UNIVERSIDADE FEDERAL FLUMINENSE
INSTITUTO DE GEOCIÊNCIAS
DEPARTAMENTO DE GEOLOGIA E GEOFÍSICA
PROGRAMA DE PÓS-GRADUAÇÃO EM DINÂMICA DOS OCEANOS E DA TERRA

Vladimir Cabello Rios

Seismic Reservoir Characterization in Ucayali Basin, Peru

NITERÓI, RJ

2024

Vladimir Cabello Rios

Seismic Reservoir Characterization in Ucayali Basin, Peru

Dissertation submitted to Universidade Federal Fluminense as a partial requirement of the graduate program in Ocean and Earth Dynamics to obtain the title of Master in Geology and Geophysics.

Advisor: PhD. Wagner Moreira Lupinacci

NITERÓI - RJ

2024

Seismic Reservoir Characterization in Ucayali Basin, Peru

Vladimir Cabello Rios

/Dissertation submitted to Universidade Federal Fluminense as a partial requirement of the graduate program in Ocean and Earth dynamics to obtain the title of Master in Geology and Geophysics.

Approved on July 17th, 2024.

_____

PhD. Narelle Maia de Almeida (UFC)

_____

D.Sc. Sérgio Adriano Moura Oliveira (LENEP)

_____

PhD. Leonardo Márcio Teixeira da Silva (PETROBRAS)

_____

PhD. Wagner Moreira Lupinacci (Advisor - GIECAR/GGO/UFF)

Acknowledgments

First of all, I would like to thank God for the opportunity to conduct this study. Also, the way God put all things and generous person because without them I would not have been able to accomplish this amazing journey.

I remain eternally grateful to my parents Teresa and Joselin for their dedication in the education of my brother Gary and me from the beginning, who always stayed with me in the most difficult situations of my life. Mon and Dad, thank you so much for supporting me at any time, encouraging me to reach my goals. On behalf of my grandparents; Maria, Juana, Ismael and Jose.

Especially thanks to my dear wife for all her attention, support, patience, care, and sacrifice. To my dear son Dario, who always provides me with invaluable sweet moments and encourages me to leave some legacy of dedication. As an anecdote, my son's name Dario came from the investigation in this project.

I am pleased to thank people from Petrobras and CNPC that cross my path for their assistance and discussions in the enrichment of this document. Also, I want to give an affectionate thanks to Jose Castillo and Gerardo Pozo, they are very gifted at teaching.

I would like to address special thanks to the department of science Geology and Geophysics of UFF, particularly the GIECAR group for their consistent dedication to improving the quality of education in the department. To professor Wagner for his teaching lesson and wise recommendations, but above all, for his valuable time in reviewing the study.

Abstract

The siliciclastic rocks in the Ucayali Basin are the main reservoirs. They contain the biggest gas accumulation in Peru. The complexity of the different depositional environments of these rocks have been studied over recent years by various researchers.

Aeolian and ephemeral fluvial environments were identified in core information from many wells in the area. The complexity of the areal distribution of these sandstones according to the development wells are not continuous as 3D facies model building at first attempt. For this reason, the possibility to integrate well-log data with seismic allowed us to evaluate in qualitative and quantitative manner.

This study presents the implementation of a stochastic seismic inversion using the algorithm Ensemble Smoother with Multiple Data Assimilation (ES-MDA) coupled with a Facies Bayesian Classification to characterize the areal distribution of the most favorable facies to be reservoir. The process begins using available well-log data and validates the results at this scale, and then extrapolates the entire process using the seismic data information. Most of the entire workflow including the stochastic seismic inversion and Bayesian classification could be done using Python (open-source programing language) at different scale dimensions such as, well-log data (1D) and seismic data (2D).

Overall, the stochastic seismic inversion offers improvements compared to a specific deterministic method such as, better vertical resolution and non-unique results of the inverted elastic properties. Also, the seismic inversion coupled with the Bayesian classification allows to delineate the facies distribution according to their depositional environment in relation to amplitude and elastic properties for the main gas reservoir units in the area. Moreover, different features of aeolian and fluvial systems were identified in the different seismic sections.

Keywords: siliciclastic reservoirs, stochastic seismic inversion, ES-MDA, Bayesian classification.

Summary

List of figures

1 INTRODUCTION

The south part of Ucayali Basin, also named The Camisea sub-basin allocated the main volumes of Gas in Peru with a production that has already surpassed the average of 79,204 Boe/day. It seems to be one of the most important Peruvian sedimentary basins according to production terms. It is one of the Sub-Andean Basins of Peru, the basin is bordered by the Maranon basin to the North, Huallaga Basin to the west, Madre de Dios Basin to the south, and the Brazilian Shield to the east (Perupetro, 2006).

In the last few decades, seismic interpreters have put increasing emphasis on more quantitative techniques for seismic interpretation, as these can validate hydrocarbon anomalies and give additional information during prospect and reservoir characterization (Avseth *et al.*, 2005). Quantitative seismic interpretation seeks to understand and measure the distribution of reservoir properties and elastic parameters of rocks in subsurface. The most important techniques include post-stack amplitude analysis, seismic attributes analysis, acoustic and elastic impedance inversion, offset-dependent analysis (AVO), facies modeling, forward seismic modeling, rock-physics models, petrophysical seismic inversion and extended elastic impedance. As a result, large volumes of information allow us to reduce the uncertainty in decision-making for exploration and reservoir oil and gas departments (Simm & Bacon, 2014).

Seismic quantitative interpretation has several tools as aforementioned, one of the most important is the seismic impedance inversion (acoustic and elastic). Impedance inversions take into account the full waveform of the seismic trace, not just the amplitudes. In general, impedance inversion is a tool to derive seismic attributes (I_p, V_p/V_s, $Poisson's\ ratio$) that can be linked to rock properties (lithofacies, porosity, pore fluids, etc.) using rock-physics models and statistical techniques (Avseth *et al.*, 2005). A popular approach to the facies identification problem is the use of crossplot templates of "impedance type" properties such as I_p and V_p/V_s (Ødegaard & Avseth, 2004). However, in the area the only one study regarding this topic was submitted by Huamán (2018).

Seismic inversion can be basically divided into deterministic and stochastic. The solutions of the deterministic inverse problem are formally shown by (Tarantola, 2005) and have been widely used since then. However, deterministic inversion tends to run into problems such as the impossibility of estimating uncertainty and the strong bias of the result due to the low-frequency model. To address these aspects, it is preferable to use

stochastic inversion due to it can generate several realizations of the model that seek to describe the potential variabilities of rocks in the subsurface (Simm & Bacon, 2014). Currently, there are several methods to carry out stochastic seismic inversion (Buland & Omre, 2003). The method applied by Liu & Grana (2018) for stochastic seismic inversion method is called Ensemble Smoother with Multiple Data Assimilation (ES-MDA). This method is able to tackle the problem of nonlinearity of the direct model in Aki-Richards equation (Aki & Richards, 1980) for largest angles and in the domain of rock-physics.

Recently, it is common to use elastic seismic inversion results for facies classification, because ambiguities in lithology and fluid identification base only on normal-incident reflection amplitudes and impedance (I_p) can be often effectively removed by adding information about V_p/V_s - related attributes (Avseth et al., 2005). For instance, Mukerji *et al.* (1998) performed facies classification based on acoustic impedance (I_p) and elastic impedance (I_s) using Bayes' theorem. The methodology involves passing one or more elastic parameters to a volume directly related to the properties of reservoirs and/or the facies using the relationship between them. Unfortunately, studies about seismic facies characterization are scares in the area, the only one was summited by Huamán (2018).

In this dissertation, a workflow for seismic quantitative interpretation in reservoir sandstones in Ucayali Basin is presented. To do this, a stochastic seismic inversion was carried out using ES-MDA and, with the elastic volume (I_p and V_p/V_s) results from this step a Bayesian facies classifications were performed. The facies were defined based on data from three wells in the study area. For study purposes five types facies were reduce to two main groups reservoir (sandstone and fine sandstone) and non-reservoir (shale, carbonate and anhydrate) facies. To carry out the entire workflow, the Python programming language was used.

The main objective of the study is to understand the distribution of these facies in the different reservoirs observed in the field and unhide the depositional behavior in the structure in relation to amplitude, elastic properties and facies distribution. The selected area for the study is a seismic crop where 3 wells which have the necessary well-log data to perform this study are available. The target zones are framed between Upper Nia at the top and Copacabana at the bottom of the sequence.

By the other hand, another main objective is to validate the applicability of stochastic inversion using ES-MDA and Bayesian facies classification to gas reservoir sandstones. Some companies performed seismic inversion and rock-physics internally, but any of them apply results in their currently making-decision geological 3D model. For this reason, the application of stochastic seismic inversion using the ES-MDA to gas reservoir in Ucayali basin can serve as a basis for future applications.

2 UCAYALI BASIN

The south part of Ucayali Basin, also known as the Camisea sub-basin, presents a remarkable structure style and plays an important role in hydrocarbon production. This sub-basin is located between the southern Ucayali Basin and northern Madre de Dios Basin, Figure 1. The western limit of this sub-basin is the basement-involved structure of the Otishi High. The Tambo Fault, probably a lateral ramp of the Otishi High, constitutes a sharp limit between the different structural styles of the north and the south (Zamora et al., 2019).

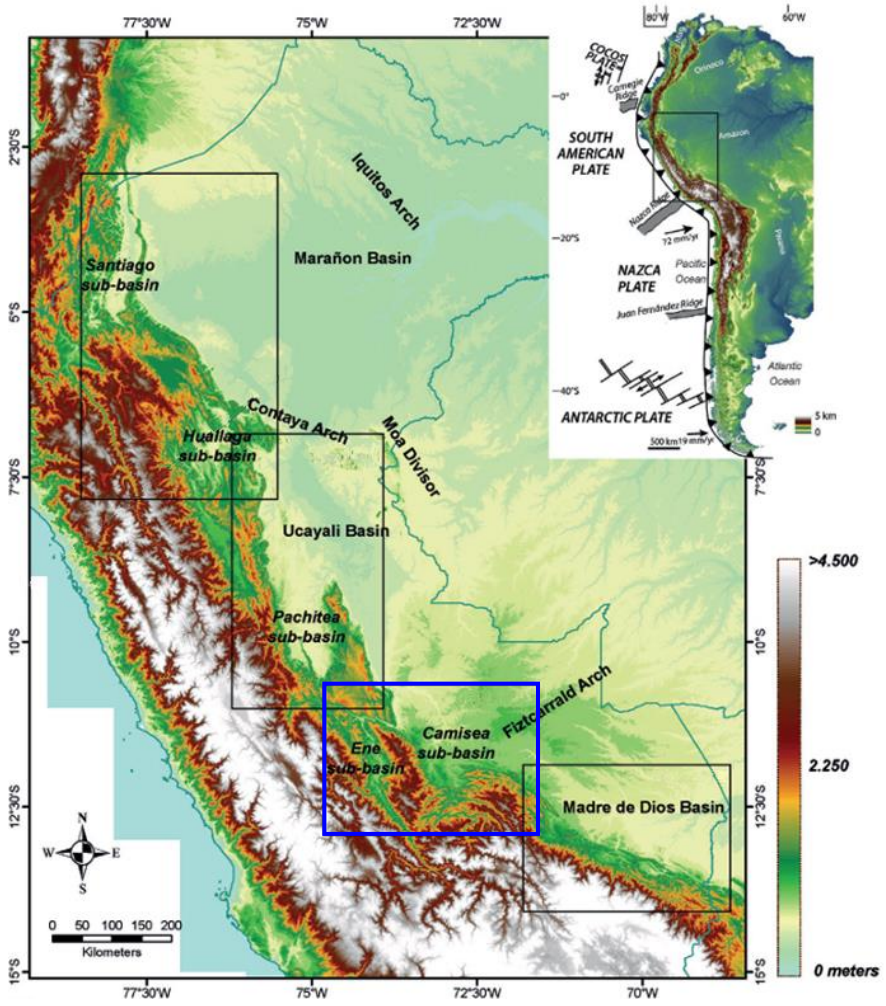

Figure 1 –Shows the Marañón, Ucayali and Madre de Dios Basins overlaying the topography map of Peru. Peruvian Sub-Andean sub-basins (Santiago, Huallaga, and Ene) are isolated from the major Amazonian foreland basin system. The Camisea sub-basin (blue rectangle) is located between the southern Ucayali Basin and northern Madre de Dios Basin. Adapted from Zamora *et al*. (2019).

The predominant structural style in the basin is the thin-skinned, generating trends of anticline and syncline which has almost the same NW-SE direction, Figure 2. The geometry of these anticlines is controlled by inverse faults with vengeance in the Forland, out-of-sequence thrusts (OOST) commonly ends up in triangle zones and back-thrust (Espurt *et al*., 2011).

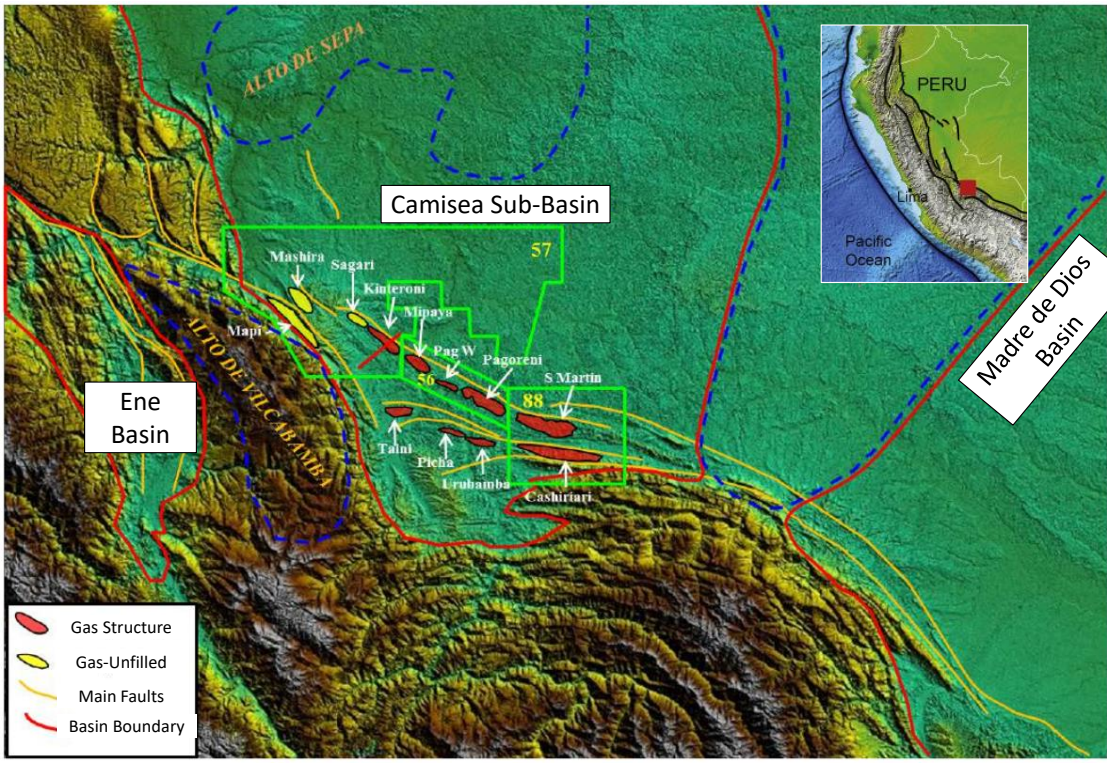

Figure 2 – The NW-SE trend of anticlines which most of them are gas accumulated structures.

Regional studies suggest that the folding in the Peruvian Sub-Andean begins in the middle Miocene, and it remains active (Hermoza, et al., 2005). On the other hand, other studies propose that the current configuration of the basin was formed by the third Quechua orogeny (Simon, 1993a). Overall, the structures affect only rocks from Silurian age which form thin folded layers disconnected from older layers of rock (Coward, 1983). Figure 3 presents the long-lived sedimentary record in The Sub-Andean zone of Peru from Ordovician to present (Zamora *et al*., 2019), and the blue rectangle highlight the statigraphy portion of the study.

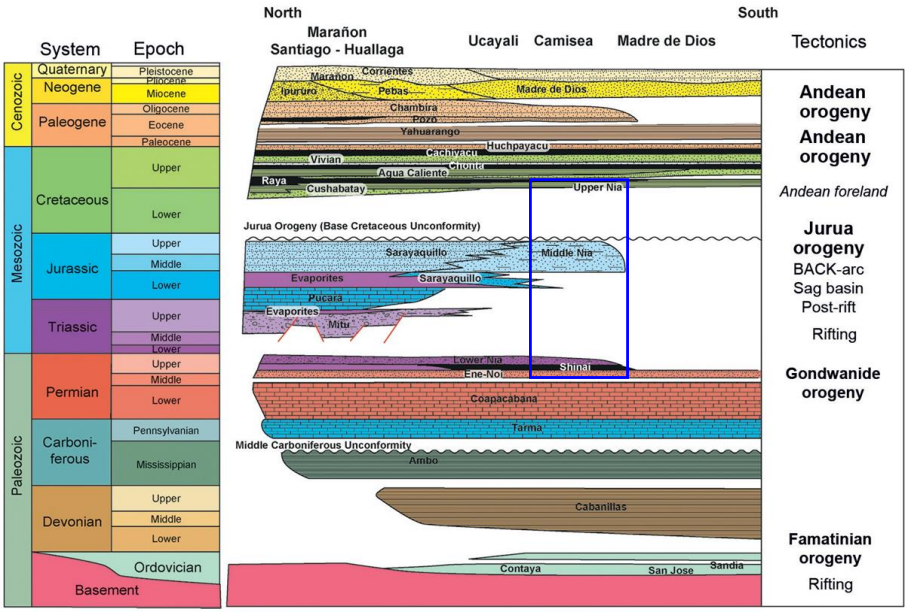

Figure 3 – Schematic chronostratigraphic along the strike of the Sub-Andean Zone. Adapted from Zamora *et al.* (2019), blue box represents the stratigraphy studied portion.

2.1 Stratigraphy

The stratigraphy of South part of the Ucayali Basin, more specifically the sub-basin Camisea consists of rocks from Ordovician to Quaternary, with a thickness of around 8000 meters, which are above a Precambrian basement of granite. All these units are affected by many erosive events which the most expressing is at base of the cretaceous. It has a dipping of 2 degrees and erodes the Permian and Pre-Cretaceous reservoirs in the NE-SW direction (Disalvo *et al.*, 2008). In this study will be described the stratigraphy units involved in the seismic inversion approach which include Ene, Lower Noi, Upper Noi, Shinai, lower Nia, Middle Nia and Upper Nia units, Figure 4.

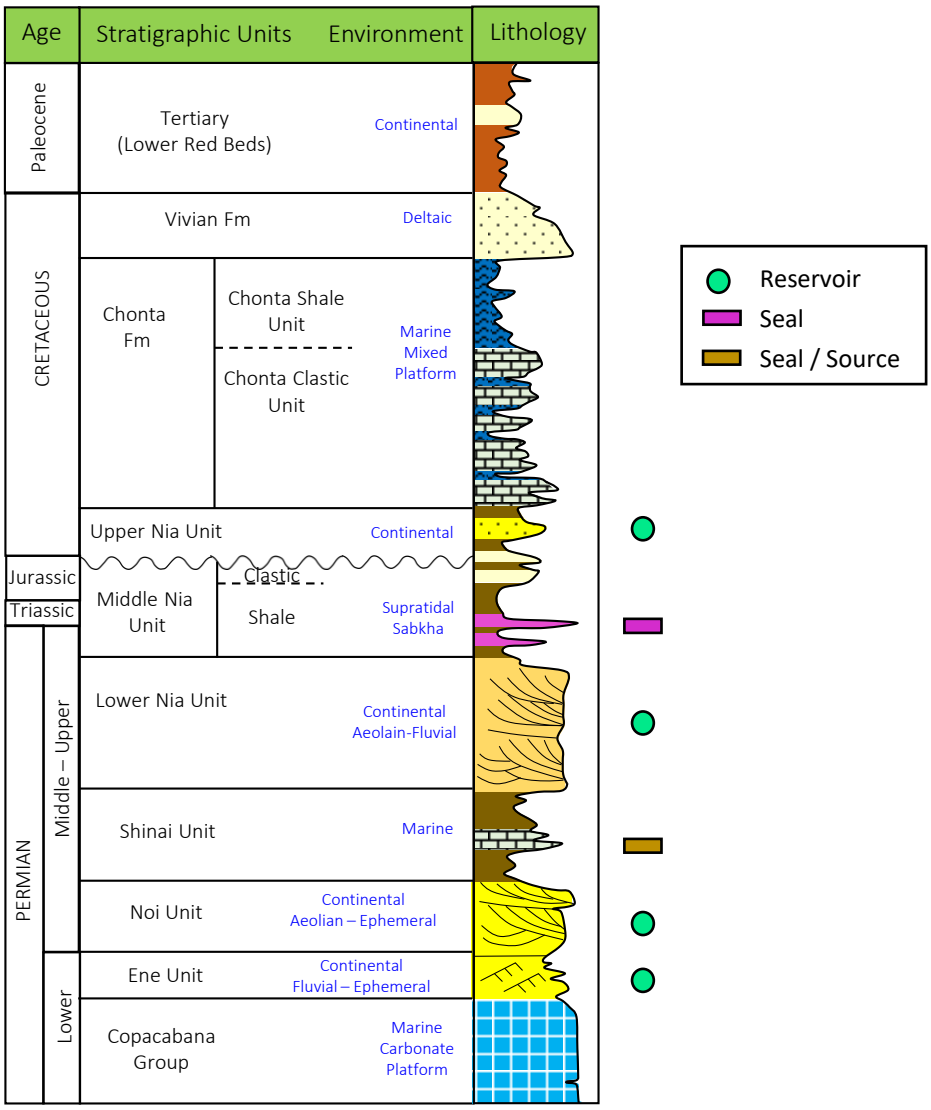

Figure 4 – Generalized stratigraphic column of the south part of the sub-basin Camisea. Adapted from Peña *et al*. (2018).

Regarding the providence of the sediments for the reservoir to be included in this study, there has been recently established some sceneries. Ene-Noi and Lower Nia reservoir sands (Upper Permian), Peña *et al*. (2018) interpreted a possible source of sediments from the Southeast and East (from a source of ~552-612Ma). Probably is the similar source that Bahlburg *et al*. (2009) describes as a "Late Neoproteroizoic Mobile Belt" (~541Ma). Also, Peña *et al*. (2018) proposed the source of sediments that was located in the peleogeographical highlands known as "Alto de Manu" and "Alto de Paititi", some another evidence come from seismic interpretation that shows a pinch-out and truncation of these reservoir units above these paleo-highlands.

For the Upper Nia (Albian - Cenomanian) reservoir sands, the source of sediments could be from the East (from a source of ~1035Ma - ~1048Ma, which could be the "Sunsas Mobile Belt" according to (Bahlburg *et al*., 2009). Additionally, Peña *et al*. (2018) based on both paleocurrents from well-log data and a gneiss age (1060+- 6 Ma) from the Otishi mountains. They concluded that the Otishi mountains could be another possible source of sediments.

2.1.1 Ene Formation (Upper Permian)

The Ene Formation is immediately above Copacabana Group, its sediments are considered to be deposited in an ephemeral fluvial lacustrine environment with a range of thickness from 25 to 34 meters in this part of the sub-basin. At the base of this unit is mainly composed by a thin layer of 3-4 meters of dark gray shale with high organic material (Seminario *et al*., 2005), followed by a present of sandstones composed of fine to very fine grain of quartz and feldspar, cemented with dolomite.

2.1.2 Noi Formation (Upper Permian)

The Noi formation is apparently deposited in a more complex environment which could be separated into two members, Lower Noi and Upper Noi.

In the east part of the Camisea sub-basin the Lower Noi is interpreted as longitudinal dune cords type Erg, Figure 5. The Lower Noi member is composed of fine to medium grain of red sandstones, the grains are composed of quartz (85%), feldspar (10%) and lithic (5%) with porosity values of 13% and permeability from 4 to 440 millidarcy. Additionally, the member presents variable thickness from 15 to 80 meters (Grosso *et al*., 2017).

The Lower Noi seismic amplitude map shows rib-type bands corresponding to the longitudinal dunes and adjacent interdunes, with a homogeneous spacing of about 3000 meters. The geomorphologic width of the dunes is 800 to 1000 meters and the interdunes are about 2000 meters. The direction of the paleocurrents is towards the NE according to well-log data, and the FMI images indicate levels of high-angle cross-stratification, corresponding to an aeolian environment (Grosso *et al*., 2017).

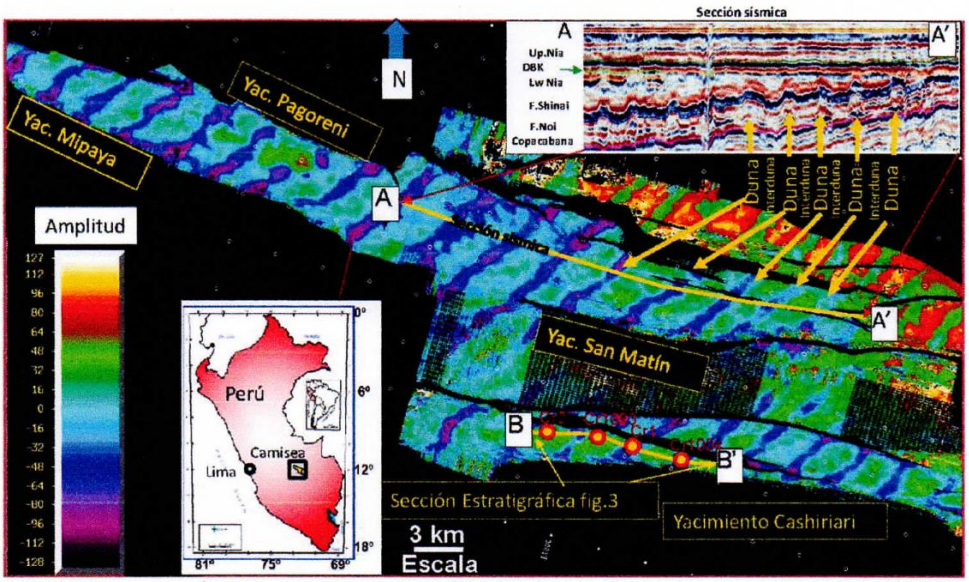

Figure 5 – Seismic amplitude map of the Lower Noi member showing the geometry of the dunes and interdunes. Adapted from Grosso *et al*. (2017).

This complexity of dunes and interdunes are also distinguished in core information. Dune facies are characterized by cross-stratification of high angle. On the other hand, interdune facies are associated with parallel and cross stratification of low angle, presence of anhydrite associated with bioturbated paleosol. The action of the water table during aeolian construction provided favorable conditions to the accumulation and preservation of interdune deposits (dry and wet) in these probable hybrid dry-wet aeolian systems (Colombo *et al*., 2019). A continuous layer of anhydrite from 2 to 9 meters is deposited above this member, representing a regional flood due to a sudden rise in the water table associated with vadose cementation of the sandstones with anhydrite in an arid climate. Moreover, the differential compaction of the interdunes reaches values of 45% to 75% and it probably has caused the folding of the overlying units of Upper Noi, Shinai, Lower Nia, and Middle Nia, this folding is also appreciated in seismic interpretations (Grosso *et al*., 2017).

The Upper Noi member corresponds to a grain growth of siliciclastic sequence of subfeldspathic sandstones, dolomites, sandy claystone and varicolored claystone, with an approximate thickness of 30 meters at least in Kinteroni field. The Upper Noi member is composed of fine to coarse grain of sandstones, and with a moderate present of cements (8–16.5%), the composition of these cements can be dolomitic, calcareous, feldspathic, silicic, hematitic and argillaceous. Towards the base of the Upper Noi member is observed a high degree of bioturbation, deformation bands by diagenesis. The middle part of the

Upper Noi member is characterized by the presence of massive sandstones that graded to sandstones with plane-parallel lamination occasionally altered due to fractures partially filled with dolomite. Towards the top, the main sedimentary feature is high angle cross bedding in sandstones (Rojas *et al*., 2013).

According to sedimentological studies in the Upper Noi, four facies associations related to a specific system environment were recognized, such as lacustrine, evaporitic (*sabkha*), ephemeral fluvial and aeolian deposits Figure 6. All of them were part of a marginal aeolian system, which was influenced by clime, eustatic and tectonics changes typical of that period of time. Moreover, petrophysical studies of this reservoir indicates the presence of both primary and secondary porosities with ranges of values between 8 and 18%, and permeability in the order of 1 millidarcy to 1400 millidarcy (Rojas *et al.*, 2013).

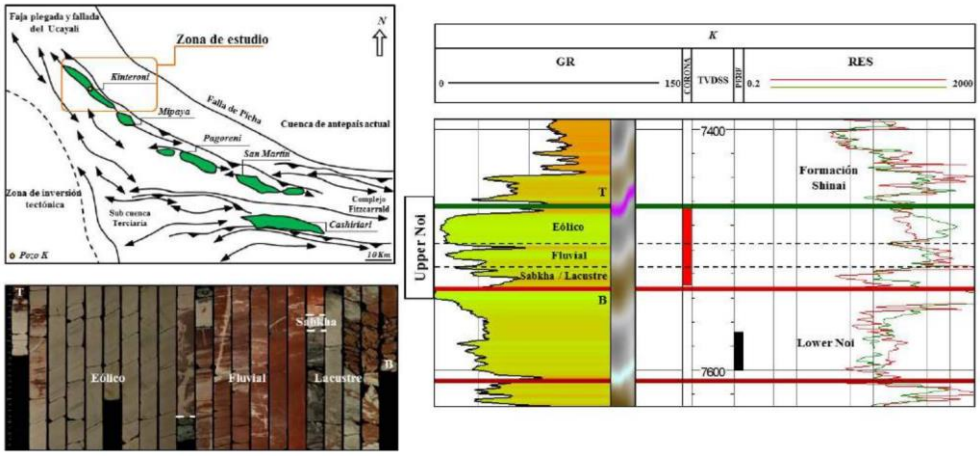

Figure 6 – Location of Kinteroni field (*orange box*), on the left down part drill core picture and lithological column of the Upper Noi member, Camisea Sub-basin, Peru. Adapted from Rojas *et al*. (2013).

2.1.3 Shinai Formation (Upper Permian)

Immediately after the deposition of the aeolian system of the Noi interval, the region is affected by a rise of sea level. This condition allowed the deposition of dark shaly and calcareous sediments (marine) with some intervals of chert mainly the center part of the interval, the thickness average of this formation is around 80 meters in the area (Seminario *et al*., 2005). In the Kinteroni field the average thickness is 90 meters.

2.1.4 Lower Nia Formation (Upper Permian)

The Lower Nia Formation is above a geological Permian unconformity and is below a sabkha surface which is followed by an important pre-cretaceous unconformity, the formation is deposited in a pre-cretaceous time (Upper Permian). The Lower Nia Fm. is composed of fine to medium grains of sandstones (feldspar-rich and lithic) showing very good sorting, reddish appearance and the average thickness of 120 meters, the Cretaceous unconformity reduce and even disappear the Lower Nia formation to the southeast part of the basin (Rojas, 2013).

Generally, Lower Nia is considered to be deposited in a desert aeolian environment with ephemeral fluvial episodes, Sabkha and, lacustrine (Disalvo *et al*., 2002); (Seminario *et al*., 2005); and (Disalvo *et al*., 2008). The intercalation of dunes and interdunes are the most representative facies in the whole section Figure 7.

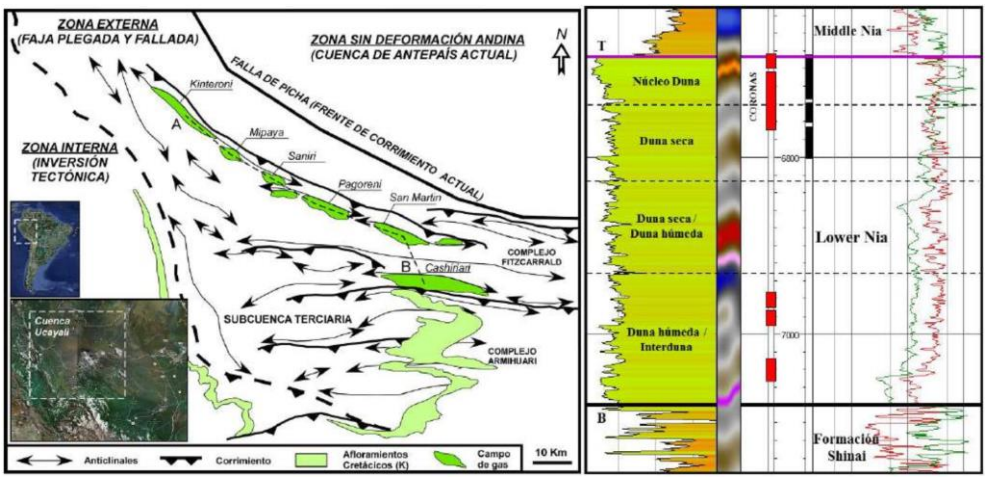

Figure 7 – Location of Kinteroni filed in the Camisea sub-basin, on the right part lithological column of the Lower Nia, Camisea sub-basin, Peru. Adapted from Rojas *et al*. (2013).

Three main sections could be identified, the lower section shows a basal aeolian dunes that shows grain fall and cross bedding grading, with coarse to conglomeratic laminae. Those laterally continuous deflation lags within the aeolian sandsheet deposits could represent periods of alternating aeolian accumulation under dry-wet conditions (Bristow & Moutney, 2013). On the other hand, the middle section is the most heterogeneous part and shows intercalations between small dunes and damp to wet interdune facies. The abundance of interdune deposits showing a facies association such

as eolian sand sheets and climbing sand with parallel stratification suggests that the interval was accumulated under wet conditions. Finally, the upper section is represented by homogeneous dune deposits with excellent reservoir properties and composed of fine sandstones with high angle cross bedding suggesting dry conditions of the system.

Overall, Lower Nia formation is interpreted as a Wet aeolian system, based on the position of water table in relation to the paleo-depositional surface and facies association (Kocurek & Havholm, 1993) . Lower Nia is characterized by the present of aeolian dunes with intervening interdunes that exhibit evidence of sedimentation that is influenced by damp and/or wet surface conditions. In such systems the behavior of the accumulation surface over time is controlled by changes in the level of the water table, sustained-water table decreases aeolian deflation, enhancing the preservation of wet interdunes (Frank & Kocurek, 1996). Therefore, the accommodation in Lower Nia formation in the three aforementioned sections are controlled by the continuous rise of water table resulted in stabilization of dunes and interdunes, and development of the laterally continuous paleosol horizon on the top of the stratigraphic sections.

2.1.5 Middle Nia Formation (Permian-Triassic)

The lithology is composed of clays with intercalation of limestone, dolomite and particularly in the area with level of anhydrate which is considered to be deposited in a restricted marine environment. According to new studies of thermochronology Middle Nia Shale is proposed to be deposited in a period between Permian and Triassic, (Peña *et al*., 2018).

2.1.6 Upper Nia Formation (Cretaceous)

Lithology is constituted by fine sandstones of reddish-to-reddish gray color, with horizontal or cross parallel lamination. In the basin the Unit presents an average thickness of approximately 25 m with good lateral continuity with porosities vary from 18- 20% and permeabilities of 50-1500 millidarcy (Seminario *et al*., 2005). In the area of the study the thickness tends to increase up to 70 meters on average.

Core information in the Kinteroni field of the sedimentary interval of Upper Nia is interpreted as generated in an alluvial environment, with mainly non-channelized deposits in regions with a seasonal or strongly intermittent discharge. Also, deposits of ephemeral shallow lakes are recorded which could represent the distal part of a

distributary fluvial systems (Ribes *et al*., 2015). In a more regional aspect, the interval cored in Kinteroni field represents the proximal area of a sedimentary complex environment which could be interpreted as a combination of an ephemeral fluvial system and a sheet-flood dominated fluvial distributary system with a sedimentary stacking pattern generated by the superposition of non-channeled flows with shallow channels of low sinuosity.

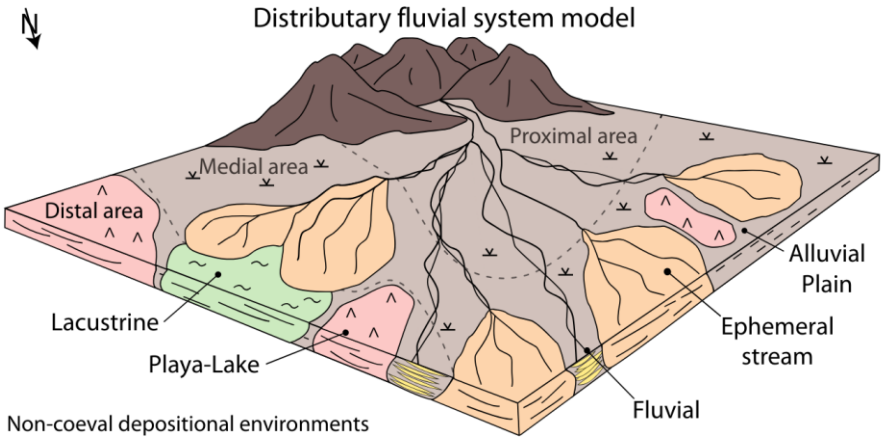

Figure 8 – Schematic depositional model of a sheet-flood dominated fluvial distributary system. The proximal area is characterized by unconfined flow in alluvial environments which could represent Upper Nia in the Kinteroni field. The medial area is characterized by ephemeral streams (unconfined terminal splay), and the distal area exhibits playa-lake and lacustrine environments. Adapted from Ribes *et al*. (2015).

2.2 Structural Style

The main structures in the Camisea sub-basin are anticlines and synclines , which are formed by low-angle thrust faults of hundreds to thousands of meters of rejection (Suppe, 1983). The angle of the main fault planes depends upon the lithology, commonly the angles are less than 16 degrees when they go through the Silurian-Devonian rocks, and close to the upper part of this cycle the angles tend to be horizontal. Once the faults cut the upper part of the Paleozoic and Cretaceous sections, the angles are around 10° a 20º, then go back to be horizontal in the tertiary base, and finally change the direction forming fold-thrust belt and, go up to surface (Disalvo *et al*., 2002).

All these angular variations produce secondary oblique faults to the mayor fault which segmented the trend. As a result, minor anticlines are formed as a consequence of these secondary oblique faults, a clear example is the trend of structures from northwest to southeast in this region; Kinteroni (*study area of thesis*), Mipaya, Saniri, Pagoreni, San Martin and San Martin Este (Disalvo *et al*., 2008). This structural trend of anticlines and synclines showed in Figure 9 is the most distal part of the Andean deformation front and has an approximate length of 110 kilometers (Venturo & Huamán, 2013).

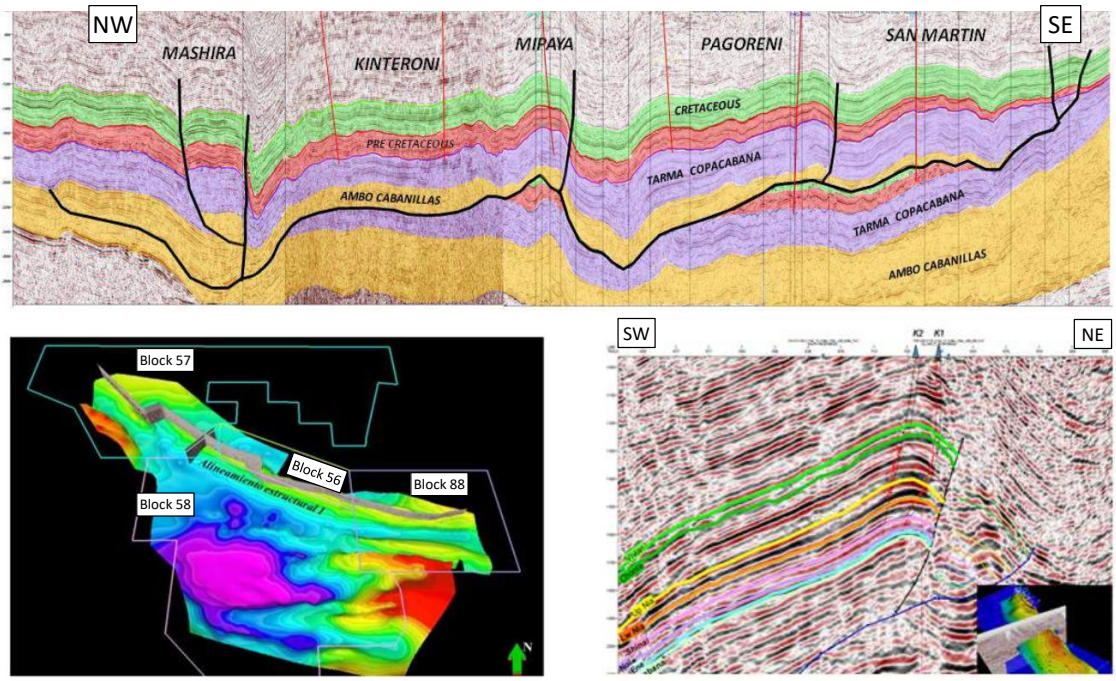

Figure 9 – Composite seismic line showing the trend of anticlines and synclines from northwest to southeast. Adapted from Venturo & Huamán, (2013).

The architecture of this thin-skinned thrust system is characterized by faulted detachment folds and associated kink-band hanging-wall anticlines, Figure 10. These thrust faults commonly terminate in triangle zones in Paleogene-Neogene strata at the leading edge of the fold-thrust belt (Espurt *et al*., 2011); (McClay *et al*., 2018a). The top of the Ordovician-Silurian syn-rift sequence and the base of the Devonian-Mississippian post-rift units host the basal detachment of the thin-skinned system in the Camisea sub-basin, and this characteristic is the main difference with the northern sectors (Huallaga and Santiago sub-basins).

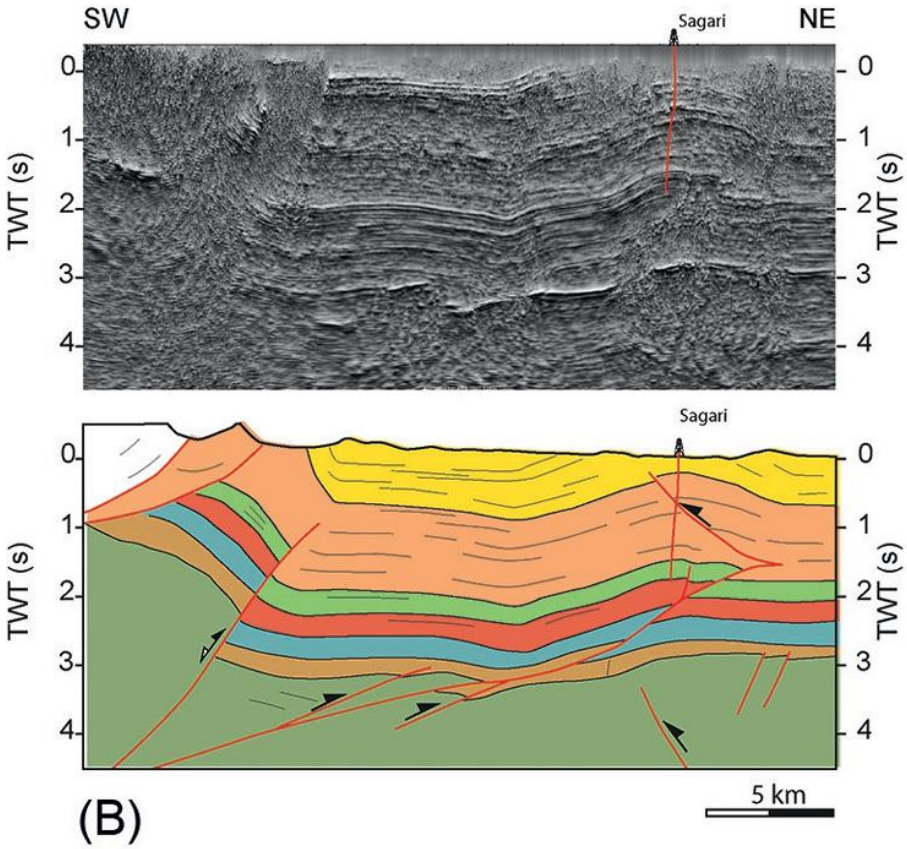

Figure 10 – Seismic attribute line (*RMS x 90° Phase change*) highlighting the structural features and interpretation. The seismic line crosses the Sagari-Kinteroni structure and shows the insertion of the basement deforming the sedimentary sequence and producing triangle zones within the Cenozoic sequence. From Zamora *et al*. (2019).

Currently two main ideas regarding the deformation in the hinterland part are adopted by geoscientists Figure 11. On one hand, the hinterland part of the Camisea sub-basin has been interpreted as a duplex system within Ordovician-Silurian strata and a large displacement hinterland passive roof backthrust (Espurt *et al*., 2011). On the other hand, (Gil Rodriguez *et al*., 2001); (McClay *et al*., 2018b) considered the hinterland of the Camisea fold-thrust belt as a system of large inverted Precambrian basement fault blocks that are uplifted and exhumed as the Andean deformation moved west from the hinterland to the foreland, and transferred displacement onto the thin-skinned sedimentary wedge at the edge of the basin. The last model implies much less shortening in the Paleozoic sequence 28 km (McClay *et al*., 2018a) vs 53 km (Espurt *et al*., 2011), and correlates better with the length of shortening transferred to the Camisea sub-basin

(~23 km; Espurt *et al.*, 2011). It is also mechanically more feasible (McClay *et al.*, 2018a).

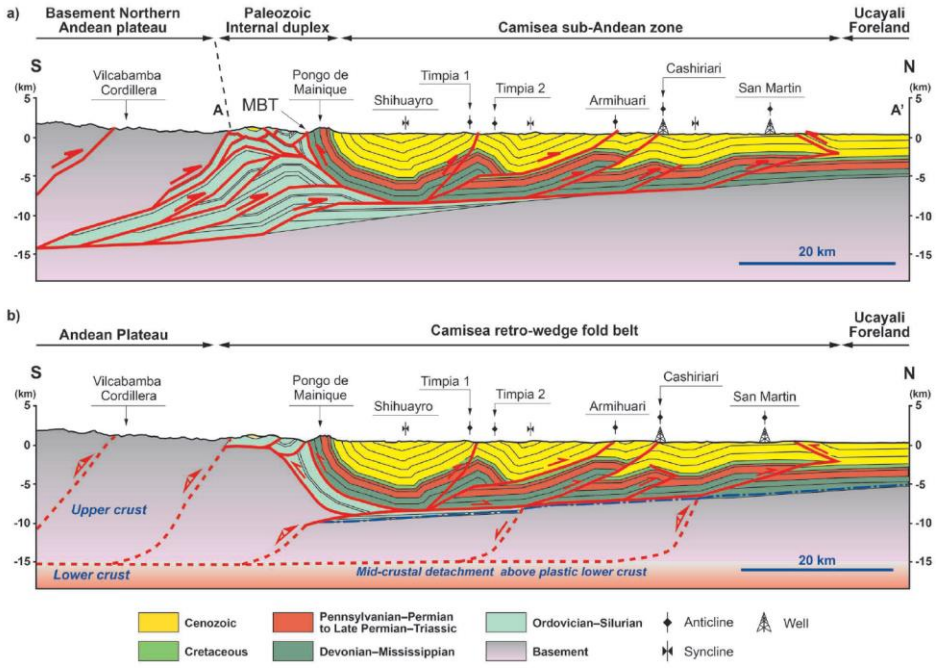

Figure 11 – Regional cross sections. (a). Regional cross section showing duplexing of the Paleozoic strata, modified from (Gil Rodriguez *et al.*, 2001); (Espurt *et al.*, 2011). (b). Regional cross section showing inverted domino-style basement faults linking to thin-skinned thrust-related folds in the Camisea frontal fold belt. From Torres & MaClay, (2014).

3 THEORY

This section aims to clarify some mathematical, physical and statistics that are the foundation for understanding the methodological stages of this work and their influences on the results. Initially, a statistical concept called Bayes' theorem will be introduced, which is the basis of the methods that will be used in this work, such as the application of Ensemble Smoother with Multiple Data Assimilation for Stochastic Inversion and Bayesian Classification for facies prediction using borehole log data and seismic volumes. Moreover, the section will state and develop the mathematical fundamentals bound up with data such as, poroelastic properties, facies and seismic data in order to get an idea how these will be used in the methodology of the study.

3.1 Bayes' Theorem

Understanding Bayes theorem is an essential part in this study, because the process to link facies with a specific value of poroelastic properties could be done by this method.

For explanation purpose, E represents a generic event and $P(E)$ its probability. For instance, E could state the occurrence of sand facies in a reservoir and *P(E)* the probability to find this specific sand facies at a given location. Probability theory is based on axioms of Kolmogorov:

(i) The probability $P(E)$ of an event E is a real number in the interval [0,1]:

$$0 \leq P(E) \leq 1, \tag{3.1}$$

(ii) The probability $P(S)$ on the sample space S is 1:

$$P(S) = 1, \tag{3.2}$$

(iii) If two events, are mutually exclusive, then the probability of the union $E_1 \cup E_2$ is the sum of the probabilities of the two events $P(E_1)$ and $P(E_2)$:

$$P(E_1 \cup E_2) = P(E_1) + P(E_2), \tag{3.3}$$

Based on these axioms, the probability of complementary event $\bar{E} = S \backslash E$, is given by:

$$P(\bar{E}) = 1 - P(E), \tag{3.4}$$

Since $P(E) + P(\bar{E}) = P(S) = 1$, it is possible to derive that probability of the union of two events, not necessarily mutually exclusive could be written as follows:

$$P(E_1 \cup E_2) = P(E_1) + P(E_2) - P(E_1 \cap E_2), \quad (3.5)$$

Where $P(E_1 \cap E_2)$ is the probability that both events will happen. For mutually exclusive events, the intersection of two events in the empty set ($E_1 \cap E_2 = \emptyset$), and the probability of the intersection is $P(E_1 \cap E_2) = 0$.

A main concept in statistic and probability is the definition of conditional probability, which explains the probability of an event based on the result of another event.

Overall, the probability of an event can be defined more accurately if additional data related to the event is available. For instance, seismic velocity depends on porosity, rock composition and fluid saturation. Thus, if one of these properties is known, then the probability of seismic velocity could be estimated.

Considering two events A and B, the conditional probability $P(A|B)$ can be defined as:

$$P(A|B) = \frac{P(A,B)}{P(B)}, \quad (3.6)$$

Two events A and B will be independent, only if the join probability $P(A,B)$ is the product of the probability of the events $P(A,B) = P(A)P(B)$. Thus, given two independent events A and B, the conditional probability $P(A|B)$ could be reduces as follows:

$$P(A|B) = P(A), \quad (3.7)$$

A common tool to estimate conditional probabilities is Bayes' theorem using the conditional probability $P(A|B)$ as a function of the conditional probability $P(B|A)$, which should be easier to calculate in many geological applications. Therefore, Bayes' theorem states that the conditional probability $P(A|B)$ is given by:

$$P(A|B) = \frac{P(B|A)P(A)}{P(B)} \propto P(B|A)P(A), \quad (3.8)$$

Here $P(A)$ is the probability of A, $P(B|A)$ is the probability of the event A given the event A, and the $P(B)$ is the probability of B. The expression $P(A)$ represents the

prior probability of A since it measures the probability before taking into account additional data associated with the event B.

Additionally, $P(B|A)$ is considered the likelihood function of the event B to be observed for each possible outcome of the event B. The term $P(B)$ represents the minimal probability of the event B and it is a normalizing constant to ensure that $P(B|A)$ satisfies the axioms. The resulting conditional probability $P(B|A)$ is also named the posterior probability of the event A, since it is computed based on the outcome of the event B.

3.2 Ensemble-Based Methods

The main goal of this seismic reservoir study is to predict the elastic properties from seismic data. Overall, inverse notation regarding seismic reservoir characterization could be written as follows:

$$\mathrm{d} = f(\mathrm{m}) + e \tag{3.9}$$

Seismic data is represented by **d**, elastic attributes is represented by $\mathbf{m} = [V_p V_s \rho]^T$, which could be P-wave velocity, S-save velocity, and density. Finally, the seismic forward model is represented by $\boldsymbol{f}$, mapping the elastic attributes **m** into seismic data **d**, and the error represented by $\boldsymbol{e}$.

This notation aims to describe the main goal of reservoir characterization which is to estimate the unknown variables **m** from the seismic measurements **d**, considering that the forward model is the best possible physical relation between model parameters and data. Keep in mind that physical relations $\boldsymbol{f}$ in equation (3.9) are often nonlinear, such as the full Zoeppritz equation.

In the study, a model-based inversion method was used in which, first it was built an ensemble of initial reservoir models of physical properties as the prior (V_p, V_s and Density); next, it was calculated the corresponding elastic attributes using a well-known equation (Zoeppritz); then it was computed the synthetic seismic response, and evaluate the misfit between the synthetic and the observed data to update the prior models until convergence.

This inversion method uses an algorithm based on the ES-MDA (Ensemble Smoother with Multiple Data Assimilation) method where the mismatch is estimated by re-parameterized of the data in a lower-dimensional space using SVD (Singular Value Decomposition) in order to optimize the procedure (Golub & Van Loan, 2013). This method is characterized by two things: the way the algorithm inverts the data and the way the algorithm optimizes the process. It applies nonlinear models to invert the properties of interest, and it iteratively performs a Bayesian updating step of the model ensemble.

Kalman filter allows to derive different ensemble-based data assimilation methods, one of them is the Ensemble Smoother (ES).

3.2.1 Ensemble Smoother with Multiple Data Assimilation

Due to the undesirable computational cost of Kalman Filter for nonlinear relations, the ensemble-based method uses an ensemble of models to approximate the model covariance with the empirical covariance of the ensemble members. The Ensemble Smoother (ES) globally update the prior model by simultaneously assimilating the measurements (Leeuwen & Evensen, 1996), using the same Kalman Filter equation each ensemble member is updated (Emerick & Reynolds, 2013):

$$\mathrm{m}_i^u = \mathrm{m}_i^p + \tilde{\mathrm{K}}\left(\tilde{\mathrm{d}}_i - \mathrm{d}_i^p\right) \tag{3.10}$$

For $i = 1, \dots, N\_e$ where N_e are the numbers of ensemble members, u and p denoting the updated (current iteration) and prior (previous iteration) variables respectively and $\tilde{\mathrm{K}}$ represents the Kalman gain matrix obtained from the ensemble as:

$$\tilde{\mathrm{K}} = \mathrm{C}_{\mathrm{md}}^p\left(\mathrm{C}_{\mathrm{dd}}^p - \mathrm{C}_{\mathrm{d}}\right)^{-1} \tag{3.11}$$

Here $\mathrm{C}_{\mathrm{md}}^p$ represents the cross-covariance generated by the prior vector of model parameters m^p and the corresponding predicted data d^p, $\mathrm{C}_{\mathrm{dd}}^p$ express the $N_d \, x \, N_d$ covariance matrix of d^p (N_d is the number of assimilated data), and $\tilde{\mathrm{d}}$ plays the role of a stochastic perturbation of the observed data sampled derived from a gaussian distribution $[\![\mathcal{N}(\mathrm{d}, \mathrm{C})]\!]_{\mathrm{d}}$ where d represents the N_d dimensional vector of observed data and C_{d} represents the $N_d \, x \, N_d$ covariance matrix of observed data measurement errors. In order to enhance the convergence, multiple times data assimilation should be performed in the ES-MDA (Emerick & Reynolds, 2013).

The equation (3.10) could be assumed as a Bayesian updating step based on the assumption that the model vector m is Gaussian. Due to the nonlinearity of the forward operator, the covariance matrices could not be computed. For this reason, an approximation of these covariance matrices is done using the empirical covariance estimated from the ensemble members, equation (3.11). The ES-MDA could be considered as a single Gauss-Newton iteration with a full step and an average sensitivity matrix obtained from the prior ensemble. By this means, multiple smaller corrections in the ensemble are executed as opposed to large Gauss-Newton demanding correction. Wu *et al.* (1999) improved the ES convergence applying at each iteration of ES-MDA an inflation parameter alpha ($\propto$) to the data error covariance matrix for the purpose of an alleviating parameter for the model variations.

Two main steps resume the ES-MDA algorithm:

1. Determinate the number of iterations and the inflation parameters $\propto_i$ for $i = 1, \dots, N$ following the notation $\sum_{i=1}^{N} \frac{1}{\alpha_1} = 1$
2. Once N was defined, for each $i = 1$ to N:
    - First, run the forward prior models and calculate the predictions $\{d^P\}_{1,\dots,N_e}$ for each ensemble member.
    - Second, generate a stochastic perturbation of each ensemble member as follow $\tilde{d} = d + \sqrt{\alpha_1 \cdot c_d}\,.\,\mathrm{Z}_d$, considering the approximation $z_d \sim \mathcal{N}(\mathrm{I}_{N_d})$.
    - Third, run an iterative process in the ensemble using equation 10 and 11 considering the replacement of C_d by $\alpha_i \mathrm{C}_d$.

The reduction of mismatch between the data and predictions is updated for each model of the ensemble. As a result, multiple model realizations are built that validate the measurements. Moreover, uncertainties which are not available with other techniques can be quantified by the covariance matrix of the updated ensemble members.

Unlike other petroleum engineering and weathering applications which could demand a large computational cost than the seismic and rock-physics forward models (Liu & Grana, 2018), the only one drawback of the method for the inversion of large seismic surveys is that the number of ensemble members (models) is much smaller than the numbers of observation, this could yield a model with underestimated uncertainty. To

overcome that problem, the method applies the SVD as a data order reduction method to re-parameterize the seismic data into a lower-dimensional data space, and then perform the ES-MDA to update reservoir models by assimilating the re-parameterized seismic data.

3.3 Bayesian Classification

It is a statistical method which gives us the versatility to provide the most likely facies classification as well as the posterior probability that could be used to quantify the uncertainty is quite robust. Bayesian classification or also called Bayesian decision is a non-iterative method that estimates the facies posterior probability using prior information about the facies model with the likelihood function that connect available data to the facies definition (Grana *et al*., 2021).

For instance, at a given location, a vector $\boldsymbol{d}$ of measurements of continuous variables, such as geophysical properties is available, and the goal is to estimate the conditional probability $P(\pi|\boldsymbol{d})$ and the corresponding most likely facies $\hat{\pi}$. The assessment of $P(\pi|\boldsymbol{d})$ can be done using Bayes' theorem equation (3.8) as follows:

$$P(\pi = k|\boldsymbol{d}) = \frac{P(\boldsymbol{d}|\pi = k)\,P(\pi = k)}{P(\boldsymbol{d})} = \frac{P(\boldsymbol{d}|\pi = k)\,P(\pi = k)}{\sum_{h=1}^{F} P(\boldsymbol{d}|\pi = h)\,P(\pi = h)} \qquad (3.12)$$

For a specific number of facies $k = 1,\ldots,F$, where F is the number of facies. In equation (3.12), $P(\pi|\boldsymbol{d})$ is the corresponding likelihood function that links the measured data to the facies definition, $P(\pi)$ is the prior model representing the prior model about the facies distribution, and $P(\boldsymbol{d})$ is a normalizing constant that ensures that $P(\pi|\boldsymbol{d})$ is a valid probability mass function. At each location $\boldsymbol{d}$, the most likely facies $\hat{\pi}$ is then obtained by operating the maximum of probability $P(\pi|\boldsymbol{d})$:

$$\hat{\pi} = \text{argmax}_{k=1,\ldots,F} P(\pi = k|\boldsymbol{d})$$

Considering all the possible values of the facies π.

If the goal is to predict the most likely facies $\hat{\pi}$ conditioned on the measured data, then it is not necessary to compute the normalizing constant $P(\boldsymbol{d})$, because of the numerator in Eq. (3.12) is proportional to $P(\pi|\boldsymbol{d})$. On the other hand, if the goal is to estimate probability of occurrence about facies distribution, then the normalizing constant $P(\boldsymbol{d})$ should be calculated.

It is common practice in geology to assume that distribution of the data, in each facies, is a multivariate Gaussian distribution $P(\boldsymbol{d}|\pi) = \mathcal{N}(\boldsymbol{d}; \boldsymbol{\mu}_{d|\pi}, \boldsymbol{\Sigma}_{d|\pi})$, where the means $\boldsymbol{\mu}_{d|\pi}$ and the covariance matrices $\boldsymbol{\Sigma}_{d|\pi}$ are facies-dependent and are often calculated from a training dataset including borehole data or core measurements. Under this assumption, the conditional probability becomes for $k = 1,\ldots,F$:

$$P(\pi = k|\boldsymbol{d}) = \frac{\mathcal{N}(\boldsymbol{d}; \boldsymbol{\mu}_{d|k}, \boldsymbol{\Sigma}_{d|k})P(\pi = k)}{\sum_{h=1}^{F} \mathcal{N}(\boldsymbol{d}; \boldsymbol{\mu}_{d|h}, \boldsymbol{\Sigma}_{d|h})P(\pi = h)} \tag{3.13}$$

3.3.1 Bayesian Facies Classification

Overall, Bayesian facies classification is, basically, the application of equation (3.13) considering the classes k by facies and $\boldsymbol{d}$ by elastic parameters, property of reservoir or profile that you want to use for classification.

These facies can be lithological, electrofacies, flow facies and/or others, so that the greater the separation between the PDFs of each facies, the better the classification result could be. Thus, here in the study a scenario with two facies (reservoir and non-reservoir) aim to predict the two groups of facies given two available measurements of acoustic impedance (I_p) and V_p/V_s ratio. In this scenario, equation (3.13) can be rewritten as form:

$$P\left(\pi = facies|\boldsymbol{I_p}, \frac{\boldsymbol{V_p}}{\boldsymbol{V_s}}\right) = \frac{P\left(\boldsymbol{I_p}, \frac{\boldsymbol{V_p}}{\boldsymbol{V_s}}|\pi = facies\right) P(\pi = facies)}{P(\boldsymbol{I_p}, \frac{\boldsymbol{V_p}}{\boldsymbol{V_s}})} \tag{3.14}$$

3.3.2 Kernel Density Estimation

In most cases available measurements do not follow a multivariable Gaussian distribution; therefore, the adoption of non-parametric approach for the estimation of the conditional probability $P(\pi|\boldsymbol{d})$ could be a suitable option.

Following the idea, the study estimates the distribution of $P(\pi|\boldsymbol{d})$ for $k = 1,\ldots,F$ using *Kernel density estimation* (KDE) in a multidimensional domain. To be more

specific, KDE tends to honor data morphology distribution instead of parameters (Silverman, 1986), it means that kernel estimation (blue line) is governed by the contribution zone of individual kernel sampling (red dash line) Figure 12.

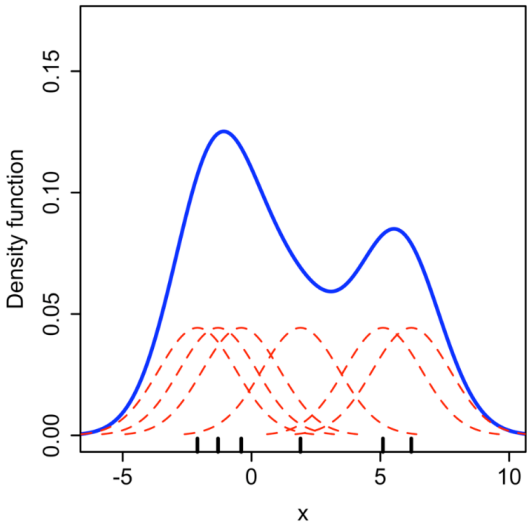

Figure 12 – Kernel density estimation constructed with six individual kernels (red dashed curves), the kernel density estimates the blue curve. The data points are the rug plot on the horizontal axis.

Kernel density estimation is governed by the following equation (Silverman, 1986) & (Bowman & Azzalini, 1997) :

$$\hat{f}(x) = \frac{1}{nh}\sum_{i=1}^{n} K\left(\frac{x - X_i}{h}\right), \tag{3.15}$$

Giving equal weight to all points $X_1, \ldots, X_n$ and n the sample number from some univariate distribution with unknown density $\hat{f}(x)$ at any given point x, K is the *kernel* which calculates the distribution morphology, the bandwidth $h > 0$ also called smoothing parameter.

The study extends the classification method to a set of multiple measurements at different depth locations and applies the Bayesian facies classification based on kernel density estimation for PDFs to a set of borehole measurements sampled. The two well logs variables at borehole location include measurement of acoustic impedance I_p and V_p/V_s ratio as well as reference facies classification.

At each location $\boldsymbol{d}$, it is assumed that prior probabilities and likelihood functions are uniformed. The Bayesian classification is applied sample by sample to calculate the

posterior probability of facies at each location in the interval. Then, the facies with the maximum (chance) probability, are predicted at each location.

4 SEISMIC QUANTITATIVE INTERPRETATION

Recent advances in seismic acquisition and processing have led to enormous progress in reservoir characterization. Over the last several years, our understanding of seismic rock properties and our ability to model those properties V_p, V_s and $density_s$ have improve substantially (Vernik, 2016). This, because Seismic quantitative interpretation assists to understand the relationship between rock properties and elastics parameters. Also, some techniques allow to obtain the non-uniqueness of the solution, using probabilistic methods that aim to estimate the most likely model as well as the uncertainty associated with the predictions (Grana *et al*., 2021). The main activities related to this area are pre-stack seismic conditioned, seismic inversion, properties and facies modelling, Rock Physics, and 4D Seismic.

4.1 Seismic Inversion

Seismic reservoir characterization aims to estimate elastic and petrophysical properties, such as P-wave and S-wave velocities, density, facies, porosity, clay volume, and fluid saturations, from seismic and borehole log data, through elastic wave propagation and rock-physics relations. Traditionally, seismic inversion refers to the estimation of elastic properties from seismic data (Doyen, 2007).

Any prediction regarding an Earth's physical property could be approximated by using a theoretical model aiming to explain the problem, and the process can be done using a forward modeling which generally requires linear or non-linear operator for accurate solution depending on the complexity. Therefore, seismic inversion aims to infer the model parameters of the system in studies that give rise to that solution; (Aki & Richards, 1980), (Rusell, 1998), and (Sen & Stoffa, 2013). The seismic inversion approaches can be divided into two groups considering the algorithm: the deterministic (matrix inversion) and probabilistic also named stochastic (Bosh *et al*., 2010).

In the first group (deterministic), these methods are relatively straightforward to generate and are based on the minimization of the difference between a modelled seismic trace and the actual seismic trace. However, these types of inversions are often smoothed results, representing a best estimation within the limits governed by the bandwidth of the seismic data. For instance, areas where the reservoir layers thickness is much lower than about ¼ of the seismic wavelength the resulting inversion could be inaccurate for

quantitative interpretation (Simm & Bacon, 2014). Band-limited, colored inversion, sparse-spike and model-based are the most important and widely used deterministic algorithms for post-stack seismic inversion (Azevedo & Soares, 2017).

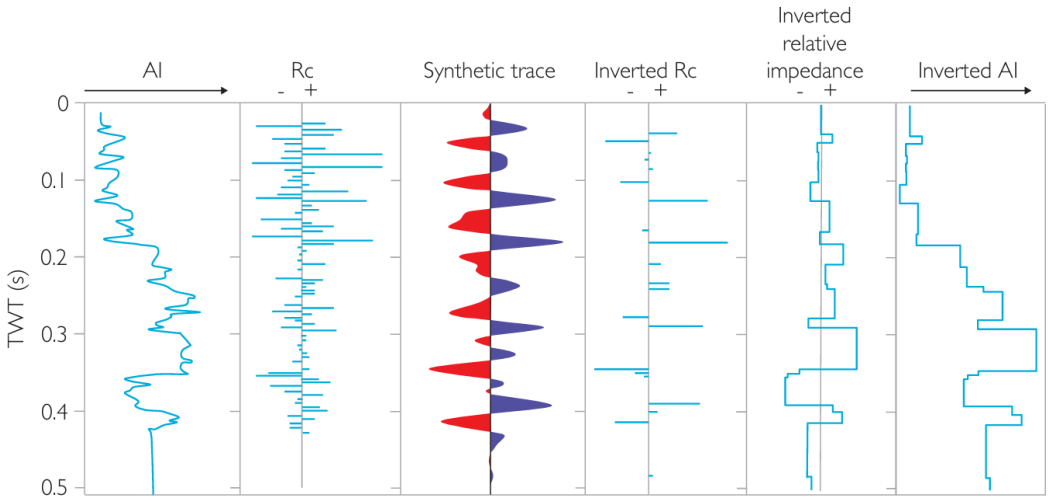

Figure 13 – Illustration of sparse spike trace inversion showing how the inverted AI trace is a blocky simplification of the well impedance. From Simm & Bacon, (2014).

Despite the well-known and widespread use of these deterministic methods, the quantification of uncertainty for deterministic methods is restricted. The only way to assess the uncertainty is by a linearization around the best fit inverse solution. For this reason, highly non-linear inverse problems such as pre-stack seismic inversion in complex geological environments could not be accurately resolved using the deterministic approaches (Tompkins *et al.*, 2011).

In the second group (stochastic), Bayesian and Geostatistical approaches could be included (Tarantola, 2005). However, in terms of computational requirements these stochastics approaches are much more demanding than deterministic methods (Bosh *et al.*, 2010). To begin, the first stochastic method mentioned *Bayesian* guarantee the propagation of the uncertainty guide by the prior probability distribution of data (e.g. well-log data), and extrapolated to the probability distribution of the model parameters space (Grana *et al.*, 2012). Once the framework is constrained, the linearity assumptions of the deterministic possible solutions are overcome (Buland & Omre, 2003). Nevertheless, the uncertainty evaluation in this method is clearly conditioned on the parameterization of the inverse problem such as, the spatial continuity pattern and the prior distribution (Scales & Tenorio, 2001). Continuing with the stochastic methods,

Geostatistical approaches use a probability density function (PDF) on the model parameters space to resolve the inverse solution (Bosh *et al*., 2010). Generally, the sampling of the model parameters to reach an inverse solution is made by Monte Carlo or geostatistical sequential simulation taking into account global optimization algorithms.

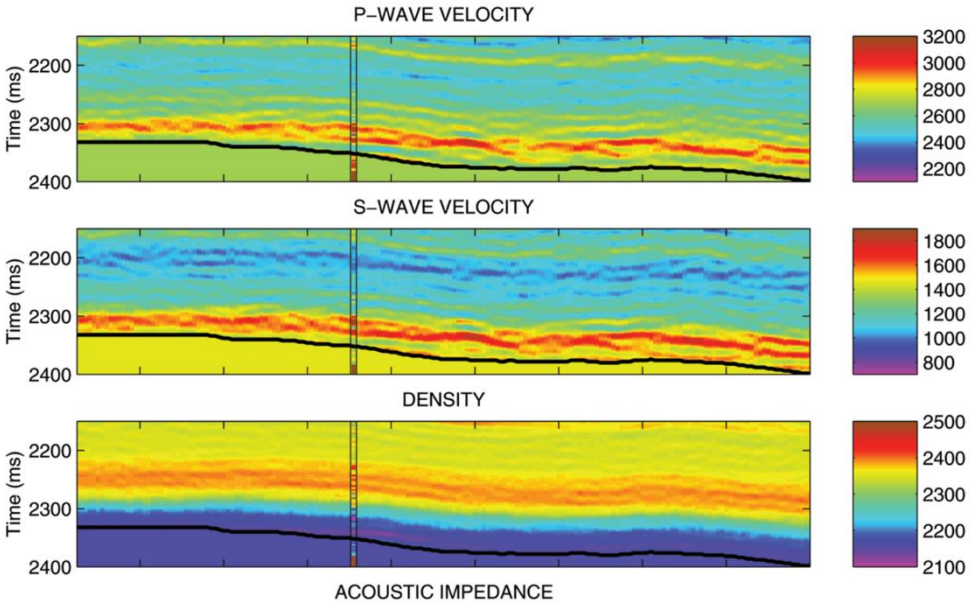

Figure 14 – Shows the P-wave, S-wave and density solution from a Linearized Bayesian Inversion in the in-line 1627. From Buland & Omre, (2003).

Overall, stochastic approaches could get decent seismic inversion results, but often in the case of using the complete Aki-Richards equation the approximation could not deal in appropriate manner for not accurately seismic processed angle (above critical angle), and in the rock-physics domain could fail for highly nonlinear models such the soft sand model or homogenous fluid mixtures (Grana, 2016). As a consequence, for nonlinear inverse problems obtaining a close-form solution is difficult, unless the adoption of a numerical method. For this reason, in the case of non-linear inverse problems, methods such *ensemble-based* can be capable of obtaining outstanding results. Using a pre-stack data from particular area of the Norne field in North Sea (Liu & Grana, 2018) obtained excellent result in the seismic inversion with the ES-MDA methodology and even compared to a Bayesian AVO linearized approach that use the same set of data. For this reason, this study adopts the same approach to get the most reliable inverse results of the petro-elastic properties and related these with a facies distribution.

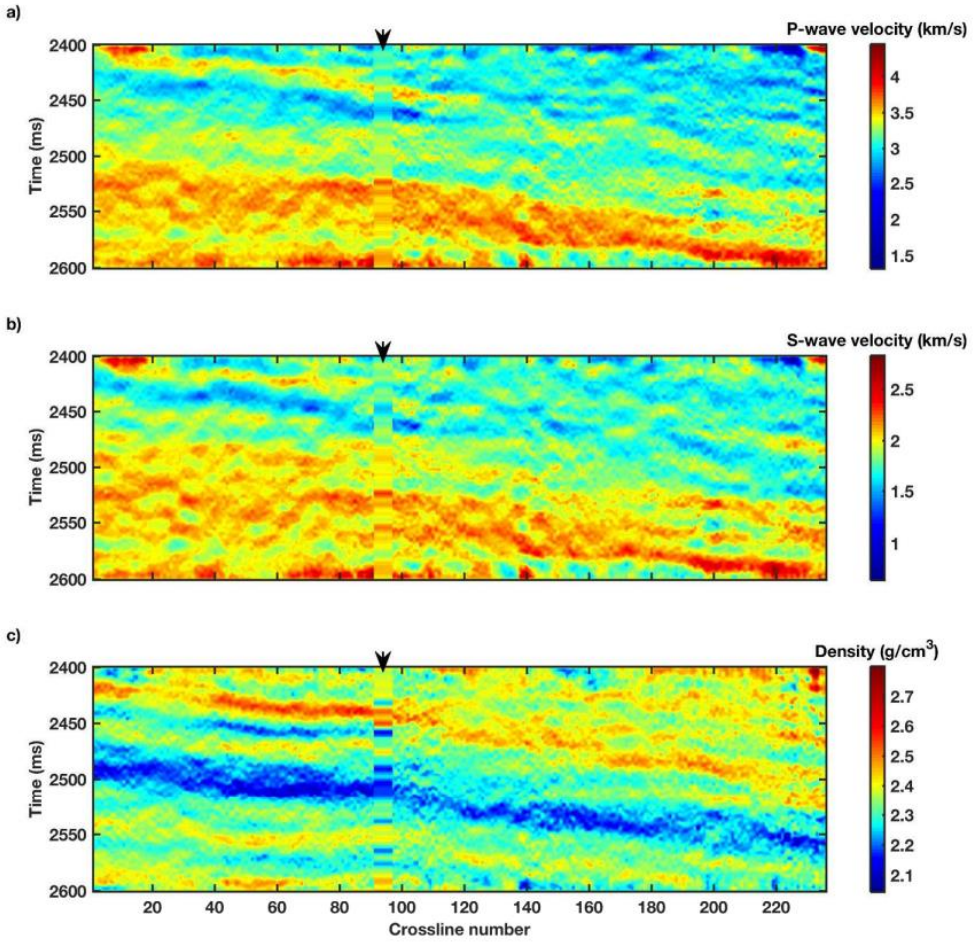

Figure 15 – Inversion results of elastic properties, from top to bottom: P-wave velocity, S-wave velocity, and density (the black arrows indicate the well location). From Liu & Grana, (2018).

Latest computational advance have emerged many other seismic approach such as those based on machine learning algorithms, which used a kind of optimization procedure to guarantee convergence with the known seismic amplitudes and in many cases constrained by a geological information. For example, (Alfarraj & Ghassan, 2019) propose a workflow using a neural-network-based inversion model to invert seismic data for elastic impedance (EI) using well-log data to guide the inversion result. In the case of prior information is sparse, for instance where seismic events corresponding to reflectors of interest remain to be identified, *Simulated Annealing* inversion could deal with this sparsity of data to resolve the seismic trace inversion problem (Mosegaard & Vestergaard, 1991) using the global optimization technique of simulated annealing to provide results that best-fit the seismic guided by an input model.

4.2 Seismic Facies Classification

Seismic facies classification was applied by (Mukerji *et al*., 1998) using data from North Sea. The acoustic impedance (I_p) and elastic impedance (I_s) from seismic inversion were used to estimate the probability occurrence of each facies. The authors applied three different approaches for facies classification and one of them is similar to what is called Bayesian classification. The estimation of the conditional PDFs $P(facies|I_p, I_s)$ was obtained from seismic inversion results using the near and far offsets at the wells location and the facies already known of these wells. This leads in a tri-variate distribution with two continuous variables (I_p and I_s) and a categorical ($facies$). These distributions were estimated using a non-parametric approach (kernel density estimation). Based on the authors' comments, the results were satisfactory not only for obtaining the most probable facies, but also for the probability of each of them, enabling an uncertainties analysis.

Recent studies in Brazil have been published applying this methodology to carbonates of the pre-salt (Texeira *et al*., 2017); (Penna *et al*., 2019); (Penna & Lupinacci, 2020). For instance, Texeira *et al*. (2017) presented a 2D Bayesian classification to discriminate carbonates with good porosity, closed carbonates and clayey-carbonates using the elastic parameters of acoustic impedance (I_p) and V_p/V_s ratio which were generated from elastic inversion. The first parameter proved to be sensitive to porosity, while the second proved to be more sensitive to mineralogy, enabling the classification of these three types of facies using seismic data.

Also studies where different kinds of gaussian distribution *(Single Gaussian and Gaussian Mixture)* were performed to link between elastic and petrophysical properties, each of these gaussian components is related to different geological lithofacies. Then a Bayesian approach for seismic inversion to estimate acoustic, impedance and lithofacies of subsurface conditioned to post-stack seismic and well data were computed (Figueiredo *et al*., 2017).

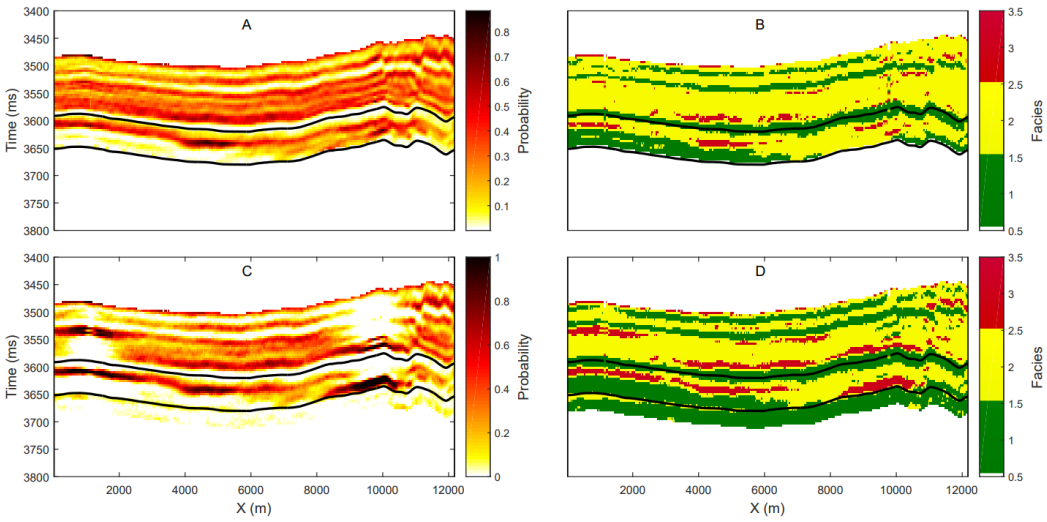

Figure 16 – Probability of reservoir facies and the more likely facies using two different distribution approach; *Single Gaussian* in A, B and for *Gaussian Mixture* in C, D. From Figueiredo *et al*. (2017).

Another common approach is the use quantitative seismic interpretation, and more specific Rock physics which establishes the relationship between elastic attributes and reservoir properties. Grana & Dvorkin (2011) carry out a seismic elastic inversion on seismic data to arrive at volumes of I_p and I_s, then a rock physic model is made at well to link the elastic properties to different rock and fluid properties.

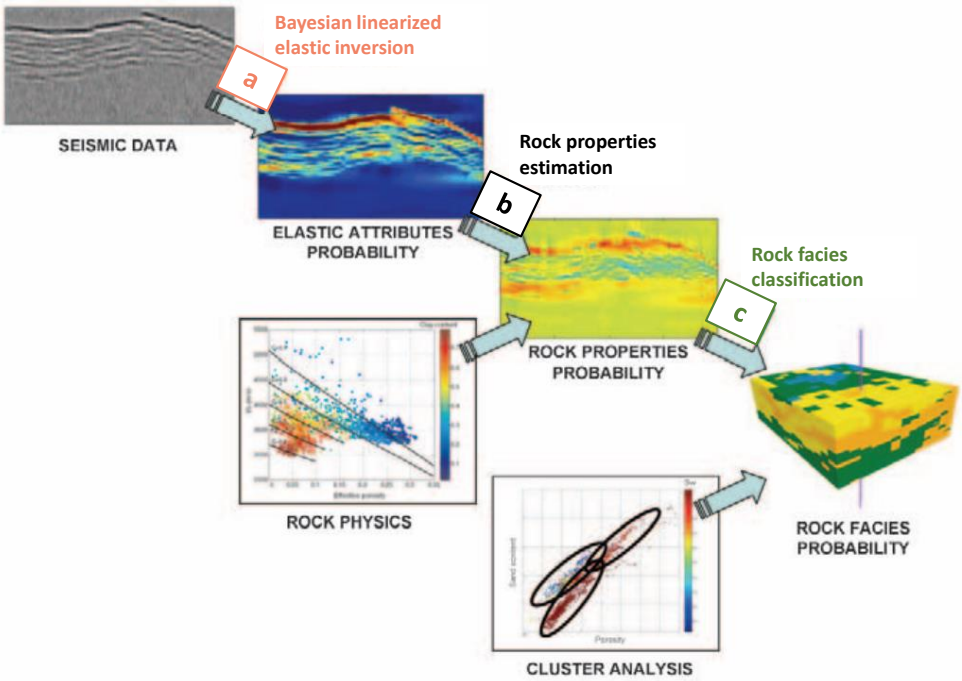

Figure 17 – Workflow of seismic facies classification. (a) Seismic data are used to obtain the probability elastic attributes, such as the P- and S-wave impedance, using a Bayesian linearized elastic inversion. (b) A rock physics model is fed into the resulting elastic attributes volumes to produce the volumes of rock properties probabilities. (c) Rock facies are classified at a well, and this classification, together with rock properties, is used to produce a facies probability volume. From Grana & Dvorkin, (2011).

An application of Bayesian facies classification to igneous rock identification using stochastic seismic inversion in the presalt interval of Santos Basin was presented by Fernandes *et al*. (2024). The study used the ES-MDA algorithm to get an acoustic impedance seismic inversion. Then, facies related to igneous rock using a priori probability were modelled, Figure 18. The results are in good agreement with the ones observed in the wells according to authors.

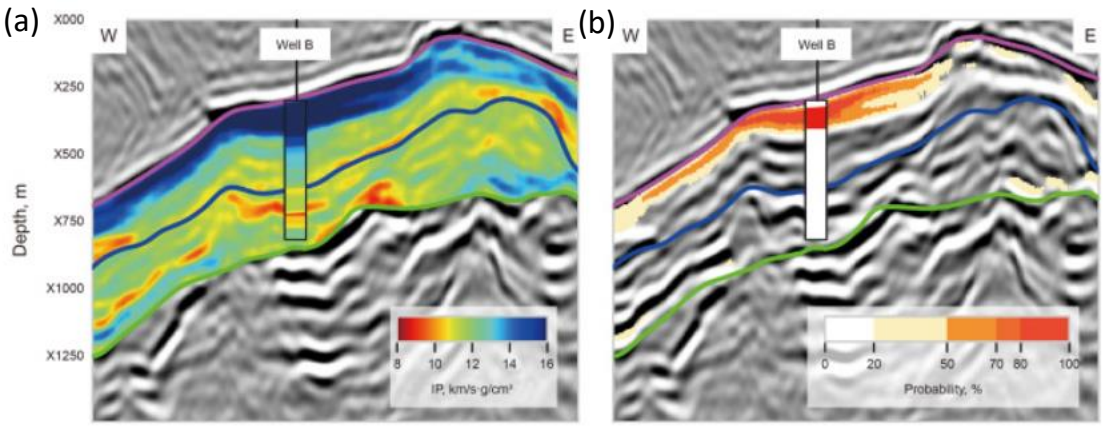

Figure 18 – Seismic section crossing Well B showing: (a) the I_p of stochastic inversion from realizations P50, and (b) their respective igneous occurrence probability estimated in Bayesian classification from P50. The lime green line represents the Pre-Jiquiá Unconformity, the blue line is the Pre-Alagoas Unconformity, and the magenta line is the Base of Salt. Adapted from Fernandes *et al*. (2024).

5 METHODOLOGY

The seismic quantitative interpretation of siliciclastic reservoirs in this specific area of the Camisea sub-basin uses two kind of data original and interpreted (*derived from a second process*). The original data consists of well-log data and conditioned pre-stack seismic data. Moreover, the interpreted data consists of an accurate seismic well tie, seismic horizons interpretation, generation of low frequency models of each property (I_p, I_s and $density$), and facies definition. The workflow of the seismic quantitative interpretation is represented in the Figure 19. The seismic interpretation was made using a Petrel software, and both the stochastic seismic inversion and seismic Bayesian classification was made using a Python open-source programing language.

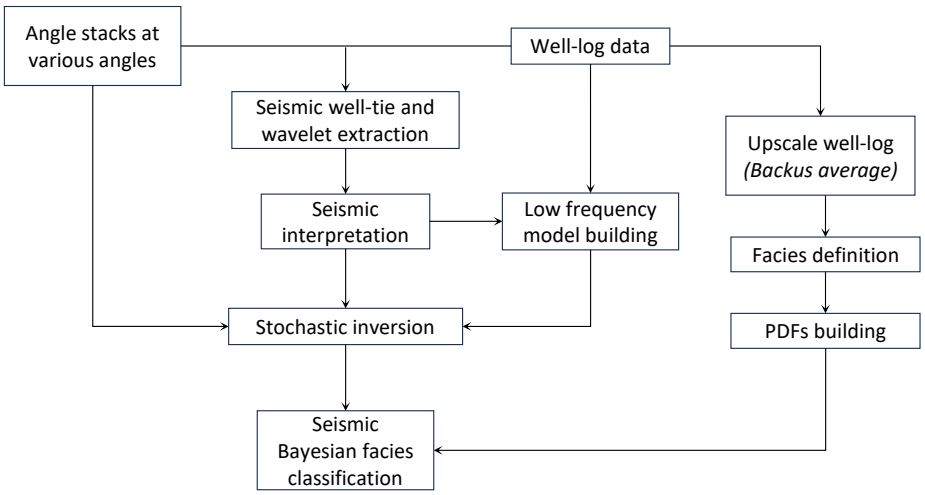

Figure 19 – Schematic workflow of the seismic quantitative seismic interpretation apply to the reservoir in Kinteroni field.

A careful seismic well tie initiates the study in order to get more reliable relation between seismic and well log data, this process identifies the best amplitude reflections related with the intervals of the main reservoirs. Moreover, a crucial step was the upscale of well data using the Backus algorithm (Backus, 1962) with a frequency of 80 Hz and 5 meters sampling. The seismic crop area has three wells which are located along the highest part of the structure, all of them were used in the building of low frequency models using a geostatistical technique with both migration velocities and well velocities data (Soares & Azevedo, 2018). To point out, the seismic crop includes 560 milliseconds in two-way traveltime thickness, 684 inlines (inline) and 285 crosslines (xline), with vertical sampling rate of 2 milliseconds and lateral sampling rate of 15 meters.

By this time, stochastic non-linear seismic inversion will be performed using previous information using the ES-MDA algorithm in time domain. After that, using the upscaled well-log data of I_p and V_p/V_s ratio conditioned to facies interpretation a PDFs was built. Then, the same PDFs used the seismic inversion results to carry out the Bayesian facies classification.

A detailed description of each part will be addressed in the following sections, such as seismic well-tie, low frequency model building, stochastic non-linear seismic inversion application and Bayesian facies classification.

5.1 Seismic Well Tie

In this subtopic the Seismic Well Tie process is described, the data of three Wells have been reviewed and analyzed during this stage. A comparison of sonic logs and checkshot information for each one of the calibration wells (K1, K2 and K3), shows that velocity trends were properly measured and corrected especially in the target zone of the study.

Figure 20 shows panels for each calibration well used in this study where sonic velocities are display in blue while checkshot in grey line colored by its value range. The group of horizontal lines represents different tops at the target zone framed between Lower Chonta at the top and Copacabana at the bottom of the sequence. An important observation is that the Nia, and Noi sandstones reservoirs are characterized by low velocities compared to high velocity trend characteristic of shale rocks. Hence, low impedance value is expected to be associated with sand lithology.

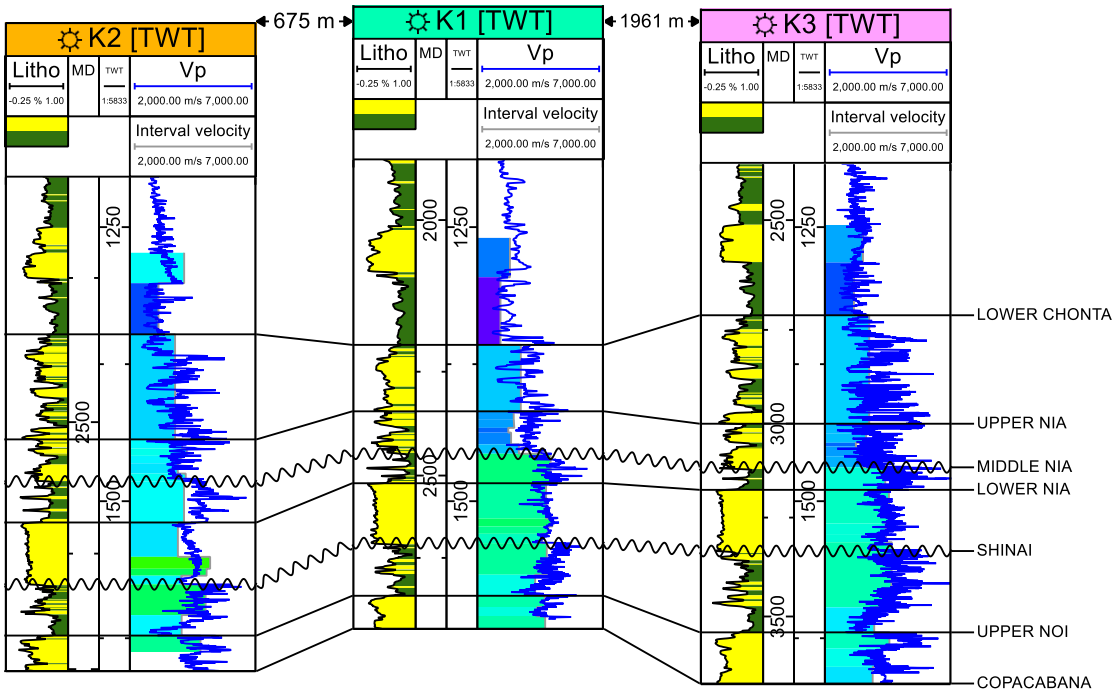

Figure 20 – Comparison between sonic velocity (blue line) and checkshot interval velocity at K2, K1 and K3 wells

In addition, an analysis of the poroelastic properties helps to determine the limitations in resolution due to frequency content of the seismic (PSTM seismic data in this case). Such analysis is represented also as log curves but at a resolution compared to seismic; also known as log curves at seismic scale. The results help to determine the degree of detail that we can expect to achieve through methods of seismic inversion.

The following Figure 21 show the poroelastic curves such as V_p, V_s, I_p, I_s, V_p/V_s and density at seismic scale (blue) and log scale (grey) for K2 well. Seismic scale log curves have been generated based on dominant frequency of PSTM seismic data using the Backus average calculation, and not as simple smoothing of the curves. These sets of curves have been provided as input in the seismic inversion process. Note that the high frequency detail observed at log scale is largely reduced in logs at seismic scale. Also, the Figure 21 shows tops of relevant units within the zone of interest from Upper Nia to Copacabana. The Backus average shows important characteristics in the poroelastic curve. For instance, the anhydrate layer above and shaly carbonate layer bellow Lower Nia is characterized as a high impedance interval but with a much lower increase in shear velocity that results in a characteristic decrease in V_p/V_s ratio associate mostly to sand intervals, particularly appreciate at well K2 (figure 21).

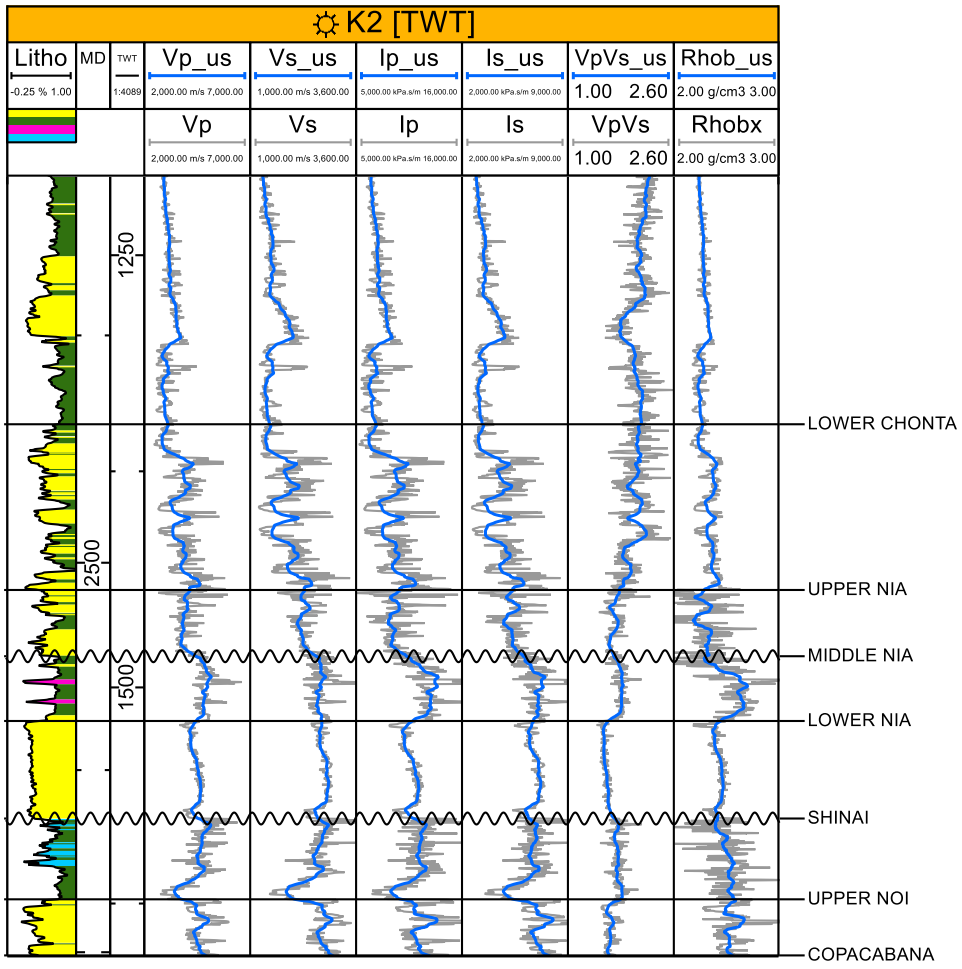

Figure 21 – Poroelastic curve at seismic scale (blue) and log scale (grey) for well K2

Post-stack calibration was performed for each calibration well included in the seismic crop volume. The methodology used sonic, density logs and checkshot information. A 25 Hz zero phase Ricker wavelet was used as a first approach to generate a synthetic trace and then replaced by an average of statistical wavelet from K2, K1 and K3. In order to evaluate the process, a cross-correlation method is used to compare the resulting synthetic trace to a composite trace that is extracted along the path of the deviated wells.

All statistical wavelets extracted from the three wells are almost identical, Figure 22 shows a comparison between the average statistical wavelet extracted from the seismic stack and Ricker wavelet. This allows for a closer reproduction of seismic character in the synthetic trace at the zone of interest.

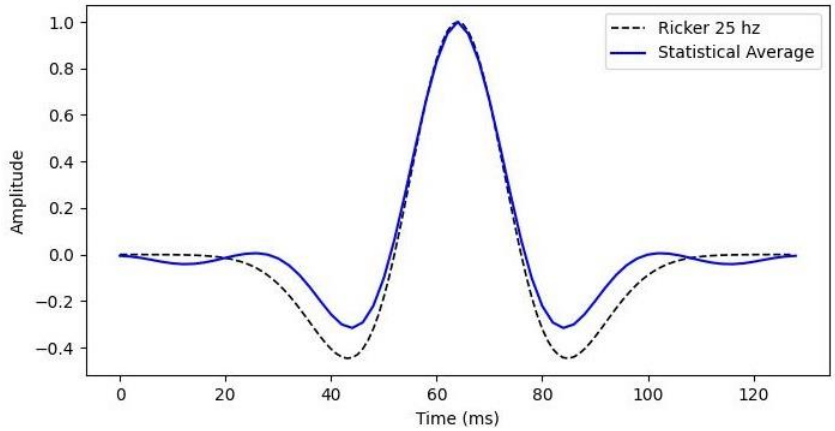

Figure 22 – Comparison between the statistical average from three wells (blue) and Ricker wavelet 25 Hz (dashed black line)

Overall, very little adjustments were introduced to checkshot curves in order to match reflections with corresponding well tops. Special emphasis was applied to match, Lower Chonta, Upper Nia, Middle Nia, Lower Nia, Shinai, Lower Noi and Copacabana. In particular, Lower Noi and Ene reservoirs were comprised within half a cycle of seismic reflection due to their thickness are bellow seismic resolution.

Figure 23 shows a composite panel of log curves from left to right including gamma ray, velocity, density, reflection coefficient, statistical extracted wavelet, synthetic trace, extracted stacked trace from seismic data, and also geologic markers (tops) are included. For the study purpose the extracted wavelet was carried out with a statistical approach.

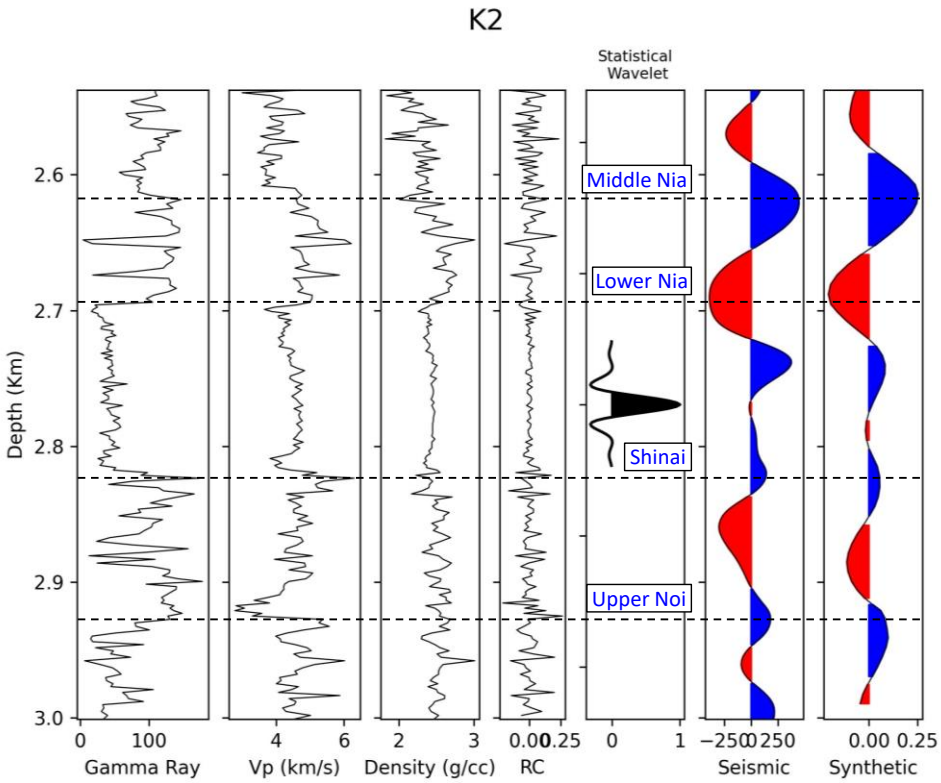

Figure 23 – Composite panel showing different well-log curves, statistical average from well K2, seismic amplitude at well location and synthetic amplitude from well-log data.

In general, the K2, K1 and K3 wells show reasonable match between seismic and synthetic trace. A method to evaluate the degree of correlation is the use of Pearson correlation coefficient (PPC). For instance, the arbitrary seismic line of stacked data where both the well path and synthetic is plotted in the Figure 24, also showing the PCC value of 0.71. For reference, tops (white circle) and seismic horizons (black line) overlain the arbitrary seismic line along the K2 well path. Observe an acceptable match of seismic events between synthetic from K2 well and stacked seismic data.

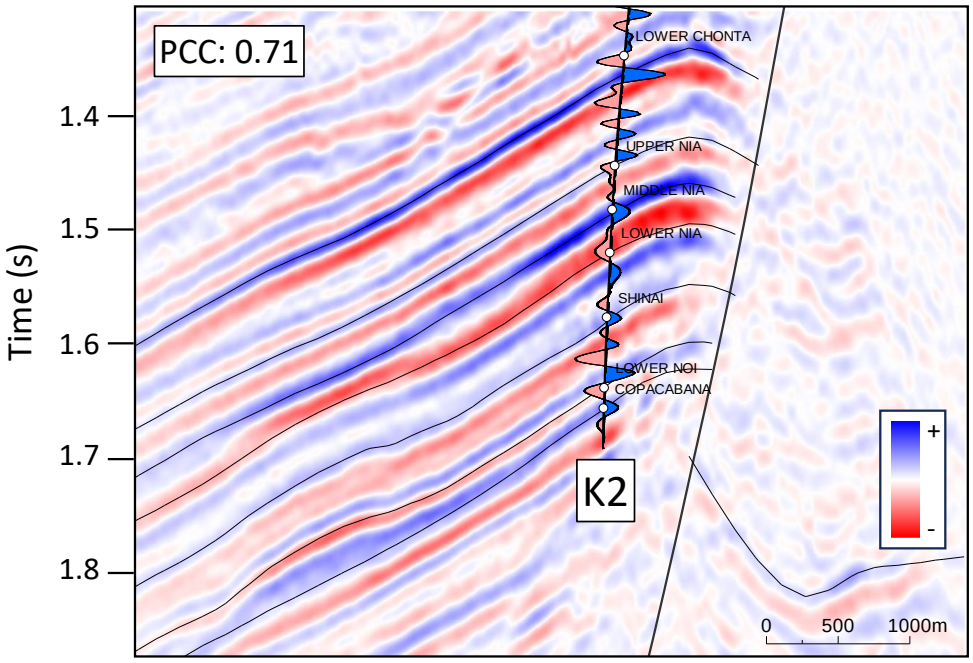

Figure 24 – Arbitrary seismic line along the path of the deviated well K2 showing the match between seismic and synthetic log.

5.2 Low Frequency Model building

In this study, low frequency models for P- and S-Impedance, as well as for density were required to be generated as prior information. The first approach to build a P-Impedance model comes from the use of velocities from migrations (PSTM velocities), where RMS velocities were converted to interval velocities using Dix approach. As a quality control the Figure 25 includes from Lower Chonta to Copacabana horizons; also, along the well path selected tops are displayed as reference (Upper Nia and Copacabana). The displays showed that RMS velocity distribution is not conformable with geometry of the geologic structure that amplitude information shows.

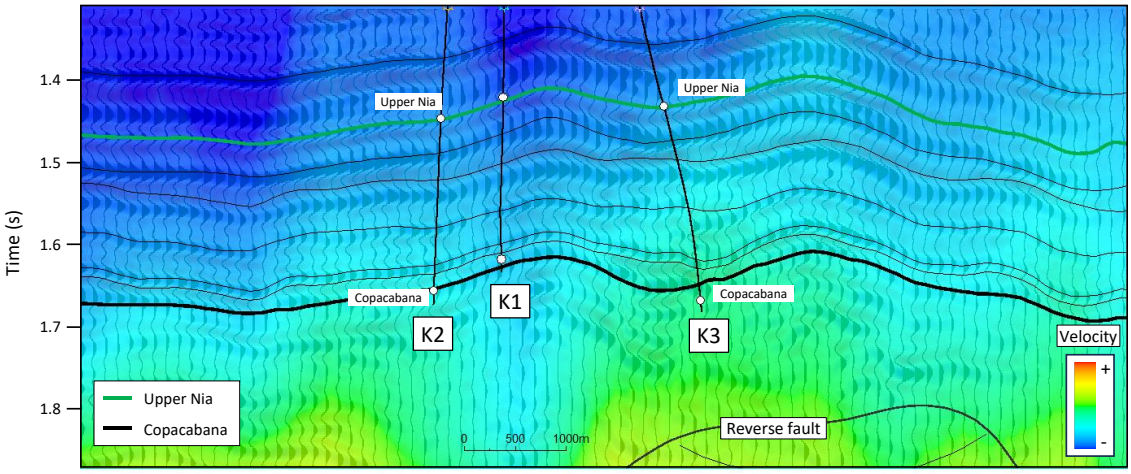

Figure 25 – RMS seismic velocity does not follow geometry of seismic amplitudes, and values of RMS are below real velocity from well-log data in the interval of interest, warn and cool colors means high and low velocity respectively.

Extraction of interval velocity curves from PSTM velocity field at each calibration well was done to check accordance with well data log and checkshot information. Figure 26 shows a composite panel of Kinteroni wells with different velocity profiles; sonic velocity at well-log and seismic scale are shown in grey and light-blue respectively, RMS velocity field from PSTM are shown in green and extracted velocities from interval velocity field from PSDM processing are shown in red.

In general, extracted RMS velocity (green) or extracted interval velocity from PSDM velocities (red) do not match closely the well measurements. The RMS velocity seems to be underestimating and the interval velocity not to accurately adjust to wells.

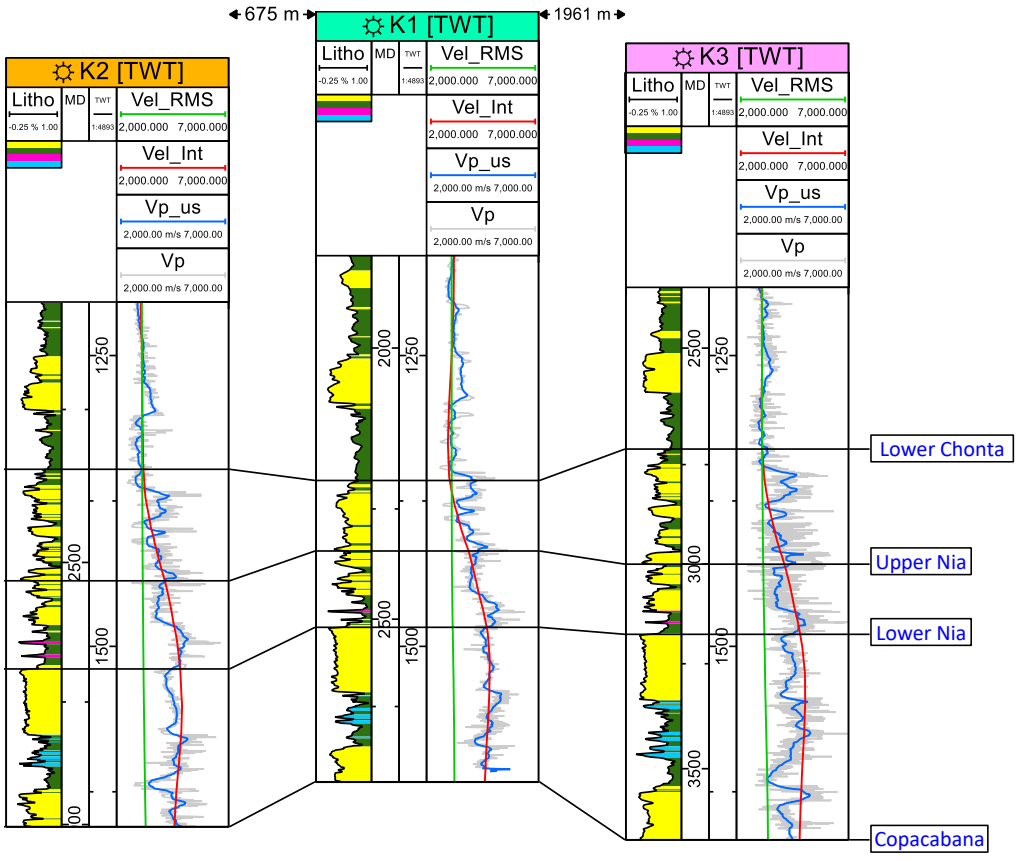

Figure 26 – Trend of RMS velocity from PSTM (green) and interval velocity from PSDM (red) compared to well velocities at each Kinteroni well at well-log (grey) and seismic (light-blue) scale.

As a result of the quality control in velocity trends from seismic and well log data that do not match the trends between them, a Low frequency model using geostatistical modeling was used by combining both migration velocities (PSTM and PSDM) and well velocities. The resulting low frequency velocity model provides a better match to trends observed at each calibration well. Figure 27 shows in the left part extracted LFM acoustic impedance curve (red), which overlays upscaled I_p from well-log (black) extracted at specific interval window for K1 well. Also, in the right part the LFM of I_p at inline 716 and well K1 path and key tops (Upper Nia, Lower Nia, and Copacabana).

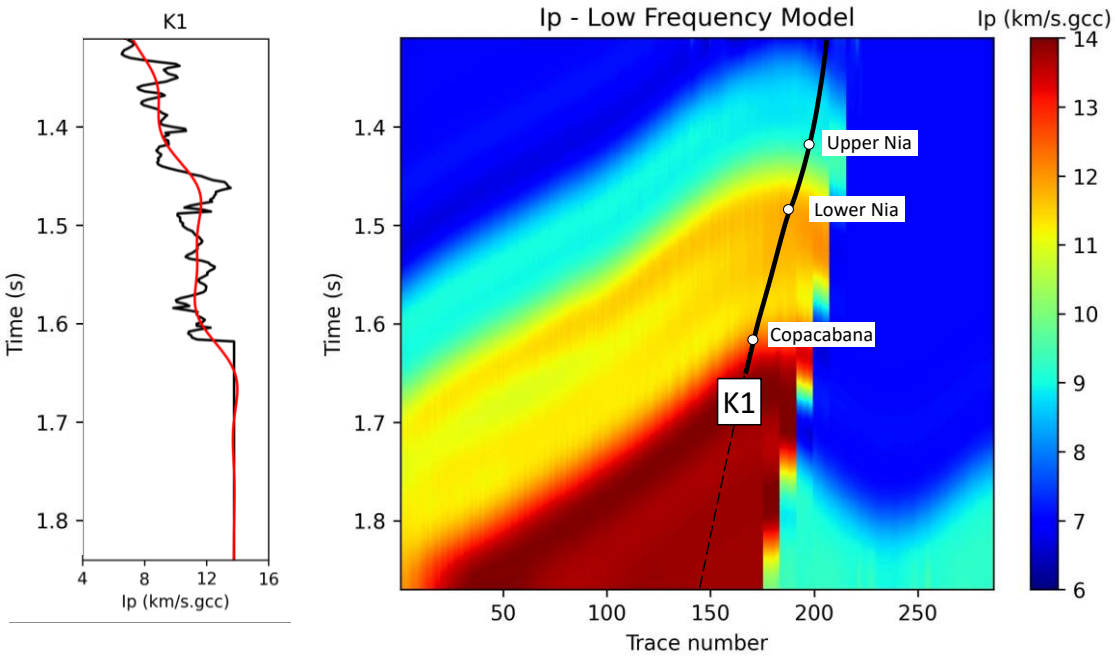

Figure 27 – In the left part, upscaled well-log (black) and LFM (red) curves of I_p. In the right part, Low frequency model (LFM) of acoustic impedance in the inline 716 and well K1 path and key tops.

The modelling of the low frequency P-velocity model was the first step to build all the suite of models needed for seismic inversion. The resulting P-impedance, S-impedance and density low frequency models (LFMs) are based on a combination of geostatistical modeling and rock physics trends that relate P and S velocity information to density.

At this point of the study, conditioned angle gather stacks (conditioned in waveform and spectra) have been generated, wells had been calibrated, wavelets have been statistically extracted from conditioned angle stacks, and low frequency models

were also built. Consequently, all the elements to conduct a Stochastic seismic inversion were satisfied.

5.3 Stochastic non-Linear Seismic Inversion application

In this section, an explanation of the seismic inversion process based on ES-MDA applied to a seismic reservoir characterization study in the Ucayali basin is described. The available data for the study includes a set of well-log data, and three partial angle stacks (near, middle, and far stack corresponding to 12°, 24°, and 36° respectively). Figure 28 shows the seismic inline 716 of the near, middle, and far angle stack across the well K1.

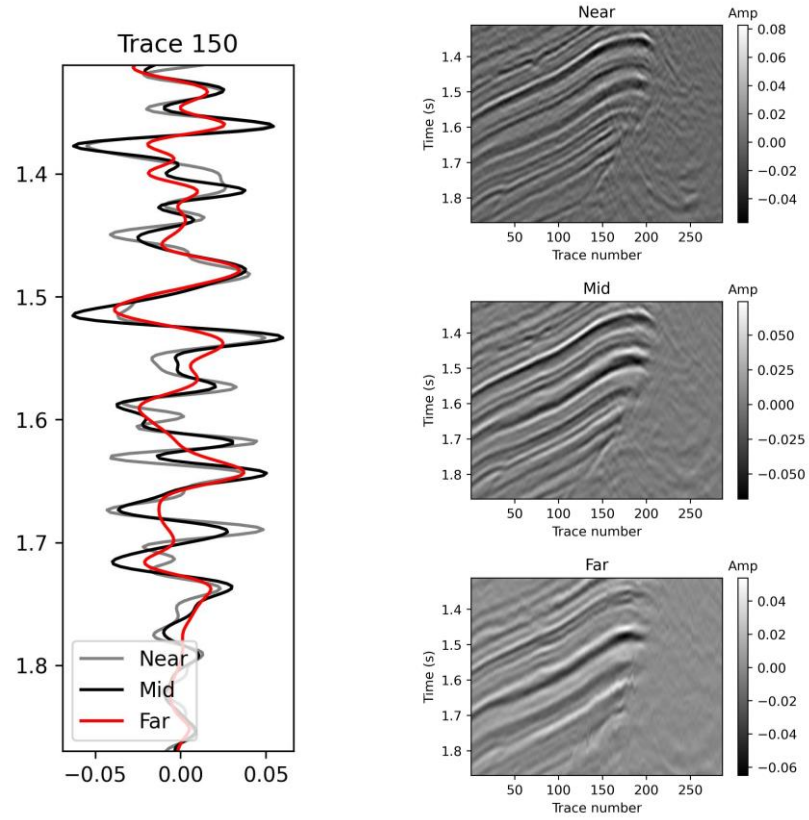

Figure 28 – In the left part, an overlain of seismic partial-stacked extracted of near, middle, and far trace with incident angles of 12°, 24° and 36° respectively at [inline 716; trace 150] position, and in the right part the seismic inline 716, from top to bottom: near angle stack (12°), middle angle stack (24°), and far angle stack (36°).

The method consists in the use of stochastic nonlinear inversion framework of three partial angle stacks (near, middle, and far) based on the ensemble smoother with multiple data assimilation (ES-MDA) to estimate elastic reservoir properties with the

measurement of the uncertainty. The stochastic seismic inversion process implemented in the study can be described as follows:

- ① Generate an ensemble of N_e initial models of elastic properties (P-wave velocity, S-wave velocity and density) using geostatistical methods to account for the spatial correlation related to the underlaying geological continuity.
- ② Compute the elastic and seismic response (predicted data $\mathbf{d}^p$) for each model in the initial ensemble using the full Zoeppritz equations.
- ③ Re-parameterize the predicted data using SVD (*Singular Value Decomposition*) and obtain a set of N_s singular values λ^p and singular vectors $\mathbf{u}^p$.
- ④ Apply the ES-MDA algorithm with Equation (3.10) and (3.11) in which the data $\mathbf{d}$ with the re-parameterized vector of singular vectors $\mathbf{u}$, to update the model parameters $\mathbf{m}$.

$$\mathbf{m}_j^u = \mathbf{m}_j^p + \mathbf{C}_{\mathbf{mu}}^p(\mathbf{C}_{\mathbf{uu}}^p + \mathbf{C}_{\mathbf{u}})^{-1}\left(\tilde{\mathbf{u}}_j - \mathbf{u}_j^p\right) \tag{5.1}$$

- Repeat steps from ② to ④.
- ⑤ After N iterations, generate the statistics (mean and covariance matrix) of the posterior distribution of model parameters $f_{m|d}(\mathbf{m}|\mathbf{d})$ conditioned by the seismic.

Before to apply the seismic inversion process, seismic information should be loaded and analyzed. In this case, a seismic crop was selected, which is a portion of a 3D seismic survey and is available in Perupetro database (bancodedatos.perupetro.com.pe).

Another necessary input in the workflow was the building of the LFMs (P-wave velocity, S-wave velocity, and density) using geostatistical techniques for this area based on both migration velocities and smoothed well log data following the low frequency trend of 0-8 Hz. The Figure 29 shows the LFM in time domain that was built in a specific time window between Upper Nia Fm. and Copacabana Fm. as top and bottom respectively. The coding workflow requires that pre-stack seismic volumes have the same geometry of the LFMs of P-wave velocity, S-wave velocity and density.

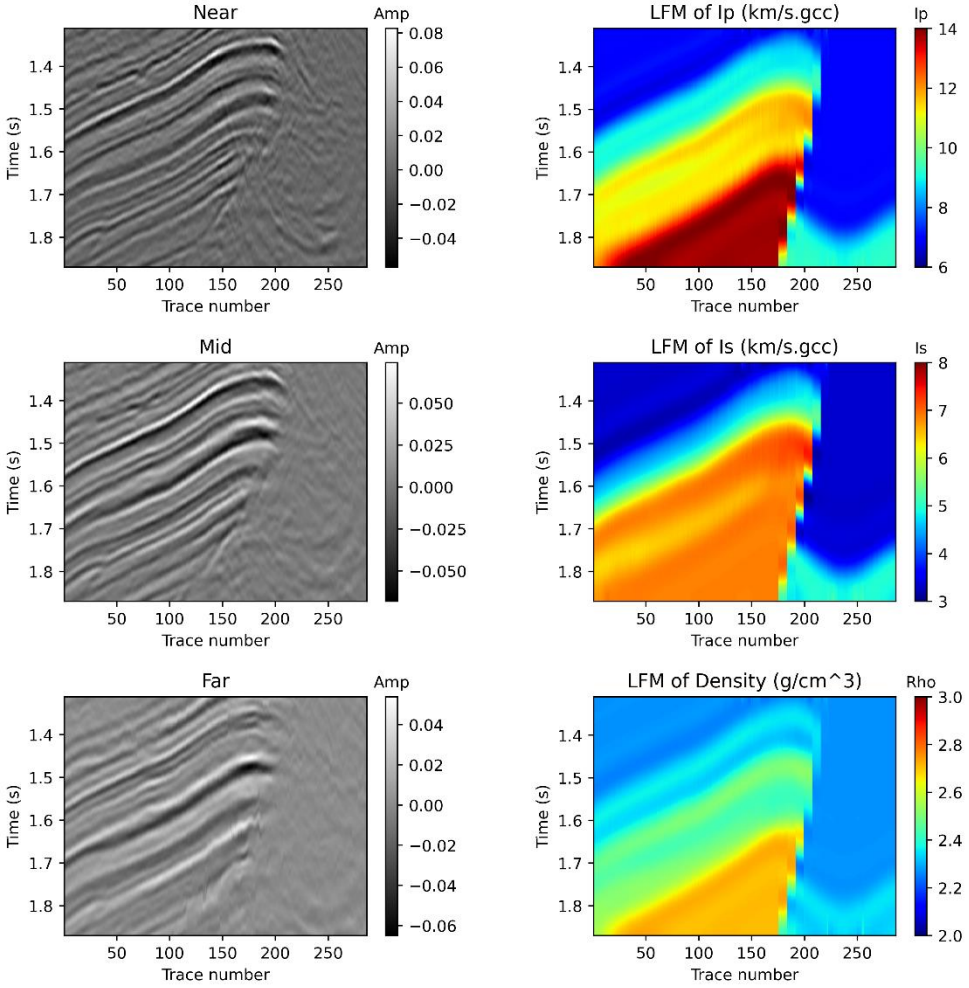

Figure 29 – Similar geometry of partial stacks and LFMs is required. The left part of the figure presents the input (*seismic partial angle stack*) of the seismic inversion, and the right part shows the low frequency models of (I_p, I_s, ρ) at inline 716.

Coupled with the average statistic wavelet from the Kinteroni wells, the information is enough to run iterations on all traces seismic. To be more specific, the whole workflow will be applied individually to each trace and then move on to the next trace. The process needs the generation of vertical spatial correlation based on Monte Carlo simulations (Dvorkin *et al*., 2014); (Fernandes & Lupinacci, 2021) to grab geology patterns. In these simulations, a premise is considered that samples that are close in time have better correlation. Thus, the tendency for samples far away from others is to become less correlated. All of the above provides the possibility to introduce a geological continuity premise to the simulations that are generated from random values.

In light of the foregoing, the workflow of the seismic inversion begins with the generation of 300 initial elastic models by stochastically sampling from the prior model space. will be aborded in following section, the initial ensemble number of models is 250, the retained singular values computed from the collocated seismic trace is 30, and the number of updating iterations is 4. Overall, stochastic prior models converge to the actual well logs and their means of the posterior ensembles shows a satisfactory agreement with corresponding elastic properties.

The associated model uncertainty can be quantified using the pointwise empirical variances calculated from the updated ensemble members. Compared to the synthetic case, the results show a larger variability in the posterior realizations; furthermore, it is noticed some inaccurate predictions of the elastic properties, fortunately in small portions of the reservoirs. Such inaccurate predictions are probably due to the limited resolution, low frequency (i.e. far angle stack) and low SNR of seismic data that do not allow to capture the local variability of elastic properties in thin layers, as well as erroneous values of density and sonic log data that does not match the real rock values, especially in the layer with high content of shale that produce washout intervals. (Liu & Grana, 2018); (Fernandes *et al*., 2024) present detailed studies where mathematical concepts were covered.

The results of the seismic inversion were P-Impedance, S-Impedance and Density, with P-impedance being the attribute with more accuracy and density the one with less accuracy. Also another volume that was generated as the result of the pre-stack inversion were V_p/V_s. At this stage of the study, we are ready to apply a Bayesian facies classification and explore relationships between inverted elastic volumes and seismic facies characterization inside the reservoirs.

5.4 Bayesian Facies Classification

The defined lithofacies in this study were based on information from well log and core data. The main reservoir zones (Upper Nia, Lower Nia and Noi-Ene) present two types of lithofacies sandstone and fine sandstone. Sandstone facies present good porosity values, followed by fine sandstones which are considered reservoirs with medium to low porosity values. The non-reservoir zones which overlie most of the reservoir facies are composed of shale facies with content of carbonate and anhydrate.

A preliminary Rock physics approach allow to correlate poroelastic parameters with facies. This analysis represented an important step in the reservoir characterization (Ødegaard & Avseth, 2004). The main objective is the use of the relation using well log data and then extrapolate that relationship using the seismic volume result from seismic inversion such Ip, Is, and density.

The analysis of compressional and shear logs, which are derived from sonic logs is a fairly routine to get a clue of trend lines related to specific facies such sandstone and shale. Generally, trends of V_p and V_s are well defined because factors such as porosity, pore shape and pressure tend to affect V_p and V_s similarly (Castagna *et al*., 2014).

Figure 30 shows acoustic-log V_p and V_s measurements of the three wells included in the study (K2, K1 and K3) from Upper Nia and Copacabana formation top, which is the reservoirs target colored by a type of facies. The dash line separates into two zones the behavior of the measurements, above the line related to sandstones facies and the bellow the line mostly related to shale, carbonate, and anhydrite facies. As a first glance, the Crossplot indicates that both curves can be used to predict at least two groups of facies.

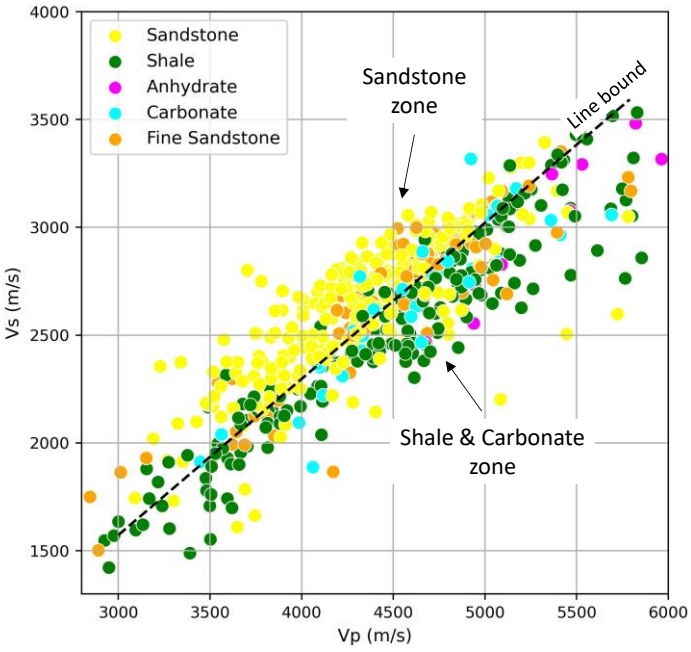

Figure 30 – Crossplot of Acoustic-log measurements of V_p and V_s of the K2, K1 and K3 wells colored by specific facies interpretation.

Another valuable tool for both QC and interpretation purposes of well log data ,and in order to assess seismic detectability is the use of the Crossplot between acoustic impedance I_p and V_p/V_s ratio (Ødegaard & Avseth, 2004), the Figure 31 shows these curve colour coded based on the five populations defined in the Crossplot domain. A noticeable behavior in the scatter data is the possibility to add a line bound which separates the sandstones zone from the shale & carbonate zone. Additionally, an anhydrate zone constitutes a small and clearly separate cluster in the high Ip.

AI and V_p/V_s estimates are among the typical outputs from elastic inversion of seismic data, and this is the main reason for presenting this analysis to evaluate the affordability to classify facies from seismic data, more specifically elastic inversion results.

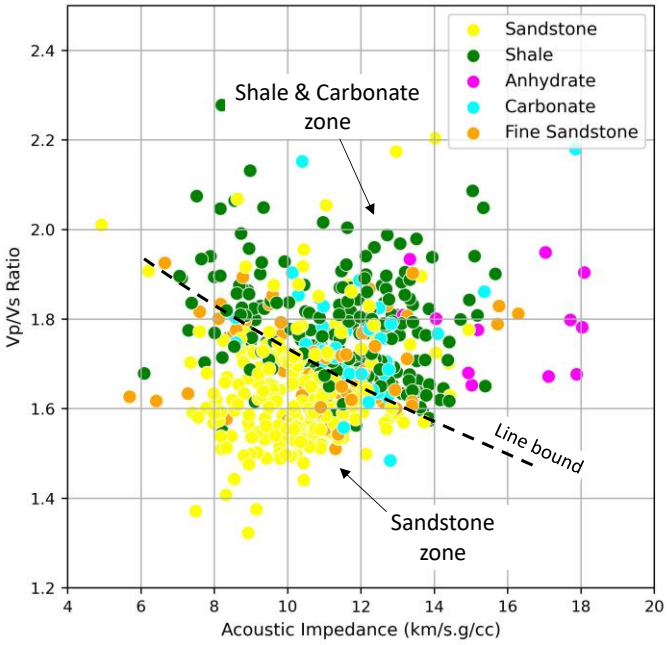

Figure 31 – Crossplot of Acoustic-log measurements of I_p and V_p/V_s for the three wells in the study (K2, K1 and K3) colour-coded by specific facies interpretation.

The probability density functions (PDFs) related to each facies were built at the beginning using a Gaussian approach and then improved by the use of Kernel approach to borehole log data upscale to seismic sample resolution (two millisecond). Additionally, Kernel bandwidth was defined using the Scott's rule (Scott, 2014). The Figure 32 shows the PDFs of V_p/V_s ratio using density Kernel estimation where different degree of overlain

between lithofacies can be observed. Nevertheless, a kind of two population reservoir and non-reservoir related to sandstone and shale respectively can be identified.

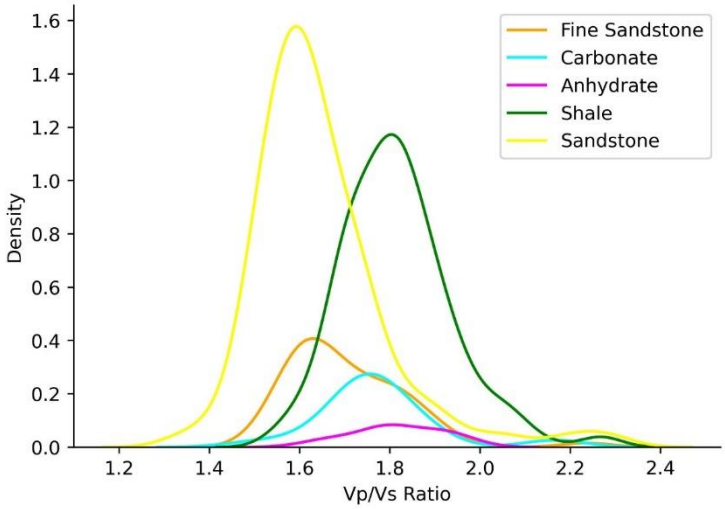

Figure 32 – Probability density functions (PDFs) of V_p/V_s ratio using density Kernel estimation for lithofacies from Upper Nia to Copacabana formation

In the case of acoustic impedance (I_p) the PDFs show three different groups related to a specific range of I_p. In the Figure 33 can be identified a much bigger population of sandstone facies that overlies a small portion of fine sandstone. Also, carbonate and fine sandstone seems to be overlaid with the same density population.

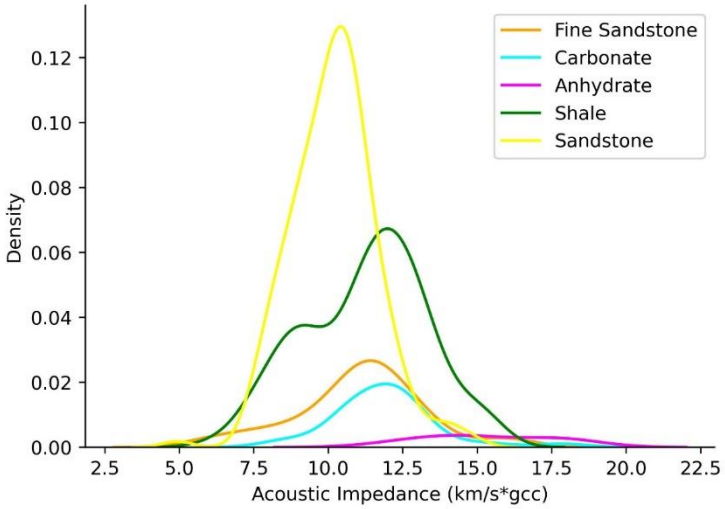

Figure 33 – Probability density functions (PDFs) of acoustic impedance (I_p) using density Kernel estimation for lithofacies from Upper Nia to Copacabana formation.

Bayes's theorem is a fundamental concept in probability theory and statistics, the posteriori distribution depends upon the priori probability of facies occurrence. A common practice is to assign the same probability of chance for each individual facies group. Thus, the posterior distribution will be defined by the PDFs.

The first attempt at least with well-log data demonstrated the possibility to characterize reservoir and non-reservoir, the strategy to merge all lithofacies into two groups is supported by the possibility to be predicted using Baye's theorem according to the aforementioned crossplot analysis in Figure 30, Figure 31, Figure 32 and Figure 33.

The analysis concludes that both facies group, such as reservoir a non-reservoir can be separated using both elastic properties I_p and V_p/V_s ratio, Figure 34. Moreover, the PDFs for both facies groups using the elastic properties seem to be separated from each other and also follows the line bound previously discussed.

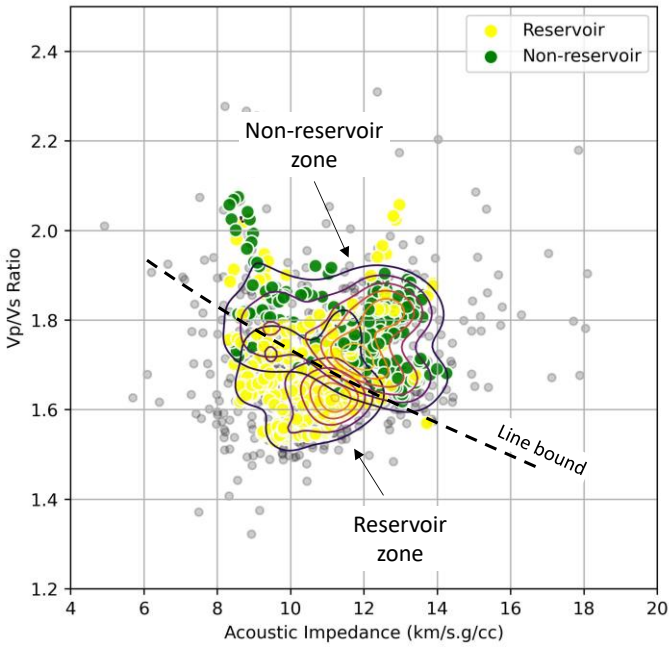

Figure 34 – Crossplot of Acoustic-log measurements of I_p and V_p/V_s for Kinteroni wells colour-coded by reservoir and non-reservoir facies interpretation, and the PDFs considering both variables.

A visual result of the Bayesian facies classification in the K1 is shown in Figure 35, the reservoir and non-reservoir facies are well predicted. The prediction supports the

possibility to obtain a framework of reservoir and non-reservoir zone which is also well defined using only seismic amplitude interpretation due to seismic amplitude quality.

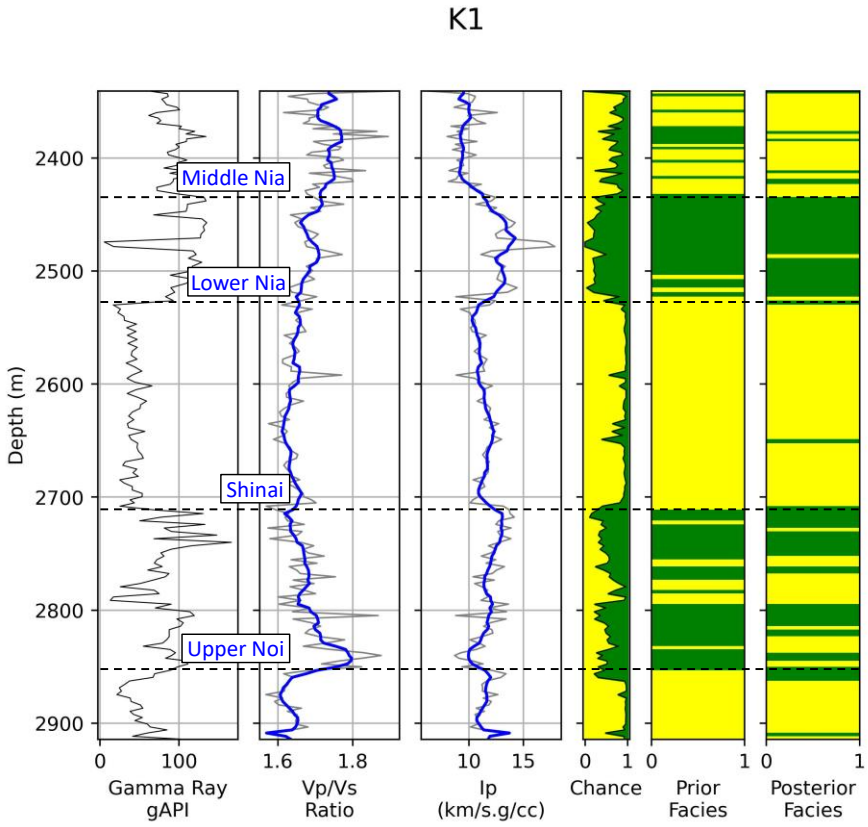

Figure 35 – Bayesian facies classification of K1 well using upscale Ip and Vp/Vs shows excellent results in the posterior facies.

Overall, Bayesian facies classification presents excellent results validated by the confusion matrix values in the three wells. According to the confusion matrix, the reservoir facies obtain 0.86 of true positive which means 14% of facies reservoir were incorrected predicted. On the other hand, the non-reservoir facies get 0.80 of true negative which means 20% of non-reservoir were incorrected predicted.

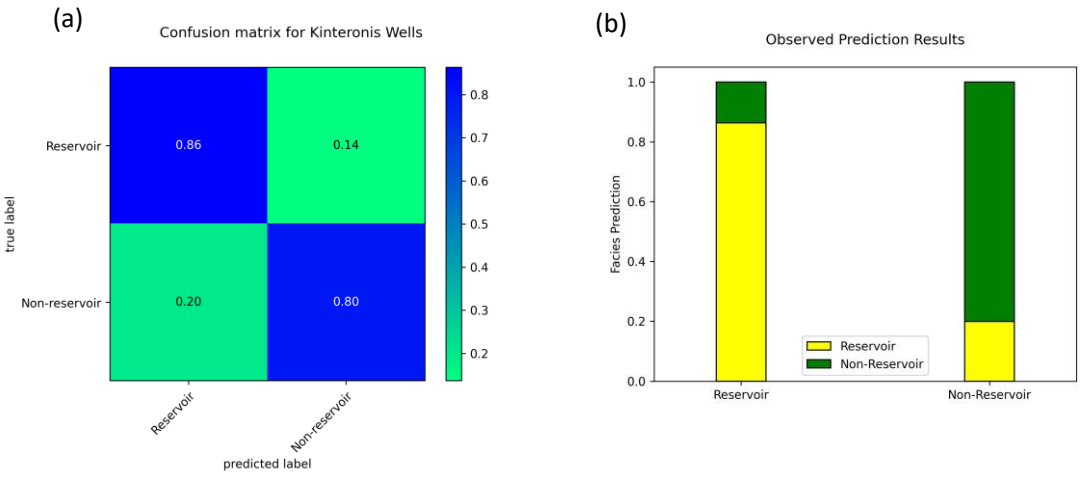

Figure 36 – The graphic shows (a) Confusion matrix of the result in the three wells of Kinteroni, (b) observed predictions results.

Despite the previous excellent results, the prediction of reservoir from non-reservoir facies could also be related to a geological framework. For instance, more than 95% of content in Lower Nia could be considered reservoir facies, which means if the geology framework were accurately defined as it is, it would be easy to say that at least 95% could be related to reservoir facies. A more challenging task and innovative will be the possibility to characterize at least in the two facies (sandstone and fine sandstone) the reservoir facies which be restricted to the Upper Nia, Lower Nia, and Noi-Ene zones. Figure 37 shows the crossplot of acoustic-log measurements of I_p and V_p/V_s for the three wells in the Kinteroni area (K1, K2 and K3) considering only data from the reservoir zones. Data points are colour-coded by reservoir facies (sandstone and fine sandstone), grey color represents data outside the upscale process. The resulting PDFs will be used to predict these two group of facies in the reservoir intervals using the seismic inversion outputs.

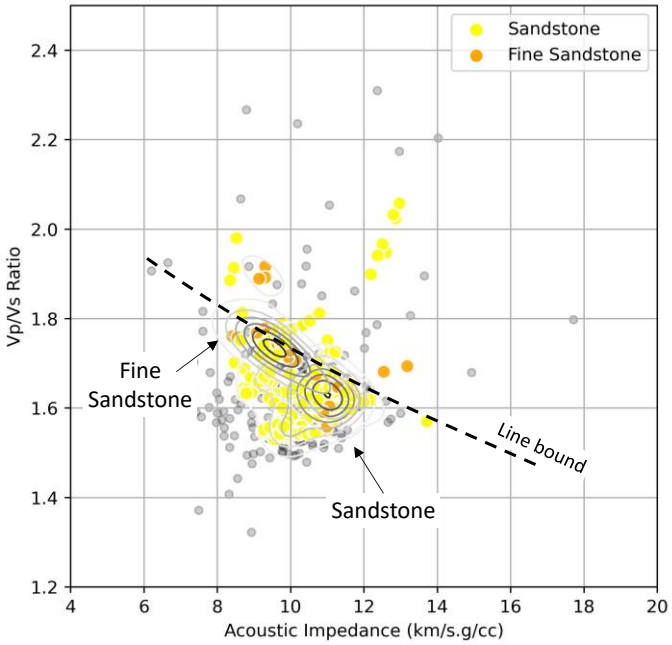

Figure 37 – Crossplot of acoustic-log measurements of I_p and V_p/V_s for Kinteroni wells colour-coded by reservoir facies (sandstone and fine sandstone), and the PDFs considering both variables, grey points represents well-log data outside the upscale process.

6 RESULT AND DISCUSSION

The whole workflow gives different kinds of outputs and results that will be described in this section. Figure 38 shows the seismic crop, wells localization, and seismic lines. In order to explain the geological and structural complex of the area an arbitrary seismic line 1 along the three wells in Kinteroni field (K2, K1 and K3) from west to east are presented. However, the focus area in this study is a seismic crop (blue polygon) that contains the K1, K2 and K3 wells. Inside the seismic crop, two arbitrary seismic limes and a crossline along their well surveys are presented as well.

The objective of the selection of these seismic limes is to show variability of rock properties using the seismic inversion results combined with a Bayesian facies classification approach.

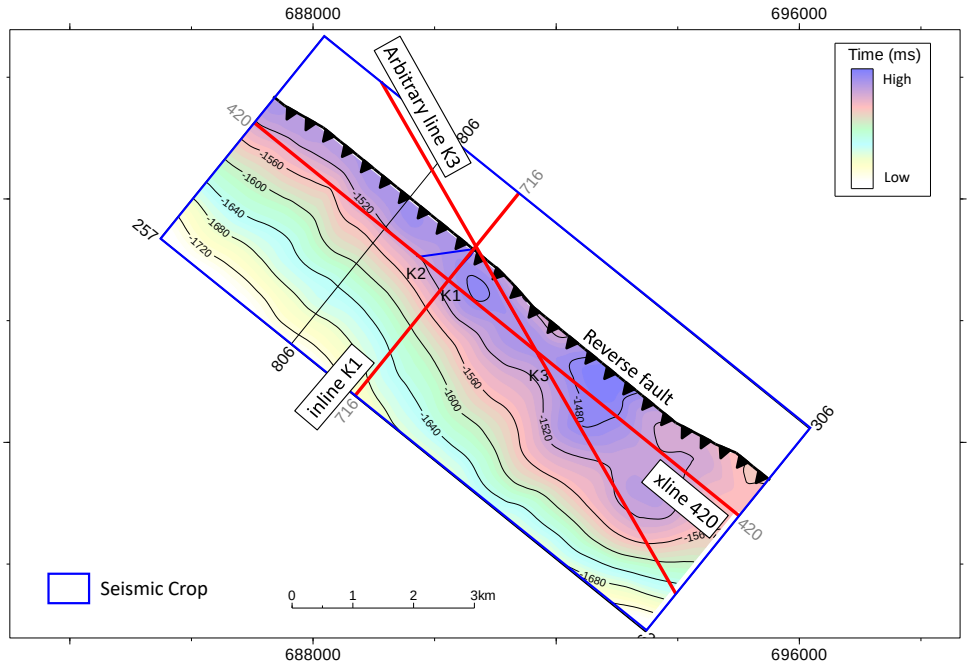

Figure 38 – Show the seismic crop where is possible to observe the highest part of the anticline and the seismic lines (red lines) to analyze the stochastic seismic inversion and the Bayesian facies classification results.

6.1 Quantitative Validation of Stochastic Inversion

6.1.1 Correlation Coefficient of Wells – Synthetic case

At the beginning of study, a preliminary 1D approach was done to demonstrate its feasibility using the set of wells from K2 well. Moreover, where both deterministic and stochastic seismic inversion were done to analyze its results and evaluate its advantage.

This real case contains several layers of clastic reservoir separated by zones of clay. The clastic reservoirs are filled with gas with a low percentage of water saturation and a high porosity brine layer in the base. The other important information is shown in the left part of Figure 39 where an overlain of seismic partial-stacked extracted from near, middle, and far corresponding to three different range of incident angles: 12°, 24° and 36° respectively at [inline 716; trace 150] position. On the right part, the middle partial-stacked traces of inline 716 is presented where a peak and trough is represented by blue and red color respectively.

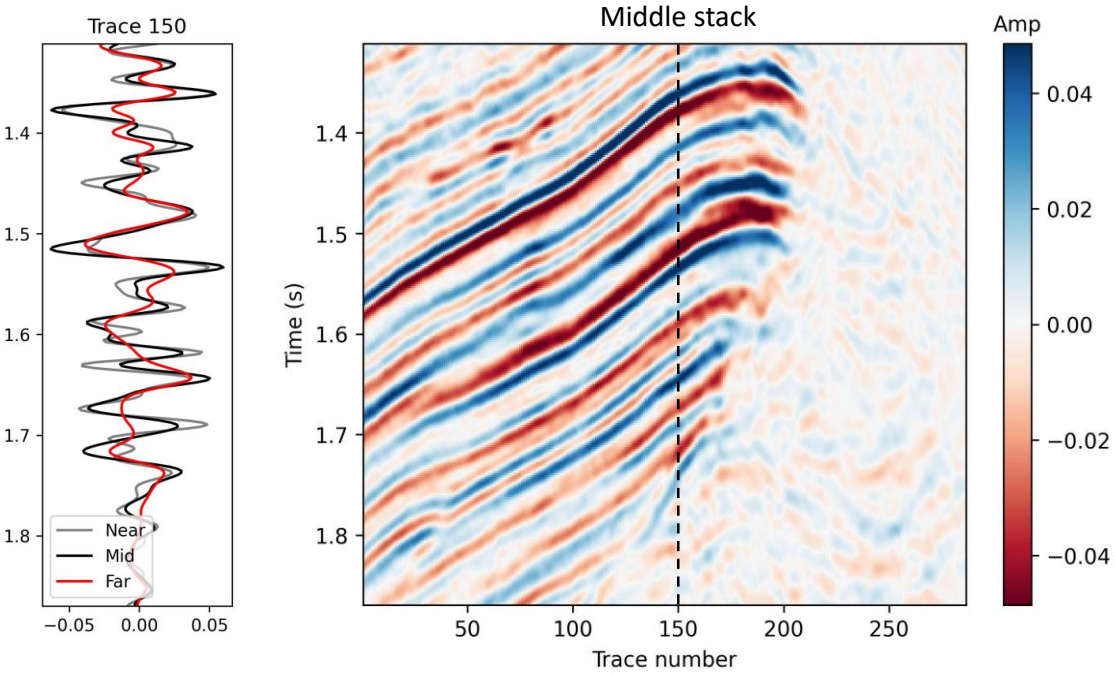

Figure 39 – In the left part, an overlain of seismic partial-stacked extracted of near, middle, and far trace with incident angles of 12°, 24° and 36° respectively at [inline 716; trace 150] position, and in the right part the middle partial-stacked traces of the inline 716.

The numbers of initial models of P-wave velocity, S-wave velocity and density generated were 300. Those prior models were stochastically sampling from prior model space, which represent the initial ensemble in the workflow. To grab the geological behavior of the underlaying continuity of the area, a vertical correlation of the model parameters was included. In the study, an exponential variogram was selected with a correlation range of 30 meters. The set of initial models is presented in the Figure 40 and it is clear that the model values cover the entire model space.

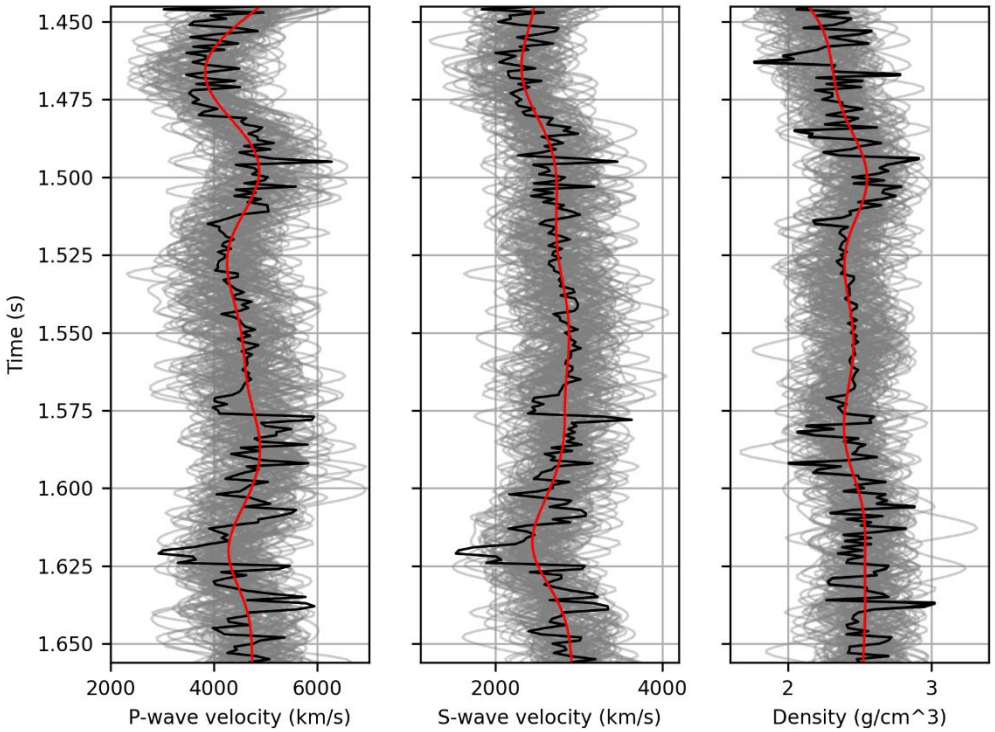

Figure 40 – Prior elastic models, from left to right: P-wave velocity, S-wave velocity, and Density (black curve represent the actual well log data, grey curves represent 200 prior models, red curves present the mean of the prior models)

For each prior ensemble model of the elastic curves the full Zoeppritz equation is used to associate reflectivity coefficients and generate the corresponding synthetic seismic trace by convolving the wavelets and the reflection coefficients. Continuing with the workflow, a re-parameterization of the measured and predicted seismic data into lower dimension space by using SVD is applied to improve the computational time consuming. Then the ES-MDA algorithm is applied to the reduced data space to iteratively update the

prior poroelastic models. In this specific case the algorithm only needs to assimilate the data 4 times to get a reasonable match. The model of elastic properties is updated in the domain (-∞, +∞), the Figure 41 shows a reasonably good match between measurements and posterior result.

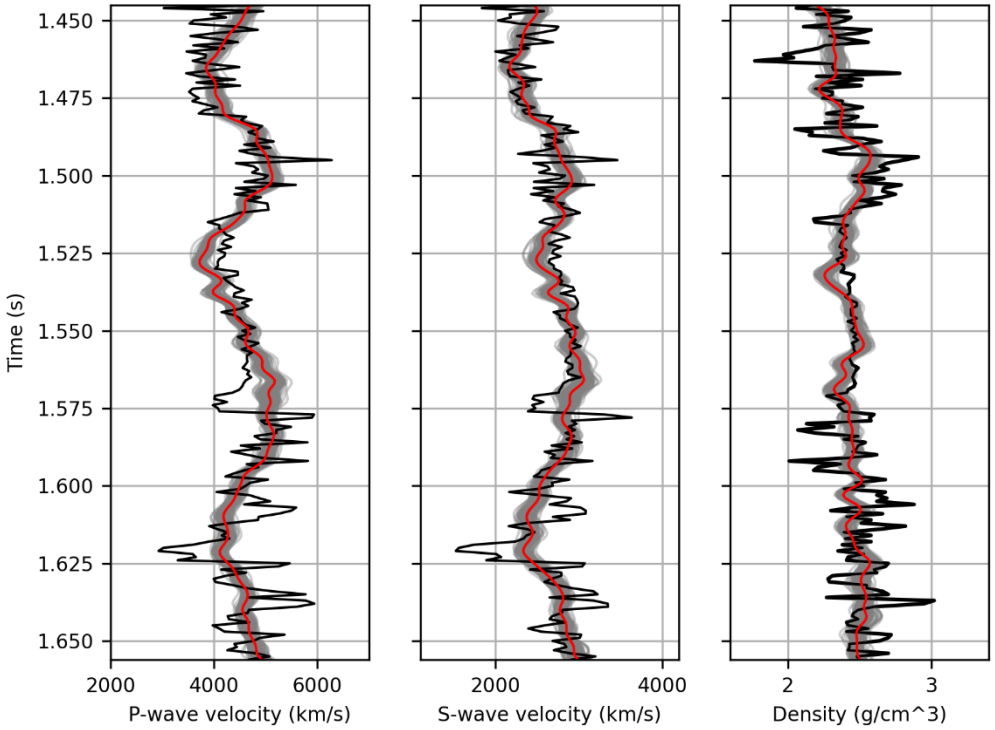

Figure 41 – Posterior elastic models, from left to right: P-wave velocity, S-wave velocity, and Density (black curve represent the actual well log data, grey curves represent 200 prior models, red curves present the mean of the posterior models)

There are several ways to measure the accuracy of a seismic inversion, linear correlation and room mean square error (RMSE) of the true model. In this case Pearson correlation coefficient (r) estimation was used to validate the uncertainty quantification in the posterior Table 1.

Pearson correlation (r)		
Well	Stochastic	Deterministic
K1	0.76	0.69
K2	0.7	0.68
K3	0.57	0.48

Table 1 – Shows the comparison between the two performed seismic inversion (Stochastic and Deterministic) using the upscaled well-log (time domain) of K1, K2 and K3 wells.

The ES-MDA parameters choices and SVD method have direct implications in the seismic inversion result. For instance, the alternative proposed inversion depends on the number of iterations N, the number of truncated singular values Ns, and the number of ensemble members Ne. In this particular study, N was selected to be 4 after due to N>4 shows an improvement in the RMSE but a substantial decrease in the coverage ratio.

After several testing, 30 singular values were retained due to higher values does not impact the seismic inversion. Therefore, for lower values of singular values, the RMSE increases and the correlation decreases. In general, the larger the number of Ne, both the number of models and the computational cost increases. For this reason, after some testing (Ne = 200, 250 and 300) Ne equal to 250 was selected as a favorable choice.

The study also compares the ES-MDA to the standard Bayesian linearized AVO inversion which is a well-known seismic inversion technique proposed by (Buland & Omre, 2003). This comparison uses the same well log dataset and seismic data from the three angle stacks: near, middle, and far stack with incident angles of 12°, 24° and 36° respectively. The inversion results by applying the ES-MDA nonlinear inversion (Figure 41) measured against to the Bayesian linearized AVO inversion (Figure 42) seen to recover better the true well logs, implying a better accuracy of our proposed method. A better result with the proposed method using ES-MDA is supported by the nonlinearity of seismic forward models for large acquisition angles. Certainly, linearization of the reflectivity coefficient expression is generally accurate for small angles, but inaccurate for large angles where the exact model becomes nonlinear (Liu & Grana, 2018).

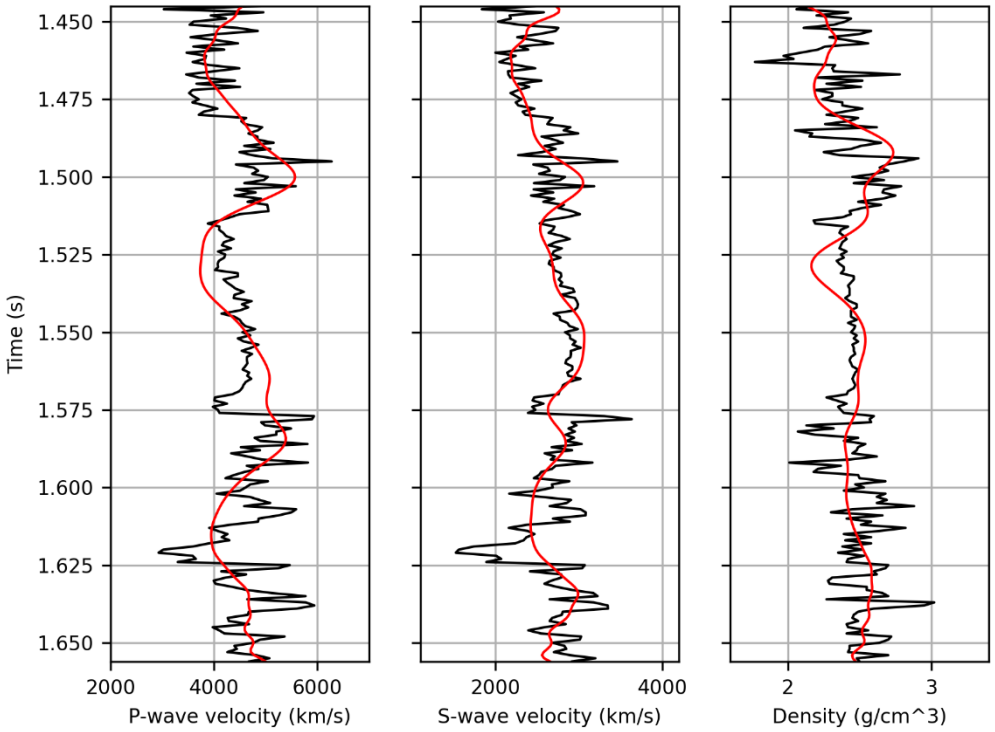

Figure 42 – Standard Bayesian linearized AVO inversion result, from left to right: P-wave velocity, S-wave velocity, and Density (black curve represent the actual well log data, red curves present the mean of the posterior models)

An acceptable way to make a quantitative correlation was through the Pearson correlation coefficient using the upscale acoustic impedance of wells compared with the seismic inversion results. Wells inside the crop have acceptable values of the Pearson correlation coefficient (r), K3 has the lowest values due mainly to the nearly position to a fault reverse plane which reduces the signal of seismic reflections. Thus, by comparing the inversion results, the proposed inversion method using the ES-MDA algorithm recovers in better way the true well logs, indicating a better accuracy of our proposed method, Figure 43.

In the study, one of main factors that improve the seismic inversion results according to the validation method was the conditioned log data used in the seismic well-tie. On the other hand, a reduction in the coefficient of correlation is closely linked to the chosen seismic inversion parameters and maybe erroneous well log data for wellbore condition.

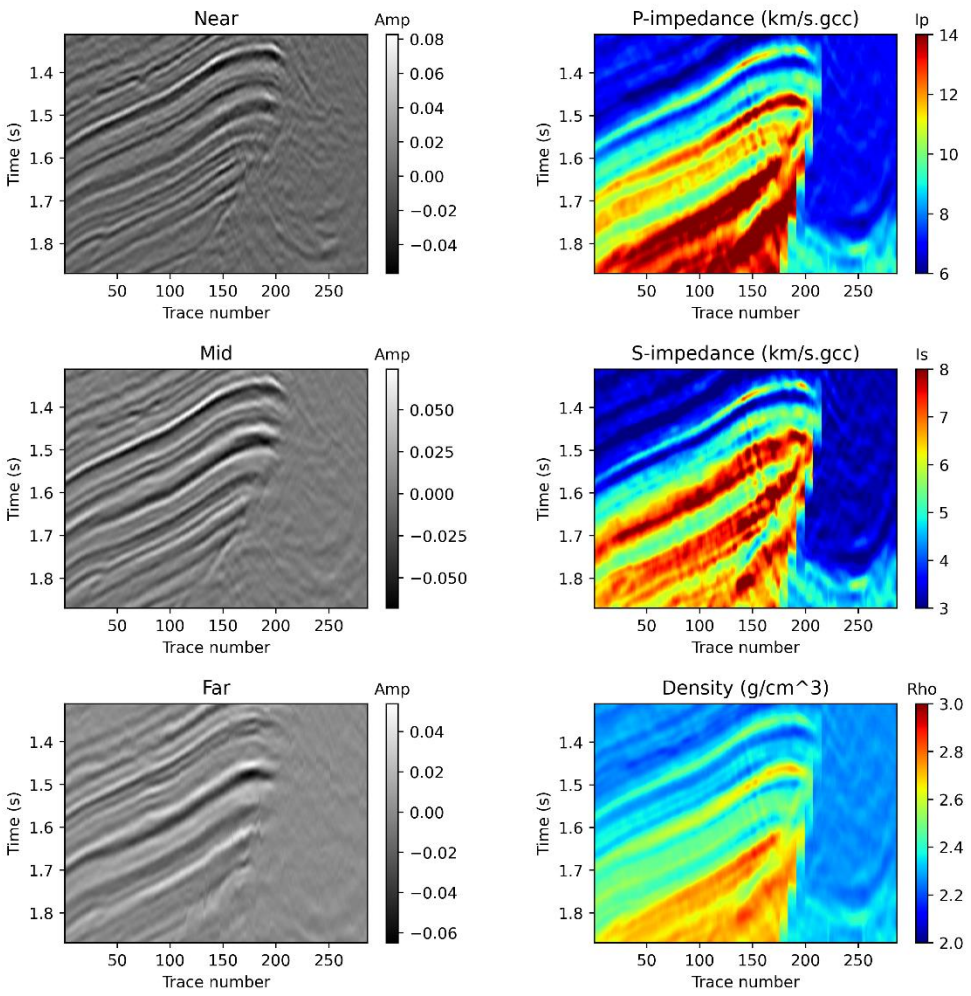

Figure 43 – The left part of the figure presents the input (*seismic partial angle stack*) of the seismic inversion, and the right part shows the outputs (I_p, I_s, ρ) of the seismic inversion of the inline 716.

6.1.2 ES-MDA Parameters

6.2 Reservoir Characterization

The study focuses on four main zones the Upper Nia, Lower Nia, Noi and Ene formation, which are the main reservoirs in terms of gas accumulation. For this reason, facies in those reservoirs should be accurately mapped. The Ene Formation, stratigraphically above Copacabana formation is considered as a fluvial environment due to its genesis, the contact between them is a well-known discordance in the region (Peña *et al.*, 2018).

Above Ene formation is deposited Noi formation, which could be divided into two stages of Aeolian system. The Lower Noi in a wet regime and the Upper Noi in a dry regime, both have considerable good reservoir properties to store gas. Above Lower Noi is founded the Shinai formation, which is considered as a regional seal, sediments are deposited in a marine context. Finally, the Lower Nia formation which is the most important reservoir in terms of volume is deposited above the Shinai formation, most of sediments in Lower Nia is considering developed in an Aeolian system.

The seismic crop used in the study were extracted in the highest part of a structure named Kinteroni-Sagari (Luque & Huamán, 2016), Figure 44. The anticline Kinteroni-Sagari is a complex thin-skinned structure. The structure is part of a giant thrust wedge, hanging-wall anticlines (McClay *et al*., 2018b).

In the area of the seismic crop, three directional wells were drilled. In order to evaluate the availability and benefits of the stochastic seismic inversion coupled with Bayesian facies classification to characterize the reservoirs in the area three seismic lines were analyzed, two of them cut the anticline (inline K1 and arbitrary line K3) and one of them is along the axis of the anticline parallel to the reverse fault (seismic xline 420).

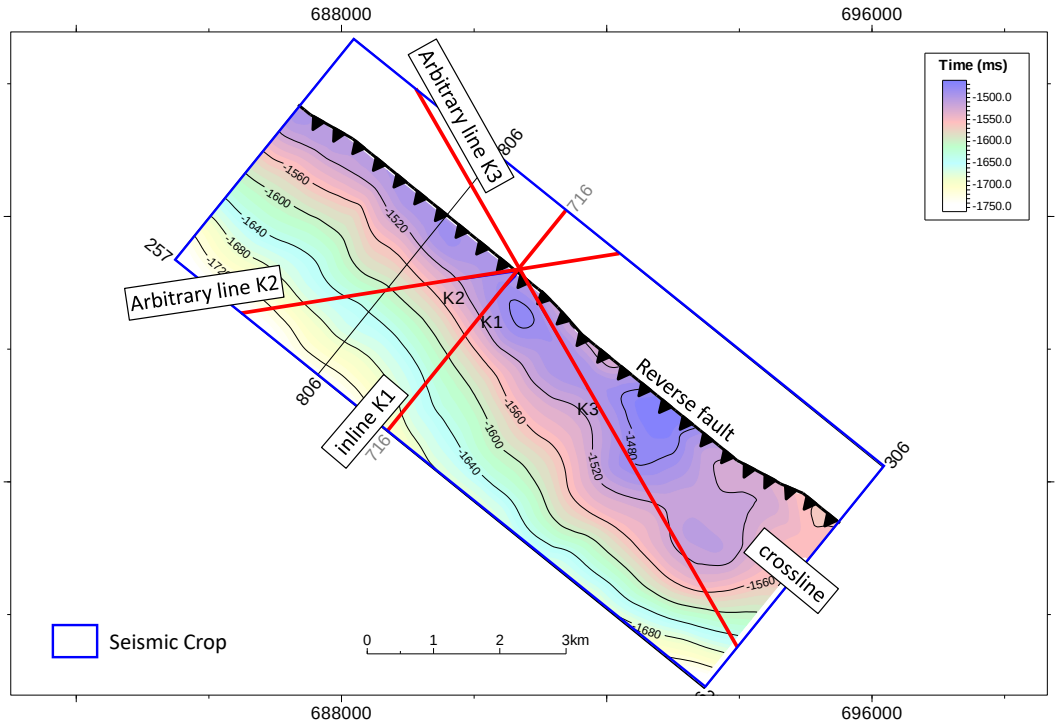

Figure 44 – Location of the seismic crop where is possible to observe the highest part of the anticline and the seismic lines (red lines) to analyze the stochastic seismic inversion and the Bayesian facies classification results.

The analysis in these sections allow us to understand the facies occurrence far away the wellbore and between them. Moreover, results in this study could guide and currently update facies propagation using only geostatistical methods.

6.2.1 Seismic xline 420

This interpreted seismic crossline 420 includes the K2, K1, and K3 wells, Figure 45. The interpreted crossline 420 (NE-SW direction) is ubicated in the east part of the main anticline structure called Sagari-Kinteroni (Venturo & Huamán, 2013). The seismic amplitudes are represented by a range of colors from bright red to bright blue, where the peak is colored in bright blue and the trough is colored in bright red. Furthermore, the seismic image of the hanging wall structure (Kinteroni) shows good quality of signal, and the amplitude seems to be balanced across the wells.

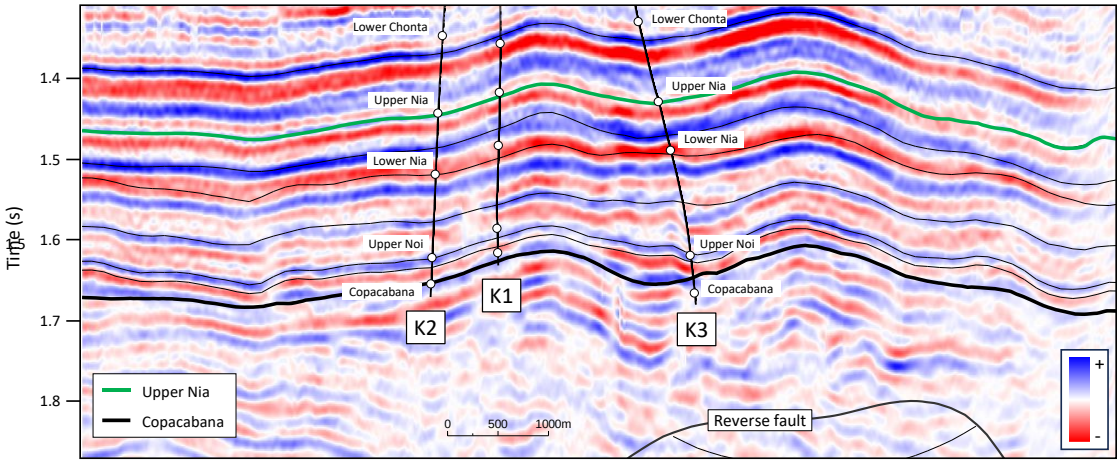

Figure 45 – Seismic inline 420 of the near stack [0-12°] shows the seismic horizons interpretation, the target zone between Upper Nia (green line) and Copacabana (black line), the position of the three Kinteroni wells, and also an excellent signal-noise ratio represented by the visual seismic quality.

In the seismic interpretation is observed that the structure is in the hanging wall of an important reverse fault. This structure could be considered the east part of a unique large anticline (Sagari-Kinteroni) and its morphology is a little wavy due to the presence of small faults and pre-existing dune deposition in the Lower Noi formation (Grosso *et*

al., 2017). The aeolian dunes in the Lower Noi formation are the most notorious geomorphology seismic expression in the area.

The seismic inversion results of the crossline 420 is shown in the Figure 46. An important layer of quality control is the anhydrate above the main reservoir of Lower Nia. The presence of this evaporite level is widely known and the values of the acoustic impedance are relatively high (values from 12000 to 13000 ($m/s * gcc$), it is marked in the upper right part of Figure 46.

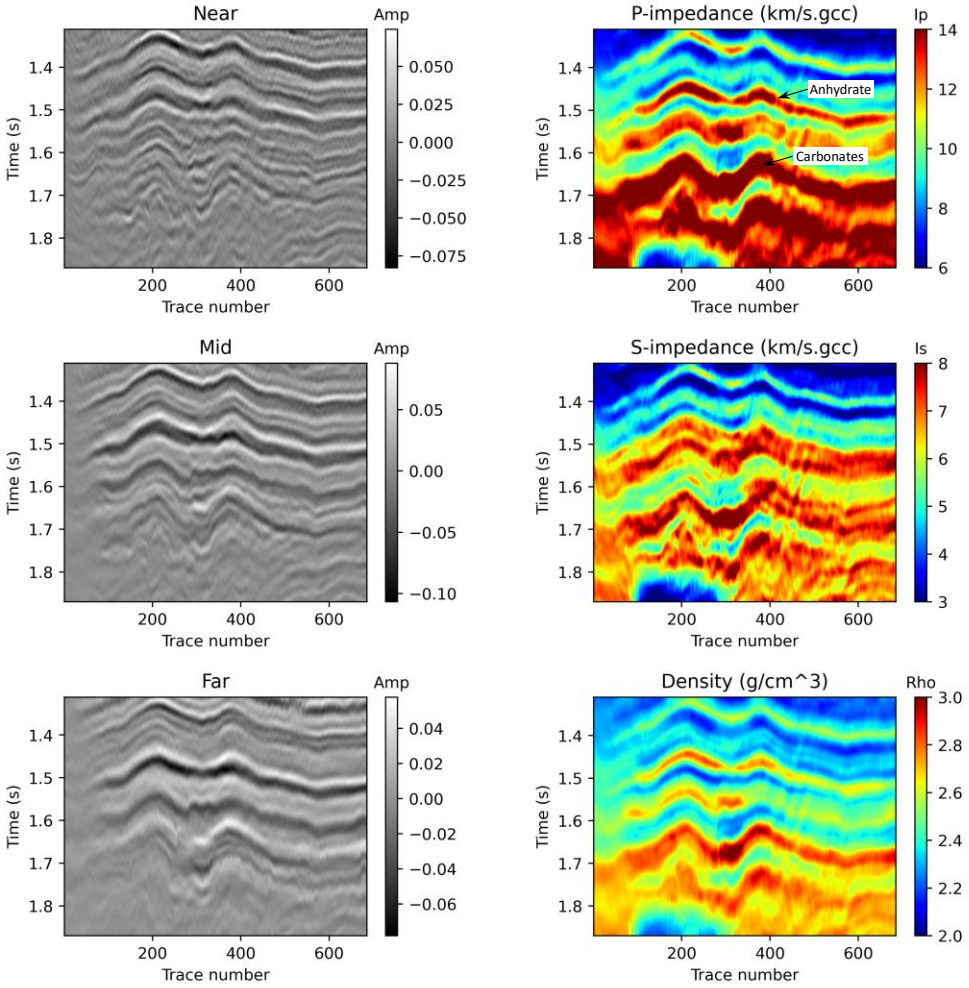

Figure 46 – The left part of the figure presents the input of the seismic inversion, and the right part shows the output of the seismic inversion of the crossline 420.

The facies variations inside the reservoirs are difficult to predict considering only seismic amplitude information. However, the acoustic impedance I_p coupled with the

V_p/V_s ratio and Bayesian classification could map these facies heterogeneity. Runing the Bayesian facies classification using the seismic inversion results in the crossline 420 identified different kind of accommodation in the three main reservoirs zone (Upper Nia, Lower Nia, and Noi-Ene) Figure 47.

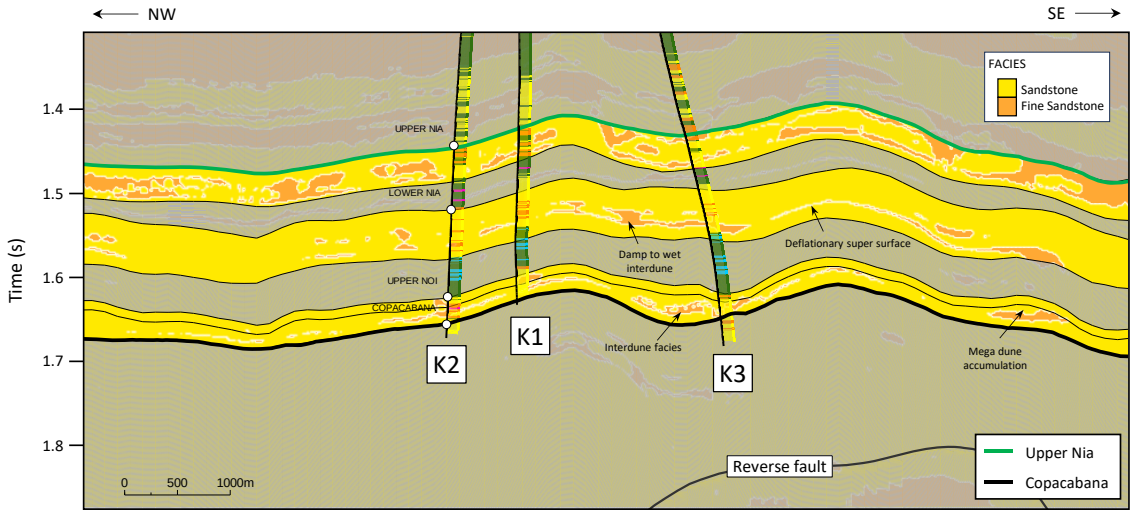

Figure 47 – Bayesian facies classification applied to seismic inline 420 using the elastic seismic inversion results of I_p and V_p/V_s.

The seismic Bayesian facies classification applied to seismic crossline 420 shows interesting results. For example, the left part of well K3 in the Noi-Ene interval, it is possible to observe a level of fine-sandstone facies which could be linked to interdune deposits. Above this level, the present of sandstone facies is related to aeolian climbing mega dune.

In the case of Lower Nia interval, the architecture of the aeolian seems to be temporally and spatially variable (dynamic) systems. The aeolian succession of Lower Nia is very similar to Permian Cedar Mesa Sandstone outcrop of about 120 meters thickness in White Cayon, Utah (Mountney, 2006). The aeolian succession of Lower Nia is not just one continuous episode of accumulation but rather it is punctuated. Thus, the thickness of Lower Nia formation is composed of repeated aeolian accommodation sequences in a sequence stratigraphy context that are each separated by major horizontal bounding surfaces that represent super surfaces, so planation surfaces where the dune field was curtailed and planed off before the next sequence accumulated later on Figure 48.

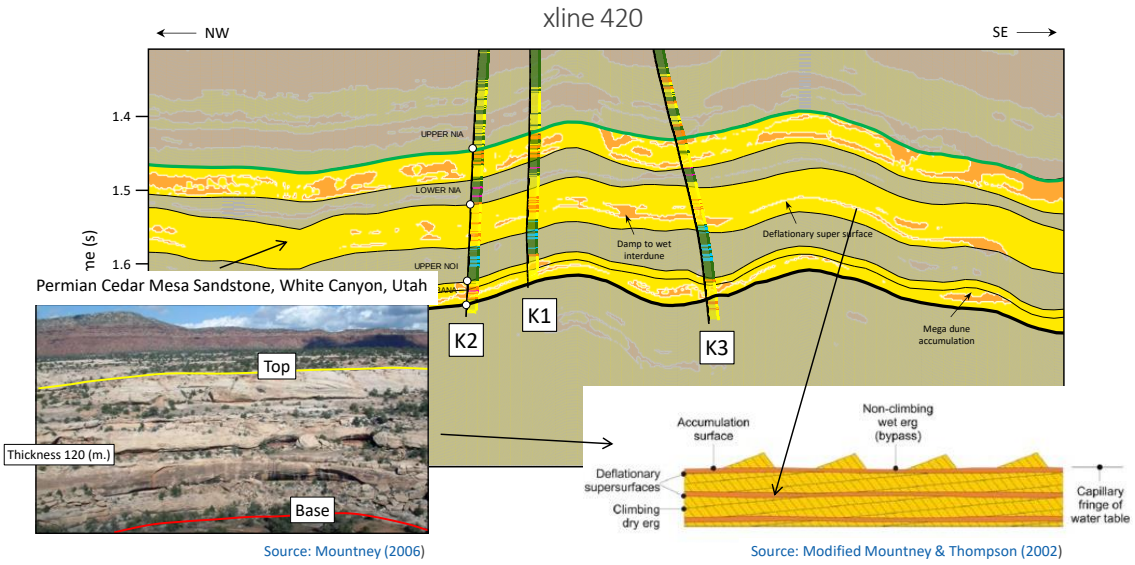

Figure 48 – Bayesian facies classification geological interpretation in Lower Nia using the elastic seismic inversion results of I_p and V_p/V_s.

The well-log and core data from Kinteroni wells identified a middle section with a more heterogenous pattern showing intercalations between small dunes and damp to wet interdune facies. Thus, the deflationary super surface could be interpreted at the presence of fine sandstones facies and bound aeolian sequences where fine sandstone facies presents a decrement in the rock property quality compare to sandstone facies related to aeolian dune and sand-sheets (parallel-laminated sandstones) probably with less influence of water table in the system (Kocurek & Nielson, 1986).

6.2.2 Arbitrary seismic line K3

This seismic line is along the well path of K3 and shows an excellent signal-noise ratio with continuity of reflectors in the reservoir window of interest between the Upper Nia and Copacabana formation.

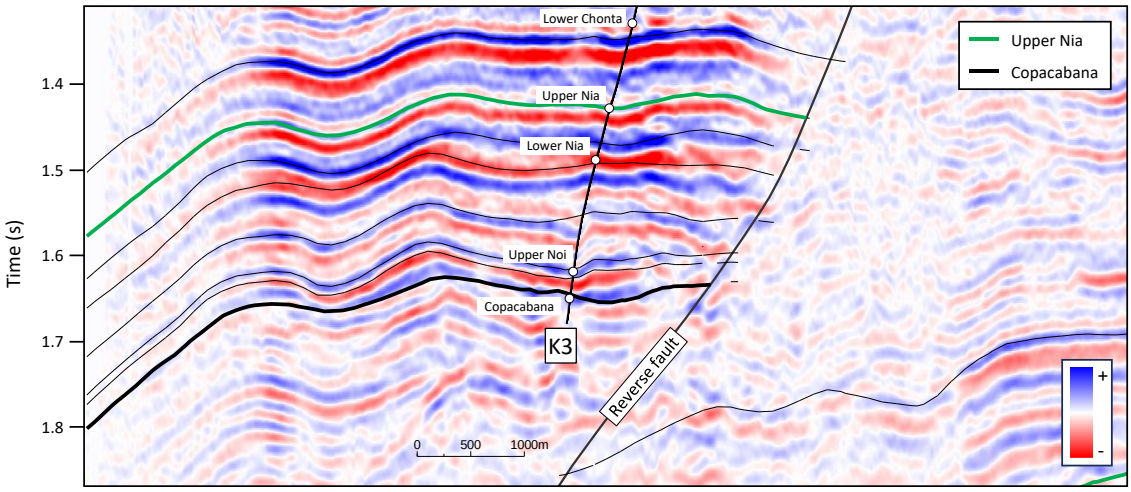

Figure 49 – Seismic Line along the survey of the K3 shows excellent signal-noise ratio, where peak and trough are represented by white and black respectively.

The seismic inversion volumes (I_p, I_s and $Density$) of the arbitrary seismic line K3 is shown in the. The geology framework in the area has two important layers of quality control. First, the anhydrate above Lower Nia formation which represents an well-known evaporite level with high values of the acoustic impedance (values from 12000 to 13000 ($m/s * gcc$), it is marked in the upper right part of Figure 50. The second layer is the Copacabana formation which is below the Noi-Ene zone, the P-impedance inversion result match so well with the high values from 12500 - 14000 ($m/s * gcc$) related to carbonates rocks of this formation.

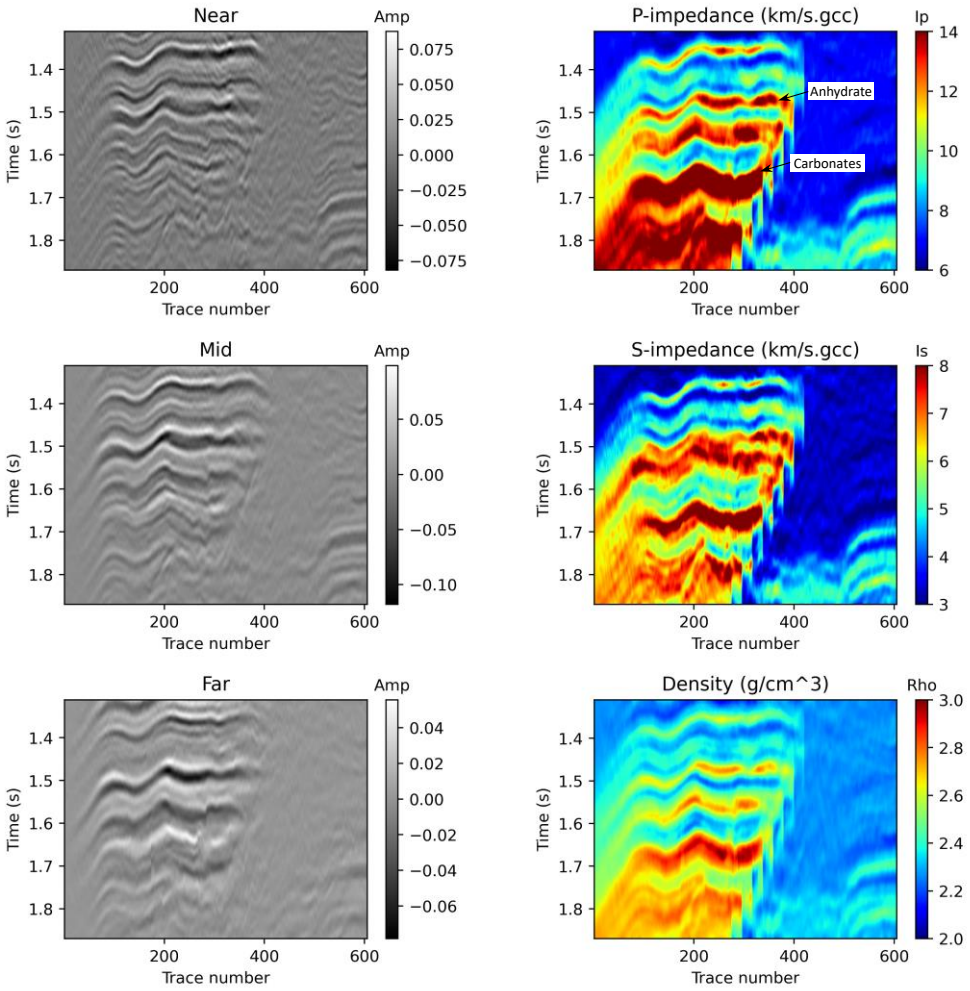

Figure 50 – The left part of the figure presents the input of the seismic inversion, and the right part shows the output of the seismic inversion of the arbitrary seismic line K3.

The seismic Bayesian facies classification applied to the arbitrary seismic line K3 shows prominent and valuable information. For instance, in the Noi-Ene zone is possible to observe that fine sandstone facies could be associated with deposits of damp interdune which occur where the water-table is close to the interdune surface (Bristow & Moutney, 2013), immediately above, the present of sandstone facies could be related to aeolian climbing and aggrading dunes or sandsheet deposits Figure 51.

In the case of Lower Nia interval, fine sandstone facies are found in an intermedia level. In most wells at this middle section shows intercalations between small dunes and

damp to wet interdune facies. Thus, a deflationary super surface could be pointed at the presence of fine sandstones facies and bound aeolian sequences.

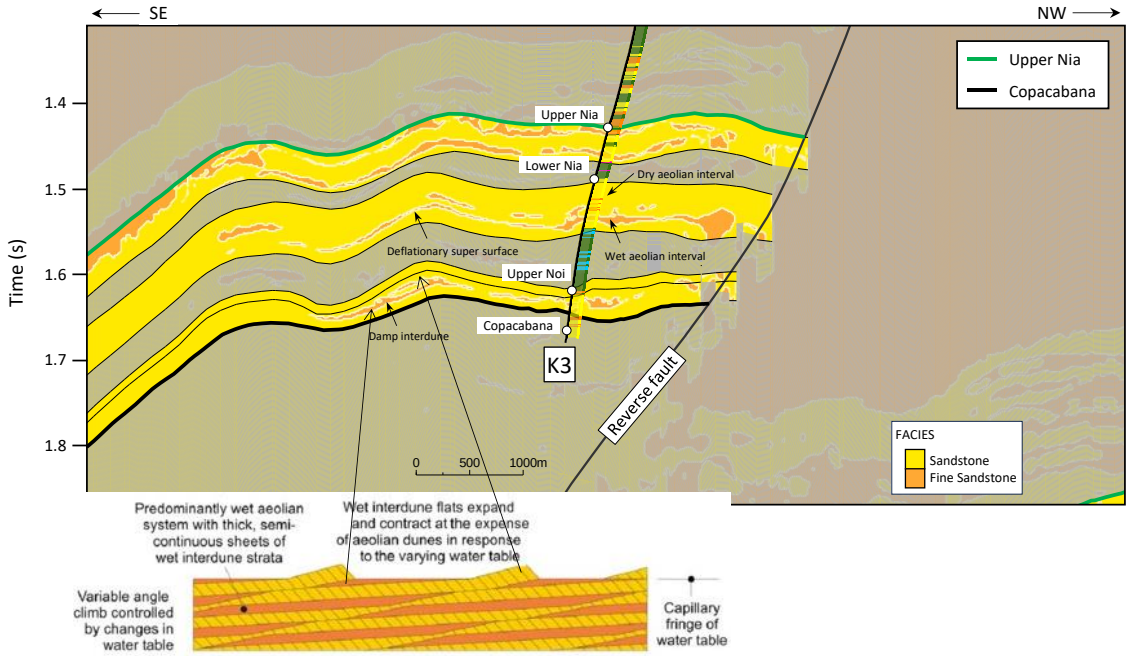

Source: Modified Mountney & Thompson (2002)

Figure 51 – Bayesian facies classification applied to arbitrary seismic line K3 using the elastic seismic inversion results of I_p and V_p/V_s.

6.2.3 Seismic inline K1

This seismic line is along the survey of well K1, the seismic line corresponds to the inline 167 in the seismic survey. Figure 52 shows the near stack [0-12°] which presents an excellent signal-noise ratio and continuity of the reflector in the reservoir window of interest between Upper Nia and Copacabana formation. Also, well survey, tops and seismic horizons are included.

The well is located in the hanging wall part of the structure, which corresponds to the highest part of the anticline. The trust fault plays an important role in the expression of the anticline and the seismic signal is also affected by the reverse fault plane mostly close to the plane. Despite the signal reduction close to the fault plane, the seismic signal in the anticline is reasonably high-quality to be used in seismic inversion process.

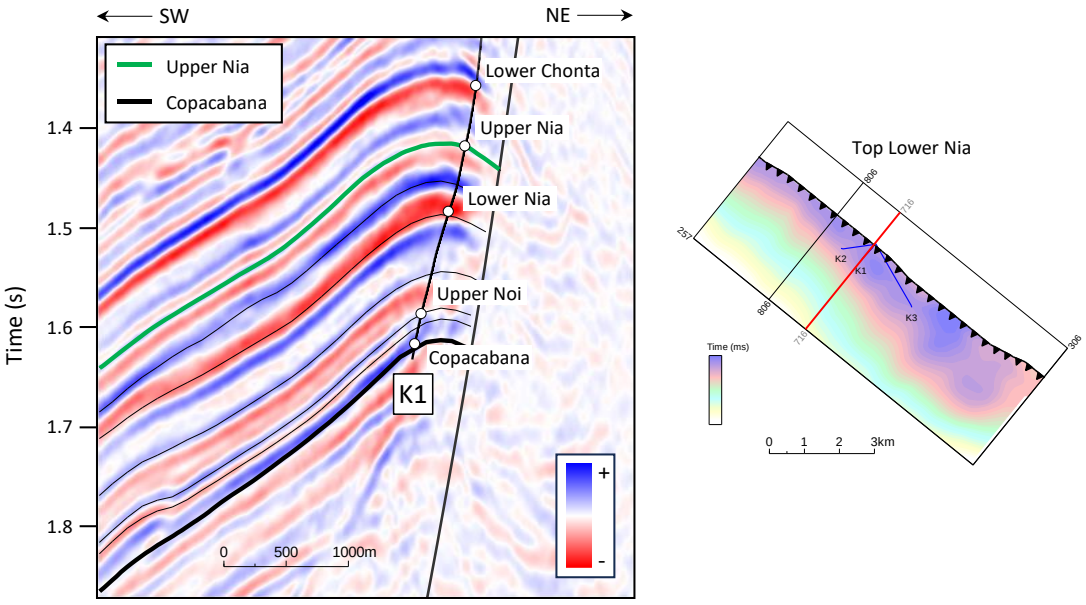

Figure 52 – Seismic XLine 716 which has the same direction of well K1 survey, the near stack [0-12°] shows excellent signal-noise ratio where peak and trough is represented by blue and red color respectively.

The elastic seismic inversion result is presented in the Figure 53. The three volumes (I_p, I_s, and $Density$) corresponds to the P50 which shows accurate visual result in tern of quality details. For instance, the top of Copacabana formation is well defined which is related to carbonate rocks with high values of acoustic impedance in range values from 12500 - 14000 ($m/s * gcc$). On the other hand, the Middle Nia formation also presents high values of acoustic impedance with values around 13000 ($m/s * gcc$) related to a level of anhydrate facies.

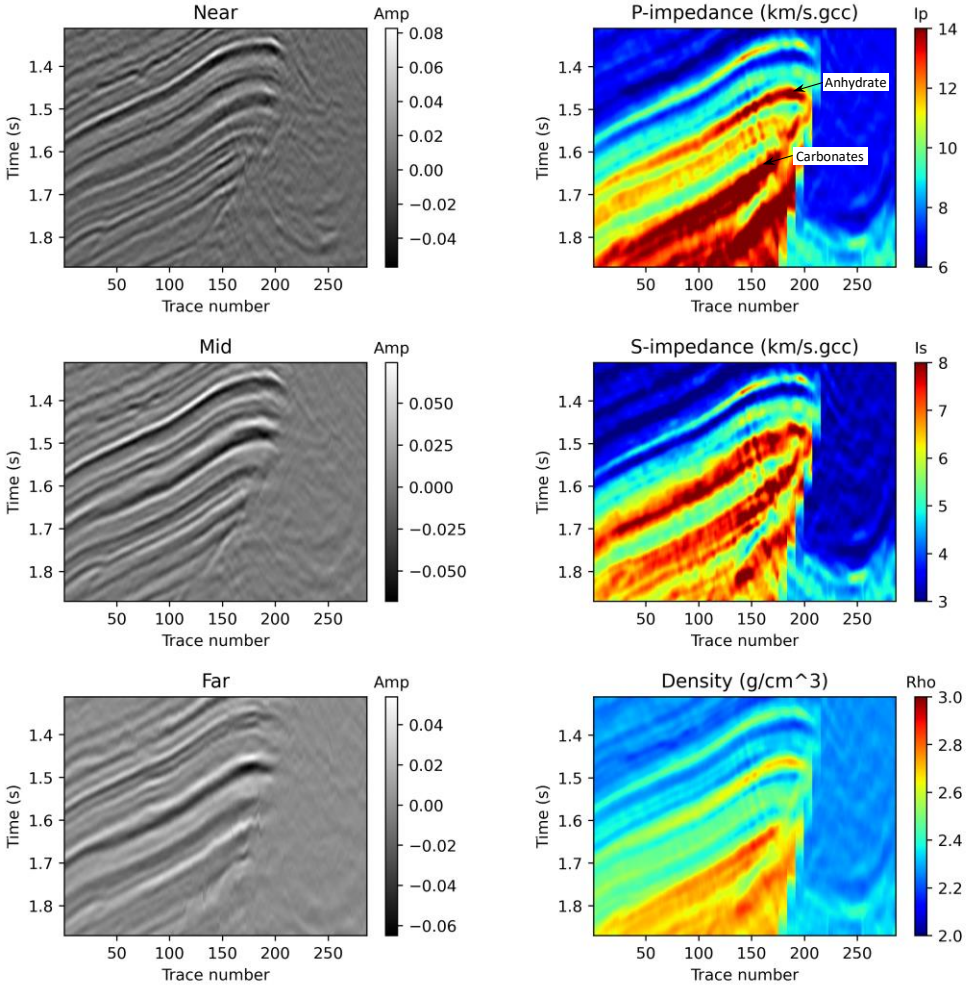

Figure 53 – The left part of the figure presents the input of the seismic inversion, and the right part shows the output of the seismic inversion of the inline 716.

The seismic Bayesian facies classification applied to seismic inline 716 in Figure 54 shows valuable information. For example, in the Noi-Ene zone is possible to observe that fine sandstone facies could be associated with deposits of damp to wet interdunes.

In the case of Lower Nia, the well K3 in the middle section shows a predominant present of fine sandstone facies. On the other hand, the seismic Bayesian results could predict these fine sandstones with less proportion compared to well-log interpretation in this middle section . Thus, the presence of fine sandstones facies in the middle section of Lower Nia suggests accumulations under wet conditions or at least different to the upper section where sandstone facies could be associated with dune deposits with excellent reservoir properties suggesting dry conditions of the system.

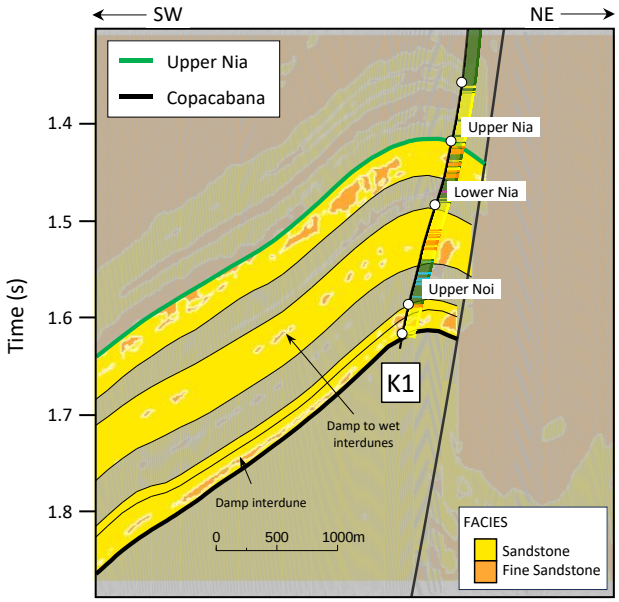

Figure 54 – Seismic inline 716 along the survey of the K2 showing the Bayesian facies classification using the seismic inversion results.

6.3 Future Perspective

There is always room for improvement, this study could serve as a basis for some possible lines of research to be implemented. Seismic reservoir characterization should be a routine workflow to be done and methodologies associated with the topic of current study should continue, such as rock-physics model, fluid substitution, seismic petrophysical characterization, improving efficiency of seismic inversion algorithm and so on. For study purposes a portion of the total seismic survey was used, future tasks that include the whole seismic survey must be done, this would imply a significantly more computational resource.

Rock-physics model could provide an easy-to-use toolbox for lithology and pore fluid interpretation of well-log data and elastic inversion results. The analysis could provide scenarios, both in terms of lithology and fluid substitutions. Also, the calibration of local conditions to the rock physic model could add basis of the influence of geologic factors such as burial compaction, diagenesis, rock texture, lithology, and clay cement to seismic properties (Avseth *et al*., 2005).

Apart from rock properties, another main goal of seismic reservoir characterization is to predict fluid properties given a set of seismic measurements by the estimation of elastic properties. For instance, the estimation of petrophysical properties, such us porosity, clay volume and fluid saturations, can also be formulated as an inverse problem and is generally referred to as rock physics inversion or petrophysical inversion (Grana, Azevedo, Figueiredo, & Mukerji, 2022). It is a more challenging work and needs to add all possible data to remove the bias in likelihood PDFs caused by zones far away of well-control, an alternative is the generation of pseudo-wells in those zones. Authors such as Dvorkin et al. (2014) and Fernandes and Lupinacci (2021) show the steps for generating spatially correlated pseudo-wells. With these pseudo-wells, the electrofacies likelihood PDFs could represent a better separation and, consequently, less confusion between them.

In recent decades, seismic inversion has been successfully extended to a kind of statistical framework for assessing the uncertainty of inferred 3D surface elastic models, which is one of the major limitations of deterministic inverse procedures. Unfortunately, these alternatives of elastic inversion algorithm are computationally expensive and only used in academia and not in the day-to-day life of the oil industry (Azevedo & Soares, 2017). Therefore, their development and implementation give the opportunity to be evaluated and shown the benefits that this type of approach brings to the reservoir characterization. This study is one of the academy purpose among others (Fernandes *et al.*, 2024). Further steps are feasible, such as the study presented by Grana *et al*. (2023) the study introduces the *Markov chain Monte Carlo* (MCMC) approach where complex prior models, such us multiple-points statistics simulations based on a training image were introduced to generate geologically realistic facies realizations. On the other hand, Ni, *et al*. (2024) presented a geostatistical seismic inversion method constrained by a seismic waveform. The correlation coefficient of seismic data is used to measure the similarity of the seismic waveforms, replacing the traditional variogram for sequential Gaussian simulation. Under the Bayesian framework, the MCMC algorithm is combined with the constraints of seismic data to randomly perturb and optimize the simulation results for obtaining the optimized parameter inversion results.

Any alternative way to improve the efficiency in the workflow is an opportunity of research. In the same row, several ways to optimize the objective function in geostatistical inversion were shown by Azevedo & Soares, (2017). A further step in the

workflow of the study is the implementation presented by Liu & Grana, (2019), they use a very common optimizer in *machine learning* for the objective function, which is ADAM (*Adaptive Moment Estimation*). The development of these types of algorithms brings interesting perspectives for future academic work. For this reason, Python programing is an essential tool for students and geosciences nowadays.

7 CONCLUSSION

This study showed a workflow for integrating information at scales of well-log and seismic for the characterization of sandstone reservoirs of a Kinteroni field in the Ucayali Basin using the Python programming language. The workflow presented made it possible to estimate and evaluate the quality and distribution of the reservoirs facies in the target zones which are framed between Upper Nia at the top and Copacabana at the bottom of the sequence in the study area.

Thankfully, partially stacked seismic volumes are available, it was possible to perform stochastic seismic inversion and use attributes such as (I_p) and V_p/V_s to perform Bayesian classification in more than one dimension. The combination between I_p and the V_p/V_s ratio bring us the benefits to the differentiation between electrofacies related to reservoir a non-reservoir. To perform the stochastic elastic seismic inversion, the algorithm *Ensemble Smoother with Multiple Data Assimilation* (ES-MDA) was selected. The study is the first work that uses this algorithm for seismic elastic inversion in Ucayali Basin.

In this work, the 50th percentile of the posterior distribution of the stochastic elastic inversion was used for the Bayesian classification of reservoir and non-reservoir facies. Previously, these electrofacies were defined based on well-log information from the three wells available in the study area (Kinteroni field) and upscaled using *Backus* approach at seismic scale. Data from the three wells were also used to construct probability density functions of conditional likelihood in the target zone.

From Bayes' theorem, it was possible to obtain the *confusion matrix* of facies prediction. The first approach for non-reservoir and reservoir facies, the results were outstanding, they were justified because target zones are well defined and restricted by seismic horizons where units contain more than 90% of specific facies (reservoir and non-reservoir). In conclusion, seismic inversion also could obtain a reasonably good result in the discretization of facies considering reservoir and non-reservoir facies. According to the confusion matrix, reservoir facies get 0.86 of true positive and non-reservoir facies obtain 0.8 of true negative.

The quantitative evaluation of stochastic elastic inversion through the coefficient of linear correlation with the upscale well profile showed that there was a gain in quality

of results compared to that of deterministic acoustic inversion. In the stochastic seismic inversion, the average success rate was 65% against 58% for the deterministic inversion.

Notorious difference in seismic inversion result was observed in the wells , such as K2 well, in which the correlation coefficient went from 49% in the deterministic inversion to 66% in the stochastic inversion. In the three wells stochastic has the advantage because it is in the statistical framework and the result is not unique. In addition, stochastic inversion is capable of providing quantitative and important information to evaluate the potential error.

The sensitivity of the ES-MDA outputs in relation to the input parameters was also evaluated. For instance, these parameters are the number of a prior ensemble members and the number of iterations. This was an important analysis, as these parameters are directly related to the required computational time for the inversion.

The analysis showed that a low number of ensemble members considering 200, produces a satisfactory result according to correlation coefficient, but it becomes noisy in the seismic section. Regarding the number of iterations (*data assimilation*), it was observed that it has little subtle impact on the difference between the original and modeled data on a randomly trace. Therefore, the best reasonable combination found was 300 prior ensemble members and 5 number of iterations.

Overall, seismic inversion results present outstanding information compared to a deterministic approach. Offering not only a single optimal solution (deterministic) instead of multiple realizations (stochastic) of the subsurface elastic properties. Indeed, these results should be integrated into the future geological models allowing greater control on the uncertainties in reservoir models because it includes a lateral spatial variability from seismic information. Moreover, the second approach of Bayesian facies classification into two groups of facies (sandstone and fine sandstone) in the target zones allow to identify different characteristics related to the depositional systems where those sediments were accumulated. For instance, in the Noi-Ene zone was possible to observe interval of fine-sandstone facies related to the deposition of damp interdune which could have less quality rock properties compared to sandstone facies which are related to climbing dunes and sandsheet deposits. On the other hand, Lower Nia presents predominant fine-sandstone facies in the middle section related to damp to wet interdune, even a fine horizontal interval of fine-sandstone facies could be associated to deflationary super surface, which

could be the limit of an aeolian successions. And Finally in the Upper Nia interval presents a less horizontal accommodations of the two group of facies due to the environment systems where these facies are accumulated, which is interpreted as a distributary fluvial system.

8 REFERENCES

Aki, K., & Richards, P. G. (1980). *Quantitative Seismology* (1st Edition ed.). W H Freeman & Co.

Alfarraj, M., & Ghassan, A. (2019). Semisupervised sequence modeling for elastic impedance inversion. *7*(3).

Avseth, P., Mukerji, T., & Mavko, G. (2005). *Quantitative Seismic Interpretation, Applying Rock Physics Tools to reduce Interpretation Risk.* Cambridge University Press.

Azevedo, L., & Soares, A. (2017). *Geostatistical Methods for Reservoir Geophysics.* Springer.

Backus, G. E. (1962, October). Long-wave elastic anisotropy produced by horizontal layering. *Journal of Geophysical Research, Volume 67*(Issue 11), Pages 4427-4440.

Bahlburg, H., Vervoort, J., Du Frane, S., Bock, B., Augustsson, C., & Reimann, C. (2009). Timing of crust formation and recycling in accretionary orogens: Insights learned from the western margin of South America. *Earth-Science Reviews, Vol. 97*(Issue 1-4), p. 215-241.

Bosh, M., Mukerji, T., & Ezequiel, F. (2010). Seismic inversion for reservoir properties combining statistical rock physics and geostatistics: A review. *GEOPHYSICS, 75*(5).

Bowman, A. W., & Azzalini, A. (1997). *Applied Smoothing Techniques for Data Analysis.* Oxford Statistical Science Series.

Bristow, C. S., & Moutney, N. P. (2013). Aeolian Stratigraphy. In *Treatise on Geomorphology.*

Buland, A., & Omre, H. (2003). Bayesian linearized AVO inversion. *GEOPHYSICS, Volume 68*(Issue 1).

Castagna, J., Al-Jarrah, F., & Chopra, S. (2014). *2. Rock-physics Foundation for AVO Analysis.* Society of Exploration Geophysicists.

Colombo, P. M., Giovanini, F. V., Veríssimo, L. W., Bernardes, F. L., Fonseca, P. G., & Assine, M. (2019). The sedimentary record of wet and dry eolian systems in the Cretaceous of Southeast Brazil: stratigraphic and paleogeographic significance. *Brazilian Journal of Geology*.

Coward, M. P. (1983). Thrust tectonics, thin skinned or thick skinned, and the continuation of thrusts to deep in the crust. *Journal of Structural Geology, Volume 5*(Issue 2), Pages 113-123.

Disalvo, A., Arteaga, M., & Chung, J. (2002). Geometria de las trampas y análisis estructural del área de Camisea y sus alrededores, Cuenca Ucayali. INGEPET 2002.

Disalvo, A., Chung, J., Seminario, F., Luquez, J., Arteaga, M., Gabulle, J., . . . de Santa Anna, M. (2008). Sistemas Petroleros Del "Gran Camisea". Sur De La Cuenca De Ucayali. Peru. VII Congreso de Exploración y Desarrollo de Hidrocarburos (Simposio de Sistemas Petroleros de las Cuencas Andinas).

Doyen, P. M. (2007). *Seismic Reservoir Characterization: An Earth Modelling Perspective* (Vol. 2). EAGE publications.

Dvorkin, J., Gutierrez, M. A., & Grana, D. (2014). *Seismic Reflection of Rock Properties.* Cambrigde University Press.

Emerick, A. A., & Reynolds, A. C. (2013, June). Ensemble smoother with multiple data assimilation. *Computers & Geosciences, Volume 55*, Pages 3 -15.

Espurt, N., Barbarand, J., Roddaz, M., Brusset, S., Baby, P., Saillard, M., & Hermoza, W. (2011). A scenario for late Neogene Andean shortening transfer in the Camisea Subandean zone (Peru, 12°S) : implications for growth of the Northern Andean Plateau. *GSA Bulletin, Vol. 123*, p. 2050-2068.

Fernandes, F. D., & Lupinacci, W. (2021). Pseudo-wells generation by spatial-correlated stochastic simulations. *1st SEG Latin American Virtual Student Conference 2021*.

Fernandes, F. D., Teixeira, L., Freire , A. M., & Lupinacci, W. M. (2024). Stochastic seismic inversion and Bayesian facies classification applied to porosity modeling and igneous rock identification. *Petroleum Science, ScienceDirect, Vol. 21*(Issue 2), p. 918-935.

Figueiredo, L., Grana, D., Santos, M., Figueiredo, W., Roisenberg, M., & Schwedersky, G. N. (2017). Bayesian seismic inversion based on rock physics prior modeling for the joint estimation of acoustic impedance, porosity and lithofacies. *Computational Physics, Vol 336*(Issue 1), 128-142.

Frank, A., & Kocurek, G. (1996). Toward a model for airflow on the lee side of aeolian dunes. *Sedimentology, Vol. 43*(Issue 3), p. 451-458.

Gil Rodriguez, W., Baby, P., & Ballard, J.-F. (2001). Structure et contrôle paléogéographique de la zone subandine péruvienneStructure and palaeogeographic control of the Peruvian Subandean zone. *ScienceDirect, Vol. 333*(Issue 11), p. 741-748.

Golub, G. H., & Van Loan, C. F. (2013). *Matrix Computation* (Fourth ed.). The Johns Hopkins University Press.

Grana, D. (2016). Bayesian linearized rock-physics inversion. *GEOPHYSICS, 81*(6).

Grana, D., & Dvorkin, J. (2011). The link between seismic inversion, rock physics, and geostatistical simulations in seismic reservoir characterization studies. *The Leading Edge, Vol 30*(Issue 1).

Grana, D., Azevedo, L., Figueiredo, L., & Mukerji, T. (2022). Probabilistic inversion of seismic data for reservoir petrophysical characterization: Review and examples. *Geophysics, Vol. 87*(Issue 5).

Grana, D., de Figueiredo, L., & Mosegaard, K. (2023). Markov chain Monte Carlo for seismic facies classification. *Geophyisics, Vol. 88*.

Grana, D., Mukerji, T., & Philippe, D. (2021). *Seismic Reservoir Modeling Theory, Examples, and Algorithms.* Wiley.

Grana, D., Mukerji, T., Dvorkin, J., & Mavko, G. (2012). Stochastic inversion of facies from seismic data based on sequential simulations and probability perturbation method. *GEOPHYSICS, 77*(4).

Grosso, S., Gabulle, J., & Chavez, F. (2017). Depósitos Eolicos Pre-cretácicos en los yacimientos gasíferos de Camisea, cuenca Ucayali, Perú. *XX Congreso Geológico Argentino*.

Hermoza, W., Brusset, S., Baby, P., Gil, W., Roddaz, M., Guerrero, N., & Bolaños, R. (2005). The Huallaga foreland basin evolution: Thrust propagation in a deltaic environment, northern Peruvian Andes. *Journal of South American Earth Sciences, v. 19*(i. 1), p. 21-34.

Huamán, V. C. (2018). Prediccion de propiedades de las rocas y distribución de fluidos en los reservorios upper y lower nia mediante el analisis de fi sca de rocas y atributos de inversión sísmica, Lote 57. *Boletin de la Sociedad Geologica del Perú*.

Kocurek, G., & Havholm, K. G. (1993). Eolian Sequence Stratigraphy—A Conceptual Framework. In *Recent Developments in Siliciclastic Sequence Stratigraphy.*

Kocurek, G., & Nielson, J. (1986). Conditions favourable for the formation of warm-climate aeolian sand sheets. *Sedimentology, Vol. 33*(Issue 6), p. 795-816.

Leeuwen, P. J., & Evensen, G. (1996). Data Assimilation and Inverse Methods in Terms of a Probabilistic Formulation. *Monthly Weather Review, Volume 124*(Issue 12), Pages 2898-2913.

Liu, M., & Grana, D. (2018). Stochastic nonlinear inversion of seismic data for the estimation of petroelastic properties using the ensemble smoother and data reparameterization. (SEG, Ed.) *Geophysics, Volume 83*(Issue 3).

Liu, M., & Grana, D. (2019). Accelerating geostatistical seismic inversion using TensorFlow: A heterogeneous distributed deep learning framework. *Computers & Geosciences, Vol. 124*, p. 37-45.

Luque, N. G., & Huamán, V. C. (2016). Modelado de Velocidades durante el procesamiento sísmico 3D PSDM y su implicancia en la configuración estructural del campo Kinteroni-Sagari, Lote 57, Camisea-Perú. *Congreso Nacional de Geologia*.

McClay, K., Scarselli, N., Tamara, J., Hammerstein, J., & Torres, D. (2018b). Structural Styles of the Camisea Fold-and-Thrust Belt, Southeast Peru. In *Petroleum Basins and Hydrocarbon Potential of the Andes of Peru and Bolivia* (pp. p. 271-296). AAPG.

McClay, K., Tamara, J., Hammerstein, J., Mora, A., Zamora, G., & Uzkeda, H. (2018a). Sub-Andean Thick and Thin-Skinned Thrust Systems of Southeastern Peru and

Bolivia—A Review. In *Petroleum Basins and Hydrocarbon Potential of the Andes od Peru and Bolivia* (pp. p. 35-62). AAPG.

Mosegaard, K., & Vestergaard, P. (1991). A Simulated Annealing Approach to Seismic Model Optimization with Sparse Prior Information. *Geophysical Prospecting, 39*(5), 599-611.

Mountney, N. P. (2006). *Periodic accumulation and destruction of aeolian erg sequences in the Permian Cedar Mesa Sandstone, White Canyon, southern Utah, USA.* Utah: Sedimentology.

Mukerji, T., Jørstad, A., Mavko, G., & Granli, J. (1998). Applying statistical rock physics and seismic inversions to map lithofacies and pore fluid probabilities in a North Sea reservoir. *SEG Technical Program Expanded Abstracts*.

Ni, X., Zhang, J., Guangzhi , Z., Wang, B., Lin, Y., & Liu, Z. (2024). Geostatistical inversion method based on seismic waveform similarity. *Applied Geophysics, Vol. 20*, p. 186-197.

Ødegaard, E., & Avseth, P. (2004). Well log and seismic data analysis using rock physics templates. *First Break, EAGE, 22*(10).

Oliveira, L., Pimentel, F., Peiro, M., Amaral, P., & Christovan, J. (2018). A seismic reservoir characterization and porosity estimation workflow to support geological model update: pre-salt reservoir case study, Brazil. *First Break, Vol. 36*(Issue 9), p. 75-85.

Peña, D., Arriola, P., Pinto, S., Santos, J., Pérez, A., & Bonora, M. (2018). PROVENIENCIA, EDAD Y PALEOGEOGRAFÍA DE LAS ARENAS RESERVORIOS - SUR CUENCA UCAYALI (AREA CAMISEA). *Congreso Peruano de Geología*.

Penna, R., & Lupinacci, W. M. (2020). Decameter-Scale Flow-Unit Classification in Brazilian Presalt Carbonates. *SPE Reservoir Evaluation & Engineering, Vol. 23*, p. 1420-1439.

Penna, R., Araújo, S., Geisslinger, A., Sansonowski, R., Oliveira, L., Rosseto, J., & Matos, M. (2019). Carbonate and igneous rock characterization through reprocessing, FWI imaging, and elastic inversion of a legacy seismic data set in Brazilian presalt province. *The Leading Edge, Vol. 38*(Issue 1).

Ribes, C., Kergaravat, C., Bonnel, C., Crumeyrolle, P., Callot, J.-P., Poisson, A., . . . Ringenbach, J.-C. (2015). Fluvial sedimentation in a salt-controlled mini-basin: stratal patterns and facies assemblages, Sivas Basin, Turkey. *Sedimentology*, p. 1513-1545.

Rojas, C. G. (2013). Caracterización diagenética de las areniscas reservorios del miembro informal Lower Nia, sur de la cuenca del Ucayali, Perú. *Boletín de la Sociedad Geológica del Perú*, p. 36-39.

Rojas, C. G., Vásquez, M. F., & Chacón, R. S. (2013). Caracterización sedimentológica del miembro informal Upper Noi, sur de la cuenca del Ucayali, Perú. *Boletín de la Sociedad Geológica del Perú*, p. 40-43.

Rusell, B. H. (1998). *Introduction to Seismic Inversion Methods.* Society of Exploration Geophysicists.

Scales, J., & Tenorio, L. (2001). Prior information and uncertainty in inverse problems. *GEOPHYSICS, 66*(2).

Scott, D. W. (2014). Kernel density estimation. *Wiley Online Library*, 1-7.

Seminario, F., Luquez, J., & Blanco, S. (2005). Las rocas reservorio productivas del Gran Camisea, Cuenca Ucayali-Perú. *INGEPET*.

Sen, M. K., & Stoffa, P. L. (2013). *Global Optimization Methods in Geophysical Inversion.* Cambridge University Press.

Silverman, B. W. (1986). Density estimation for statistics and data analysis. *CRC press, 26*.

Simm, R., & Bacon, M. (2014). *Seismic AMplitude, An Interpreter's Handbook.* Cambrigde University Press.

Simon, P. (1993a). Geology, hydrocarbon potential and prospect analysis, Ucayali basin, Perú. *v. 1*, p. 246.

Soares, A., & Azevedo, L. (2018). Geostatistics for Seismic Characterization of Oil Reservoirs. In *Handbook of Mathematical Geosciences* (pp. Pages 483-504).

Suppe, J. (1983). Geometry and kinematics of fault-bent folding. *American Journal of Sciences, 283*, 684-721.

Tarantola, A. (2005). *Inverse Problem Theory and Methods for Model Parameter Estimation.* SIAM.

Texeira, L., Cruz, N., Silvany, P., & Fonseca, J. (2017). Quantitative seismic interpretation integrated with well-test analysis in turbidite and presalt reservoirs. *The Leading Edge, Vol. 36*(Issue 11), p. 874-960.

Tompkins, J. M., Fernandez, J., Alumbaugh, D., & Mukerji, T. (2011). Scalable uncertainty estimation for nonlinear inverse problems using parameter reduction, constraint mapping, and geometric sampling: Marine controlled-source electromagnetic examples. *GEOPHYSICS, 76*(4), 263-281.

Torres, D., & MaClay, K. (2014). Structural evolution of the gas-condesate bearing traps of Camisea, Se Peru. *INGEPET.*

Venturo, D., & Huamán, V. (2013). Estilos estructurales que controlan los reservorios del Lote 57 dentro del área del Gran Camisea. *Boletín de la Sociedad Geológica del Perú*, p. 60-64.

Vernik, L. (2016). *Seismic Petrophysics in Quatitative Interpretation.* Society of Exploration Geophysicists.

Zamora, G., Louterbach, M., & Arriola, P. (2019). Structural controls along the Peruvian Subandes. In *Petroleum Basins anf Hydrocarbon Potential onf the Andes of Peru and Bolivia* (pp. p. 333-362). AAPG.